IS-T-790

INDUCTIVELY COUPLED PLASMA-ATOMIC EMISSION SPECTROMETRY: TRACE ELEMENTS IN OIL MATRICES

Charlie Albert Peterson

Ph.D. Thesis Submitted to Iowa State University

Ames Laboratory, DOE
Iowa State University
Ames, Iowa 50011

Date Transmitted: December 1977

PREPARED FOR THE U.S. DEPARTMENT OF ENERGY
UNDER CONTRACT NO. W-7405-eng-82

DISCLAIMER

NOTICE

Available from: National Technical Information Service
U. S. Department of Commerce
P.O. Box 1553
Springfield, VA 22161

Price: Microfiche $3.00

TABLE OF CONTENTS

Inductively coupled plasma-atomic emission spectrometry: Trace elements in oil matrices[†]

Charlie Albert Peterson

Under the supervision of Velmer A. Fassel
From the Department of Chemistry
Iowa State University

The simultaneous determination of up to 20 trace elements in various oil matrices by inductively coupled plasma-atomic emission spectrometry is reported. The oil matrices investigated were lubricating oils (for wear metals), fuel oil, centrifuged coal liquefaction product, crude soybean oil, and commercial edible oils. The samples were diluted with appropriate organic solvents and injected into the plasma as an aerosol generated by a pneumatic nebulization technique. Detection limits of the 28 elements studied ranged from 0.0006 to 9 μg/g with the majority falling in the 0.01 to 0.1 μg/g range. Analytical calibration curves were linear over at least two orders of magnitude and for some elements this linearity extended over 4.5 orders of magnitude. Relevant data on precision and accuracy are included.

[†]This work was supported by the U.S. Energy Research and Development Administration, Division of Physical Research.

Because metals often occur as particles in lubricating oil and coal liquefaction products, the effect of particles on the analytical results was examined. Wear metal particles in used oil did not appear to affect the analytical results. However, incomplete recovery relative to organometallic reference solutions was obtained for iron particles with a nominal mean diameter of 3.0 μm suspended in oil. It was shown that the following factors contributed to incomplete recovery for the particles: settling of the suspended particles in the flask, a difference in nebulization efficiency between particle suspensions and organometallic solutions, and indications of incomplete vaporization of the larger particles in the plasma.

High framing speed photography was employed to investigate the effect of aerosol carrier-gas flow rate and aerosol tube geometry on particle velocity in the plasma. This technique was also used to investigate the high frequency fluctuations in plasma shape and intensity of three plasma systems under various experimental conditions. Correlations with the electrical characteristics of the generators are shown in several instances.

CHAPTER I. INTRODUCTION

The Importance of Trace Elements in Oils

The concentrations of various elements in oils at the trace level are of great interest to the petroleum, fossil-fuel and edible oil industries. The extent of interest by the petroleum industry is exemplified by the recent formation of the Trace Metals Project, a joint project of five major petroleum laboratories to develop methods for determining trace metals in petroleum and petroleum products (1,2).

The occurrence and importance of trace elements in petroleum have been discussed by several authors (3-6). In an oil refinery, certain elements (e.g., Fe, Cu, Ni and V) poison the catalysts used in catalytic conversion units. This leads to decreased activity of the catalysts and/or altered product distribution (e.g., a change in the yield of gasoline relative to coke and gas). Thus, the concentration of the poisoning elements in the petroleum feedstock is of importance. Other elements affect the stability of finished products by catalyzing or inhibiting processes associated with product degradation. Concentration of metal-containing additives can be monitored by determining the concentration of the metal. In the case of fuels, especially the residual types, some elements, (e.g., Na, V) may cause corrosion or fouling of the fuel burning and power generating equipment.

From an environmental viewpoint, the concentrations of trace elements, especially toxic elements, in fuels are of interest since the elements ultimately present an environmental threat when the fuels are burned. The lead and phosphorous content of gasoline is of interest to the Environmental Protection Agency because of the poisoning effect these elements have on the catalytic converters in new automobiles.

The analysis of petroleum based oils for trace elements is also of interest outside of the petroleum industry. The determination of trace metals in used lubricating oil has become an accepted means of monitoring component wear in a variety of oil-wetted systems, most notably diesel and aircraft engines of various types (7). In fact, these determinations now constitute one of the world's largest single analytical operations. As metal components come in contact with each other, a certain amount of wear takes place.[1] In an oil-wetted system, the particles of wear are deposited in the oil. By analyzing the lubricating oil at regular intervals, the trace metal content due to normal or baseline wear can be determined. Any large deviation or rapid increase in the metal concentration may signal rapid wear or failure of a component.

---

[1]For a discussion of wear mechanisms, the reader is directed to reference (8).

With the realization by the general public and the Congress that the world supplies of petroleum are indeed limited, there has been an increasing interest in the liquefaction of coal. In several of the liquefaction processes (9,10) the coal is dissolved in a solvent at elevated temperatures and pressures. The dissolution may be performed in the presence of absence of hydrogen and/or a catalyst depending on the process. It is of interest to determine to what extent the trace elements found in the original coal are carried over into the liquid product. Many of the reasons for this interest are the same as discussed earlier for petroleum. If the liquid product is to be burned directly, questions arise concerning the environmental hazards and equipment corrosion and fouling due to trace elements in the fuel. If the liquid product is to be refined further, the effect of trace elements on catalysts and end product stability must be considered.

Other questions concerning the liquefaction process itself have been raised (11). First, the fact that certain Kentucky coals are very easy to liquefy in the SYNTHOIL process, poses the question of whether there is a constituent in these coals that acts as a catalyst for conversion or, alternatively, whether a catalyst poison is absent. Second, in some of the liquefaction processes, the solvent used to dissolve the coal is obtained from the resulting liquid product (9,10). Because of this recycling of solvent some

trace elements may actually be concentrated in the product oil.

Turning to edible oils, it has been recognized that trace metals influence the flavor and color stability and, thus, the shelf life of these products (12,13). The concentrations of these metals are, therefore, important to the edible oil processors. The trace element content of edible oils, as well as other foods, is also of interest from a nutritional standpoint.

Traditional Analytical Methods

A variety of analytical procedures for determining trace elements in oils of all types have been described. In the early years, the published methods generally employed colorimetric, spectrophotometric, polarographic or arc-spark optical emission analysis of the residue remaining after wet or dry oxidation of the oil sample. Because these procedures involved possible contamination of the sample by the oxidizing acids and/or loss of the analytes of interest during dry ashing, examination of the oil sample directly or after dilution with an organic solvent has been the favored analytical approach in recent years. For the direct examination approaches, a large number of variations of spark atomic emission, flame or nonflame atomic absorption or fluorescence, X-ray fluorescence, and neutron activation procedures have been proposed. The advantages and disad-

vantages of a number of these techniques as well as spark source mass spectrometry have been discussed with respect to petroleum oil samples by Braier and Eppolito (14,15). The most widely employed methods appear to be the rotating electrode, atomic emission technique (16) and several variations of atomic absorption procedures. Literally millions of determinations are made annually by these two methods. This extensive usage may imply that these two approaches meet all expectations with reference to speed of analysis, simplicity of analytical manipulations, powers of detection, absolute accuracy, and precision, but this is not the case. For example, in the case of lubricating oil the rotating disk electrode-atomic emission technique is admittedly subject to serious matrix effects arising from changes in the fuel dilution, viscosity and total composition (base oil plus additives) of the lubricating oil (7). For the various flame atomic absorption procedures, dilution of the oil sample with selected solvents usually reduces the matrix effects to acceptable levels. However, the atomic absorption approach possesses an operational disadvantage. Until the problem of simultaneous atomic absorption analysis is overcome, the determinations must be performed on a sequential basis. The elapsed time to complete the determination of an extended list of trace metals in a large number of samples is therefore much greater and unacceptable under some circumstances.

Inductively Coupled Plasma-Atomic Emission Spectrometry

The inductively coupled plasma-atomic emission excitation source (ICP) possesses certain unique properties and operating characteristics not found in spark or flame atomization systems (17,18). Some of these properties and characteristics are discussed below, but first an examination of the nature of the ICP may be helpful. A plasma is defined as a gas in which a significant fraction of the atoms or molecules are ionized. In the case of the ICP presently in use in this laboratory, the plasma is formed and sustained at the open end of an assembly of quartz tubes known as a plasma torch through which argon flows, as shown in the schematic diagram of the ICP in Figure 1. An alternating current (I) generated by a high frequency current generator flows through the coupling coil which surrounds the open end of the plasma torch. The current, alternating at ~27 MHz in the system in this laboratory, generates a time-varying magnetic field (H) with force lines as shown in the figure.

Plasma initiation and thermal isolation

To initiate the plasma, the argon in the plasma support and auxiliary argon streams is partially ionized by a tesla discharge. The resulting charged particles (electrons and ions) interact with the magnetic field; they are induced to flow in closed circular paths. The electron and ion flow,

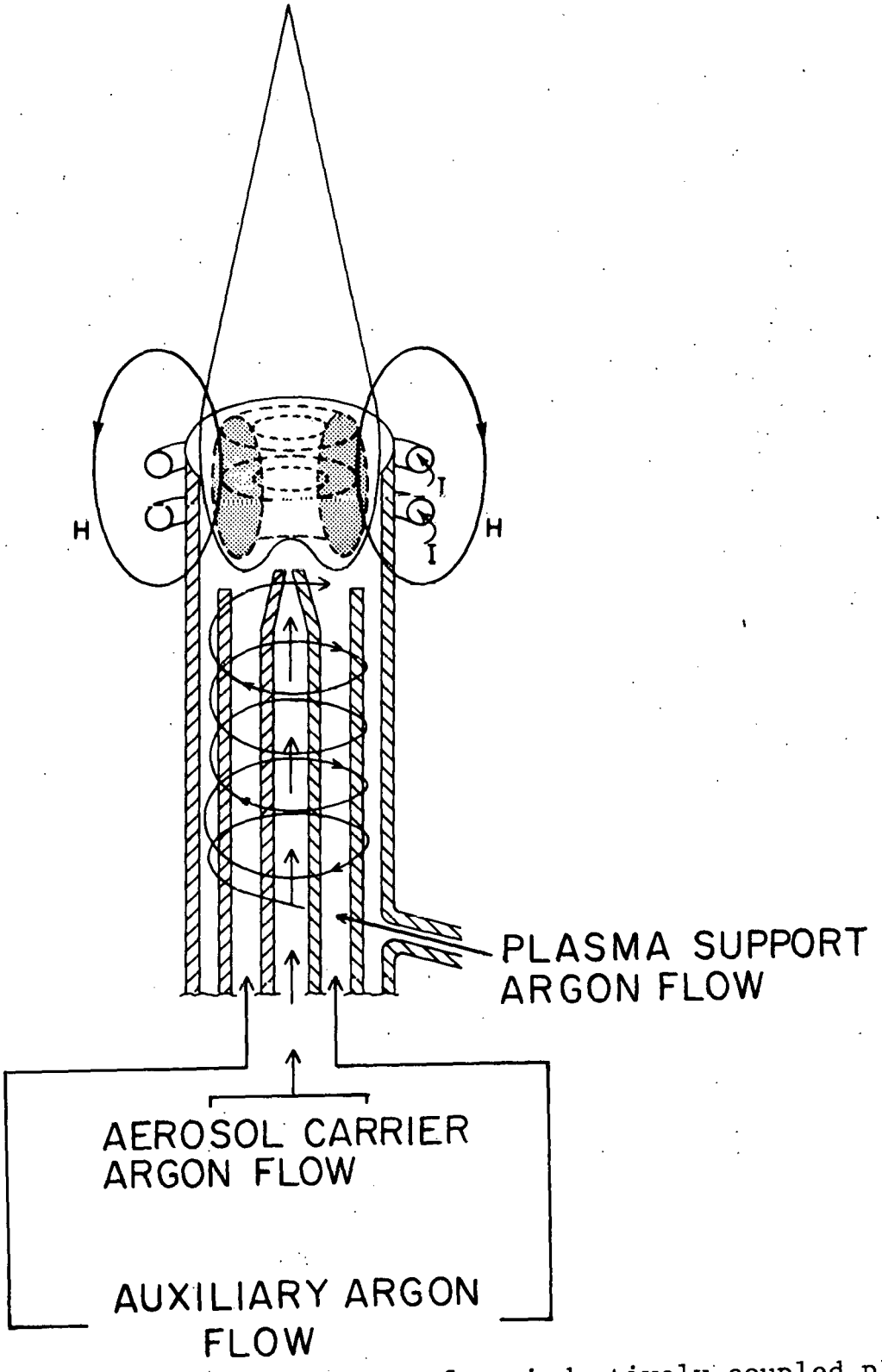

Figure 1. Schematic diagram of an inductively coupled plasma.

or eddy current as it is called, is analogous to a short circuited secondary of a transformer. Since the current in the coil and, therefore, the magnetic field are varying sinusoidally in direction and strength with time, the ions and electrons are accelerated every ½ cycle. In this acceleration, they meet resistance to flow which results in Joule heating, which in turn leads to additional ionization. In this way, a plasma of extended dimensions is formed almost instantaneously.

The plasma is isolated thermally from the plasma torch by the vortex stabilization technique suggested by Reed (19, 20), for which the support argon flow is introduced tangentially as shown in Figure 1. This tangential flow also serves to center the plasma in the torch.

Sample introduction

Once the plasma has been initiated, an argon flow of ~1 ℓ/min is introduced in the central tube as shown in Figure 1. This argon flow carries the sample aerosol. In order for the ICP to act as a effective atomization and excitation source, the sample aerosol must be injected efficiently into the plasma and remain in the high temperature environment as long as possible. As Fassel has aptly noted (21), this physical situation is difficult, if not impossible, to achieve in many other plasmas. One of the main forces acting in opposition to the injection of sample into the ICP is expansion thrust pressure. As gases are heated in the

ICP, they expand and are accelerated in a direction perpendicular to the exterior surface of the plasma. This outward movement of gas bombards the incoming particles or aerosol droplets and tends to deflect them around the plasma.

The presence of magnetic pressure in teardrop shaped ICP's which use laminar, coaxial argon introduction was first recognized by Chase (22,23) and later studied by several others (24-28). In an ICP, the electric field and, therefore, the induced current density are zero at the center of the plasma. The magnetic fields induced by the coil and eddy currents reinforce each other at the outside of the discharge and oppose each other at the center. These characteristics lead to the result that the Lorentz force produces magnetic compression around the sides of the plasma directed toward the axis. This compression opposes gas flow from the interior through the sides and confines the plasma in the radial direction. Thus, the pressure can be converted into kinetic energy only in the axial direction and an outward flow is produced along the axis in both the upstream and downstream directions. This "magnetic pumping" which is fed by an inward flow of gas through the sides of the plasma, has been observed experimentally by Waldie (24). The outward flow of gas along the axis opposes entry of particles or aerosol into the plasma and tends to deflect them around the plasma. Chase (23) has noted, however, that if the plasma support

gas is introduced tangentially as is done in this laboratory, there is a low pressure zone in the axial channel of the plasma, as postulated by Reed (19), which obscures the magnetic pressure effect (22).

In addition to tangential gas introduction, the skin depth effect has been used to facilitate sample introduction. The skin depth, i.e., the depth at which the eddy current is reduced to 1/e of its surface value, is inversely proportional to the square root of the current frequency. As the frequency is increased, the position of highest eddy current density moves toward the outer surface of the plasma. At the frequencies used in this investigation, an annular plasma is formed as shown in Figure 1. Because the axial region is somewhat cooler than the annulus, it offers less resistance to sample introduction. The annular shape can be further developed by optimizing the gas flows. This plasma configuration permits efficient sample introduction along the axis.

Advantages of the inductively coupled plasma

By the time the sample or its decomposition products reach the observation height 15 to 20 mm above the coil, they have had a residence time in the plasma of ~2 ms. During that time, they have experienced temperatures ranging from ~7000 K to ~5500 K. Both the temperature and the residence time are approximately twice as great as those found in a

nitrous oxide-acetylene flame, the hottest flame normally used in analytical spectroscopy. The relatively high temperatures and residence times and the inert environment provided by the plasma support and stabilizing gas leads to the expectation that the degree of atomization of the samples, including suspended particulates, should be greater than in flames or spark discharges. Because the atoms are released in a noble gas environment, free-atom depopulation processes, such as monoxide formation, should also be minimized. These favorable environmental factors should, in turn, overcome many of the interelement or matrix interference effects found in flames or arc or spark discharges. These expectations have been confirmed by observations on several classical interelement interference effects (29).

Other features of the annular ICP arise from the fact that analyte atoms or ions are confined to a narrow channel along the axis. The analyte emission is concentrated in this region and can be utilized more effectively by conventional spectrometers. The temperature across the channel at the normal observation height is relatively uniform, and the number density of analyte atoms or ions in the surrounding argon is far lower than in the channel. Under these conditions, the central channel of the ICP acts as an optically thin emitting source. With the proper detection and measurement system, analytical calibration curves that are linear over

five orders of magnitude change in concentration are possible.

Previous Work

Pforr (30) evidently published the first paper on the direct introduction of oil samples diluted with gasoline into the plasma. In a later preliminary report, Pforr and Aribot (31) reported detection limits of 3.6, 4.2, and 1.5 ppm (by weight) respectively for Al, Fe, and Ni. In another brief report, Greenfield and Smith (32) indicated that they successfully determined Al, Cr, Cu, Fe, Ti, Ni, Mg, and Mn in samples of engine oil. Neither Pforr and Aribot nor Greenfield and Smith provided any data on the accuracy and precision of their results. In this laboratory, Abercrombie had found that an inductively coupled argon plasma could be sustained when oil diluted 1:10 w/v with 4-methyl-2-pentanone was nebulized and the resulting aerosol carried into the plasma (33). He employed the plasma to obtain calibration curves for a number of elements in an oil matrix. These curves were linear for at least two orders of magnitude. He also found that for viscosity variations between 1.0×10^{-5} and 2.45×10^{-4} m^2/s there was little or no difference in net spectral emission intensities when equivalent concentrations occurred in oils of different viscosities. Abercrombie applied this analytical technique to used crankcase oil samples in a recovery study and obtained recoveries

which, within experimental error, approached 100% (34).

With this background, the present investigation was undertaken. The applicability of the ICP to the determination of trace elements on a simultaneous multielement basis in a variety of oil matrices was explored. These matrices included residual fuel oil, the liquid product of coal liquefaction, and edible oil, as well as lubricating oil. The behavior of metal particles suspended in oil was examined with respect to analysis by the ICP. In addition, high speed photography was utilized to examine the plasma and the influence of two parameters on particles traversing the plasma.

CHAPTER II. EXPERIMENTAL FACILITIES AND PROCEDURES

Experimental Facilities

The experimental facilities and operating conditions are summarized in Table I. More detailed discussions of the facilities may be found in references 36-38.

Although the ICP is normally operated without the auxiliary plasma argon flow (17) when aqueous solutions are nebulized, this flow is desirable for oil samples because there is a tendency for the formation of carbon-like deposits on the rims of the two inner tubes of the torch. The auxiliary argon flow provides an improved spatial separation of the plasma and these tubes.

Other operating conditions employed with organic solutions also differ from those commonly employed in this laboratory with aqueous solutions (29,37). These include the forward power, plasma and aerosol carrier argon flow rates, optimum observation height, and height of the torch with respect to the coil.

The pneumatic nebulizer used in this work has been abandoned for use with aqueous solutions in this laboratory because of the inability of the stainless steel needles to tolerate high acid concentrations (39). This was not a problem with the organic solutions used in this study, so the stainless steel nebulizer was retained. However, when

Table I. Experimental facilities and operating conditions

Aerosol generator	Pneumatic nebulizer similar to that described by Valente and Schrenk (35) with Teflon uptake tube.
Spray chamber	Borosilicate glass, 300 mm long, tapering from 40 mm i.d. to about 10 mm i.d. and (later) a 190 mm long chamber; operating angle deviates slightly from horizontal to allow free drainage of excess solution from nebulizer end (see Figure 2).
Plasma torch assembly	All of fused quartz construction as described previously (17) and shown in Figure 2. Torch positioned in center of the coil with the top of the intermediate tube ~3 mm below the bottom coil. When vegetable oils are analyzed, the top of the tube should be approximately even with the bottom of the coil (see Chapter V for explanation).
Argon flow rate	Plasma support: 17-18 ℓ/min Auxiliary: ~1 ℓ/min Aerosol carrier: 0.6 to 1.0 ℓ/min depending on sample type and solvent. For MIBK solutions, 0.9-1.0 ℓ/min.
Observation height	Position B in Figure 3, usually 18-20 mm above the load coil.
Plasma power supplies	1. Lepel High Frequency Laboratories Model T-5-3-DF1-2-J-S generator with attached impedance matching network as described in (36). Input power 45% of total power.

Table I. (Continued)

	2. Plasma-Therm Model MN-2500 E generator, 27 MHz, 2500 W forward power rating, operated at 2100 W forward power. This generator is equipped with a Plasma-Therm servo-drive impedance matching network that maintained the reflected power to ≤1 W. Load coil made from 1½ turns of 5 mm o.d. copper tubing, i.d. of coil 27 mm.
	3. Unit similar to 2 with a slightly different impedance matching network and a 2-turn load coil.
	4. Unit similar to 3 with a 2-turn coil.
Spectrometers	1. Sequential single channel
	A. Jarrell-Ash Co., Model No. 82-000, 0.5 m Ebert monochromator with a grating blazed for ~300 nm used with an EMI 6256 photomultiplier and a Keithley Model 417 picoammeter.
	B. Jarrell-Ash Co., Model No. 78-466 1.0 m Czerny-Turner monochromator with a grating blazed for 250 nm with an EMI 6256 photomultiplier and a Keithley Model 417 picoammeter or a logarithmic amplifier.

Table I. (Continued)

	2. Simultaneous multichannel
	A. Applied Research Laboratories, Model QVAC 127 multichannel direct reading spectrometer with a 2160 grooves/mm grating blazed for the 170.0-215.0 nm region. The spectral lines programmed are given in Table II. The detector electronics are described in (36). A signal integration interval of 30 sec was used.
	B. Same spectrometer as system I, but with a new holographic grating with 2160 grooves/mm and with detector electronics as described in (37). A signal averaging interval of 10 sec was used.

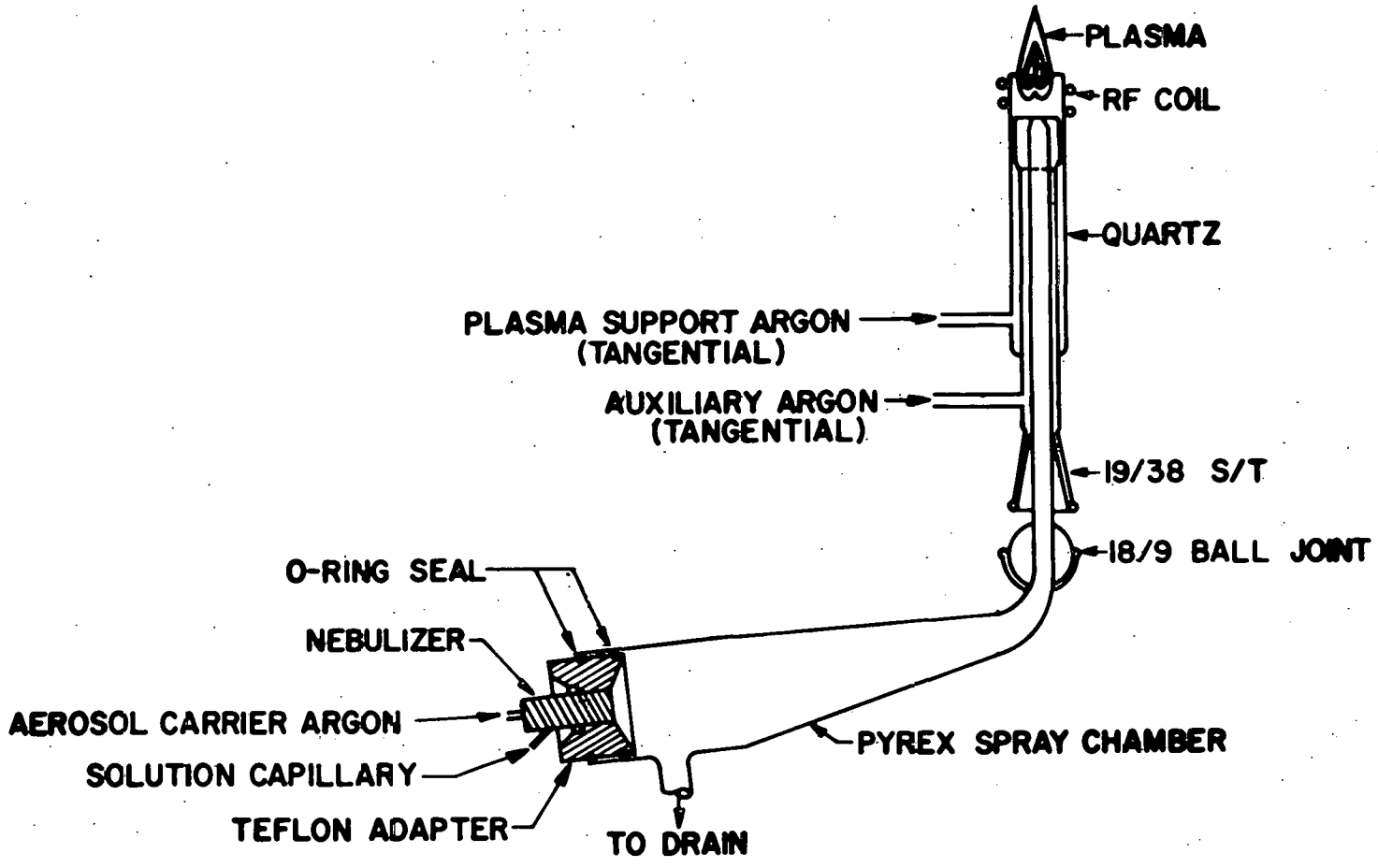

Figure 2. Schematic diagram of plasma torch assembly and aerosol generation system.

Table II. QVAC 127 line array

Element	Wavelengths (nm)								
Ag	I[a]	328.07							
Al	I	308.22	I	396.15					
As	I	193.76	I	234.98[b]					
B	I	249.68							
Ba	II[c]	233.53							
Be	II	313.04							
Bi	I	223.06							
Ca	II	315.89	II	393.37					
Cd	II	226.50	I	228.80					
Co	II	238.89	I	345.35					
Cr	II	205.55	II	267.72	II	283.56	I	357.87	
Cu	I	324.75							
Fe	II	261.19							
Ga	I	294.36							
Ge	I	265.12							
Hg	I	184.95	I	253.65					
Mg	II	279.55							
Mn	II	257.61	I	403.08					
Mo	I	386.41							
Ni	II	231.60	I	341.48	I	351.51			
P	I	255.33							
Pb	II	220.35	I	405.78					
Sb	I	217.59							
Se	I	196.03							
Si	I	288.16							
Sn	I	303.41							
Sr	II	338.07							
Ti	II	334.90							
Tl	I	377.57							
V	II	311.07							
Y	II	242.22	II	371.03					
Zn	II	202.55	I	213.86					

Number of elements 32
Number of elemental wavelengths 46

[a] I Signifies that spectral line originates from neutral atom state.

[b] This spectral line was available during only a portion of this study.

[c] II Signifies that spectral line originates from singly ionized state.

aqueous solutions from the wet ashing procedure were analyzed, the right angle glass needle nebulizer described in (39) was used with the spray chamber described in (29).

Experimental Procedures

Plasma ignition and sample introduction procedure

A step by step procedure for igniting the plasma and introducing aerosols of the organic solutions discussed in this paper is given in Table III. If an impedance matching network such as described in Table I for power supplies 2 to 4 is used, the tuning in steps 3 and 5 is accomplished automatically. The network is then switched to manual control for steps 6 and 7 and returned to servo control for step 8. For organic matrices other then those discussed here, it may be necessary to modify the detuned position of step 6, as well as the argon flow rates given in Table I.

Sample preparation for lubricating oils

Dilution procedures and reference samples Unless otherwise noted, the sample, reference and blank oils for the petroleum related matrices were all diluted 1:10 w/v with 4-methyl-2-pentanone (more commonly known as methyl isobutyl ketone, MIBK), i.e. 1.000 g of oil was diluted to 10 ml with MIBK. The reference oils were prepared from Conostan organo-metallic reference samples (Conostan Division, Continental Oil Company, Ponca City, OK) by appropriate serial dilutions with

Table III. Plasma ignition and sample introduction

1. Position torch and set argon flows as shown in Table I. Purge the nebulization chamber and torch assembly with argon for ~ one minute. The uptake tube should be immersed in the sample.

2. Close aerosol carrier gas toggle valve.

3. To ignite the plasma, turn on tesla coil discharge, and simultaneously turn up the forward power and tune to minimum reflected power.

4. Check to see that the forward power is set at ~2100 W. (Plasmas have been sustained at much lower power when an organic aerosol was injected, but 2100 W is recommended because it is easier to sustain the plasma upon the injection of aerosol at this power.)

5. Tune to minimum reflected power. This position will differ from that of step 3.

6. Start from the tune position of step 5 and detune toward the tune position of step 3; stop at a position ~1/3 of the way between the two. The plasma may sound and/or appear slightly unstable at this point.

7. Open the aerosol carrier gas toggle valve quickly so that the aerosol is introduced into the plasma in an abrupt manner. This operation is facilitated if the toggle valve is located close to the nebulizer. When the organic aerosol is introduced slowly, there is often a tendency for the plasma to rise out of the coil and to collapse.

8. Tune to minimum reflected power. The tuned position may change slowly for the first 30 to 60 minutes.

Conostan 245 base oil, a refined oil with a very low metal content. The Conostan reference samples included single element reference samples, Conostan D-12 blended reference sample, and Conostan D-20 blended reference sample. Conostan D-12 contained equal concentrations of Ag, Al, Cr, Cu, Fe, Mg, Na, Ni, Pb, Si, Sn, and Ti, whereas Conostan D-20 contained B, Ba, Be, Cd, Mn, Mo, V and Zn in addition to those elements contained in Conostan D-12. For the analysis of the U.S. Air Force (USAF) Spectrometric Oil Analysis Program (SOAP) correlation samples, the reference and blank oils provided by the USAF were simply diluted 1:10 w/v with MIBK. Because USAF-SOAP reference solutions were exhausted at the time the Al determinations were performed on the SOAP samples, a separate set of reference solutions was prepared by serial dilutions of Conostan 900 ppm D-12 blended reference sample with Condor 105 (ArRo Laboratories, Inc., Joliet, IL) as the dilution oil. The Condor oil was used instead of Conostan 245 because it more closely matched the viscosity of the original USAF-SOAP reference solutions.

Wavelength profiles obtained on multichannel spectrometer B, as described below, of Fisher ACS certified MIBK and Baker ULTREX MIBK showed no apparent difference in trace element content. Because of cost considerations, the Fisher ACS certified MIBK was used as the solvent.

Chemical oxidation procedure and reference samples For comparison purposes (see p.53) three of the used engine oils were also prepared by a chemical oxidation procedure. One gram oil samples were weighed into Kjeldahl flasks after which 15 ml of HNO_3 and 10 ml of $HClO_4$ were added. The flasks were then heated gently until oxidation was complete, as evidenced by a clear solution. After cooling, the resulting solution (~5 ml) was diluted to 50 ml with deionized water. Reference solutions and the blank solution contained an acid concentration approximately equal to that of the samples, i.e. 7% by volume of $HClO_4$. Thus, differences in nebulization caused by variation in acid concentration which have been described by Greenfield et al. (40) were avoided. The perchloric and nitric acids used for the chemical oxidation and in the reference solutions were purified by sub-boiling distillation (41).

Analytical procedures

Analytical measurements For all analytical systems, the net analyte measure was determined by subtracting the average of the blank measures (determined immediately prior to and following the sample measure) from the sample measure.

Wavelength profiles Wavelength profiles were obtained on multichannel spectrometer B for up to 20 analytical lines simultaneously by moving the entrance slit in small increments along the Rowland circle as described in references 37 and 42.

CHAPTER III. DETERMINATION OF TRACE ELEMENTS IN PETROLEUM RELATED MATRICES

General Results

When solutions such as MIBK/oil or xylene/oil are nebulized, a much denser fog is formed in the spray chamber than with aqueous solutions. The appearance of the plasma is also much different. Figure 3 is a photograph, taken through crossed polarized filters, of a plasma with an oil/MIBK (1:10) solution being nebulized. When organic liquids are introduced into the plasma, the various regions of the plasma are easily visible. The point labeled B indicates the recommended viewing region for analysis.

Wavelength scans

Wavelength scans from 190.0 to 520.0 nm are given in Figures 4 and 5 for emission from the regions of the plasma labeled in Figure 3. These wavelength scans were recorded while an oil/MIBK (1:10) solution was being nebulized. A forward power of 2050 W from power supply 4 sustained the plasma. The 1.0 m spectrometer was used in conjunction with a logarithmic amplifier. The latter assured that a large range of spectral intensities could be accommodated in one recording. Other conditions were as stated in Table I. For comparison, a scan of an argon plasma with only argon in the aerosol carrier channel is included. The relative intensity

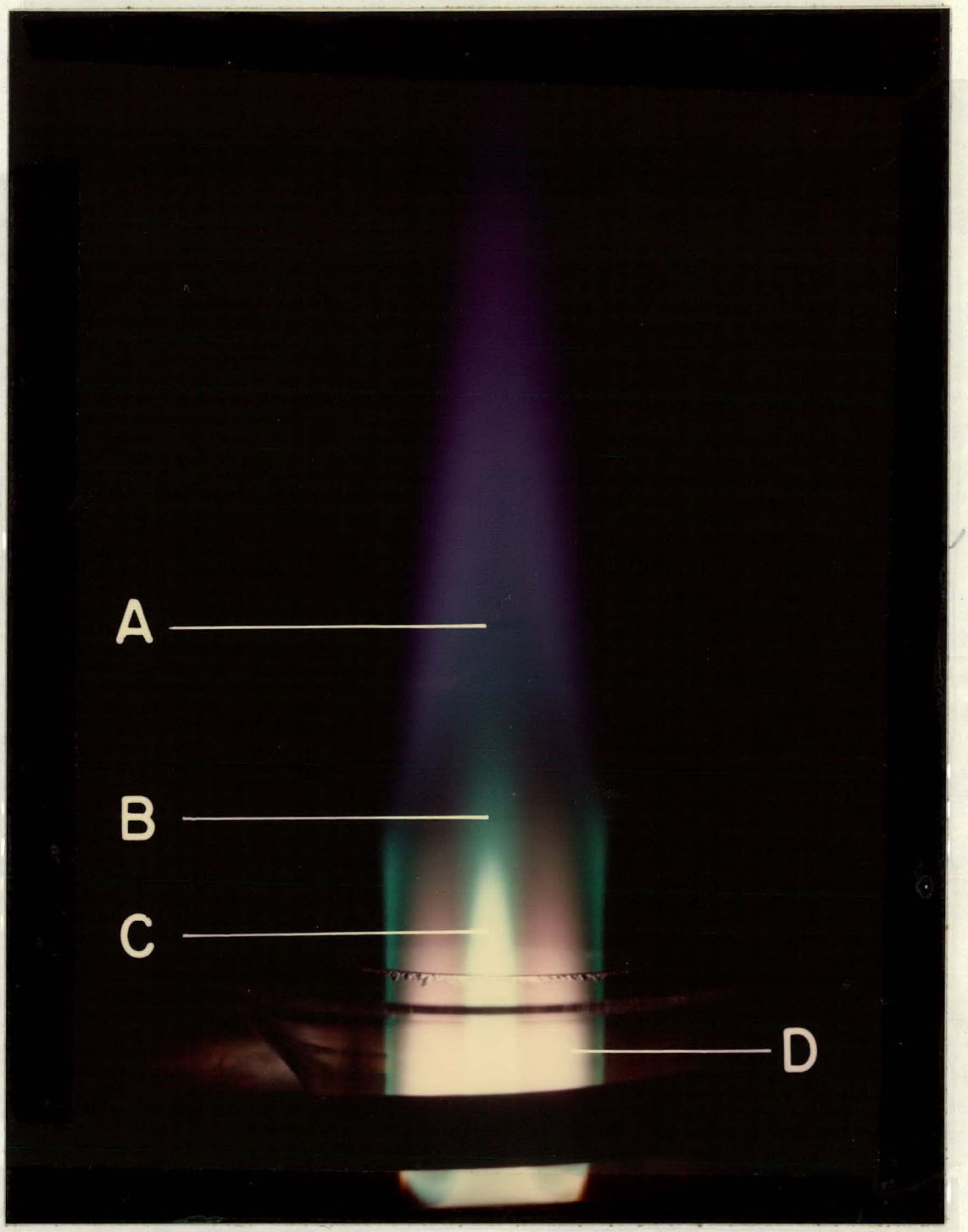

Figure 3. Photograph taken through crossed polarized filters of a plasma with an oil/MIBK (1:10) solution being nebulized. Letters locate various regions of the plasma; (A) tail flame in axial channel, (B) analytical zone in axial channel, (C) luminous zone low in axial channel, and (D) toroid.

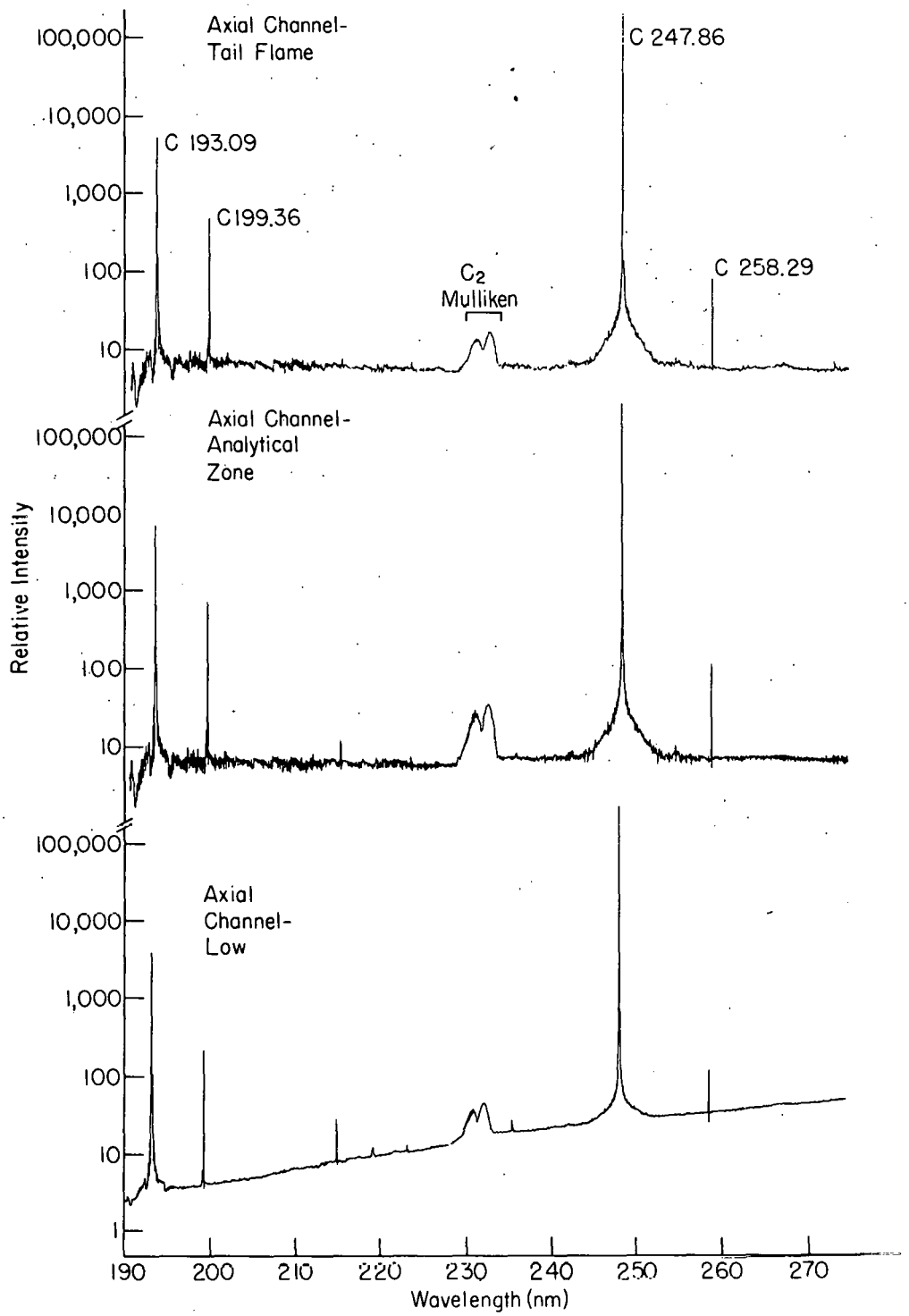

Figure 4. Wavelength scans from 190.0 to 520.0 nm for three heights in the center of the axial channel (points A, B and C in Figure 3). Scans were obtained while an oil/MIBK (1:10 w/v) solution was being nebulized.

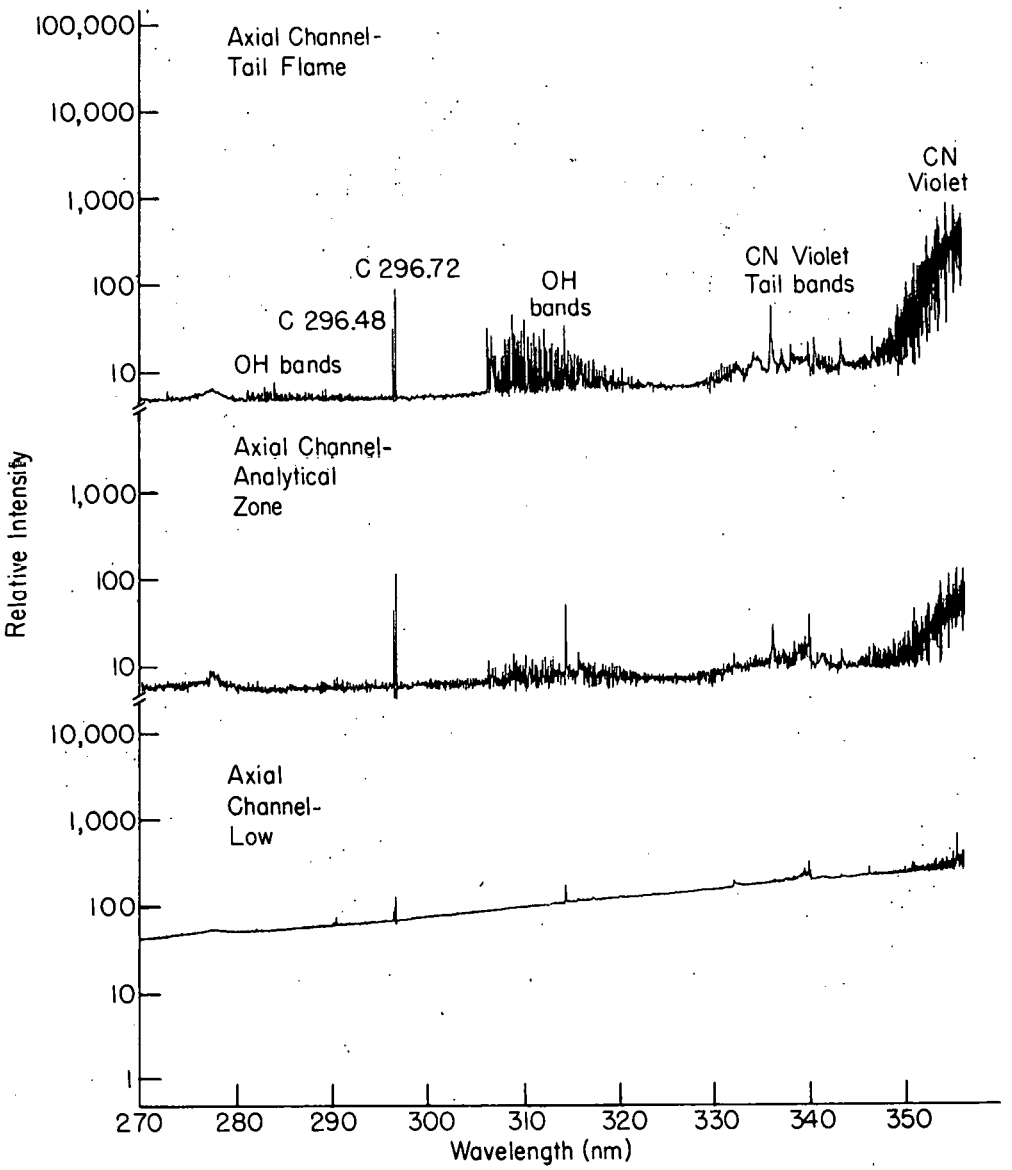

Figure 4. (Continued)

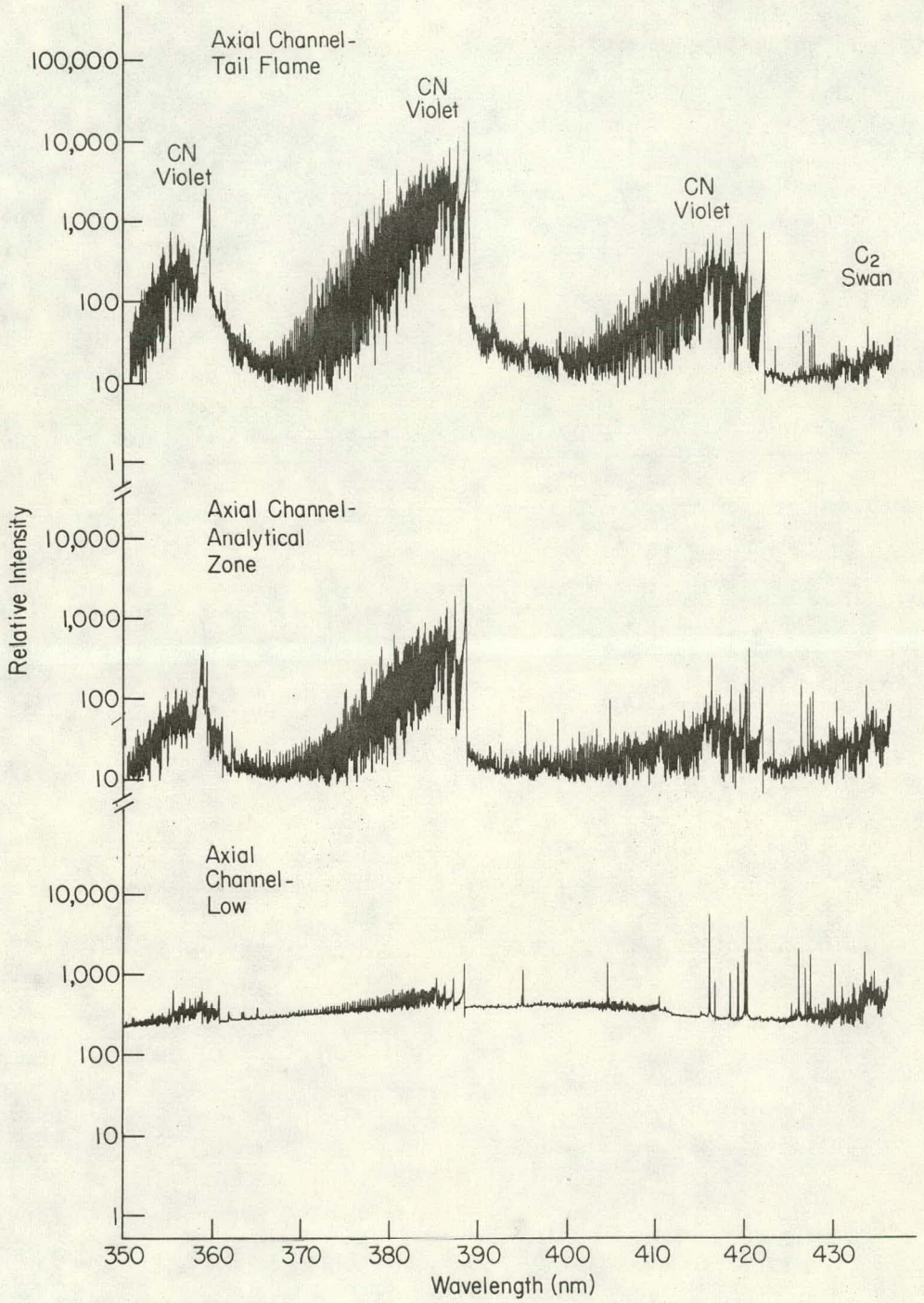

Figure 4. (Continued)

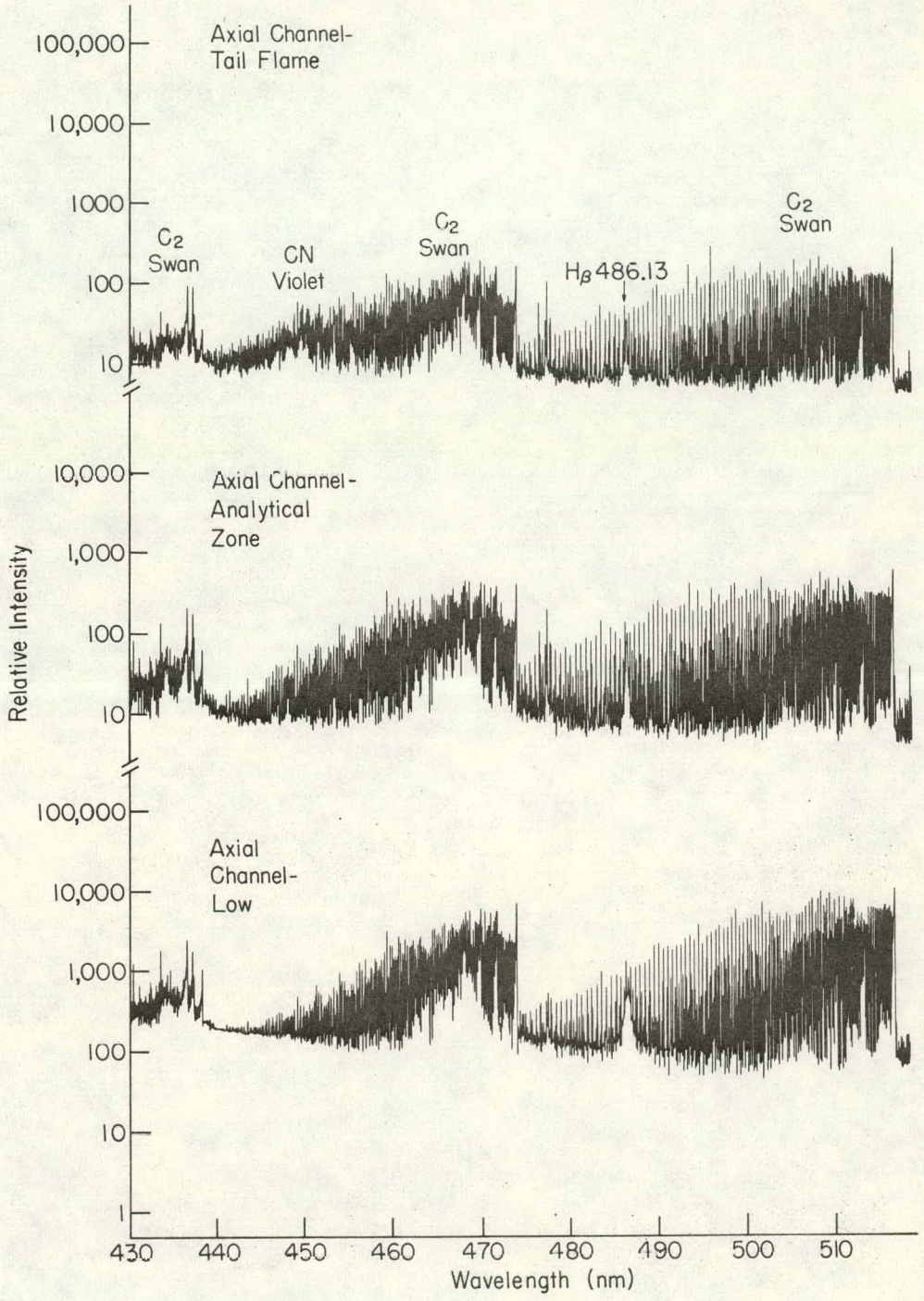

Figure 4. (Continued)

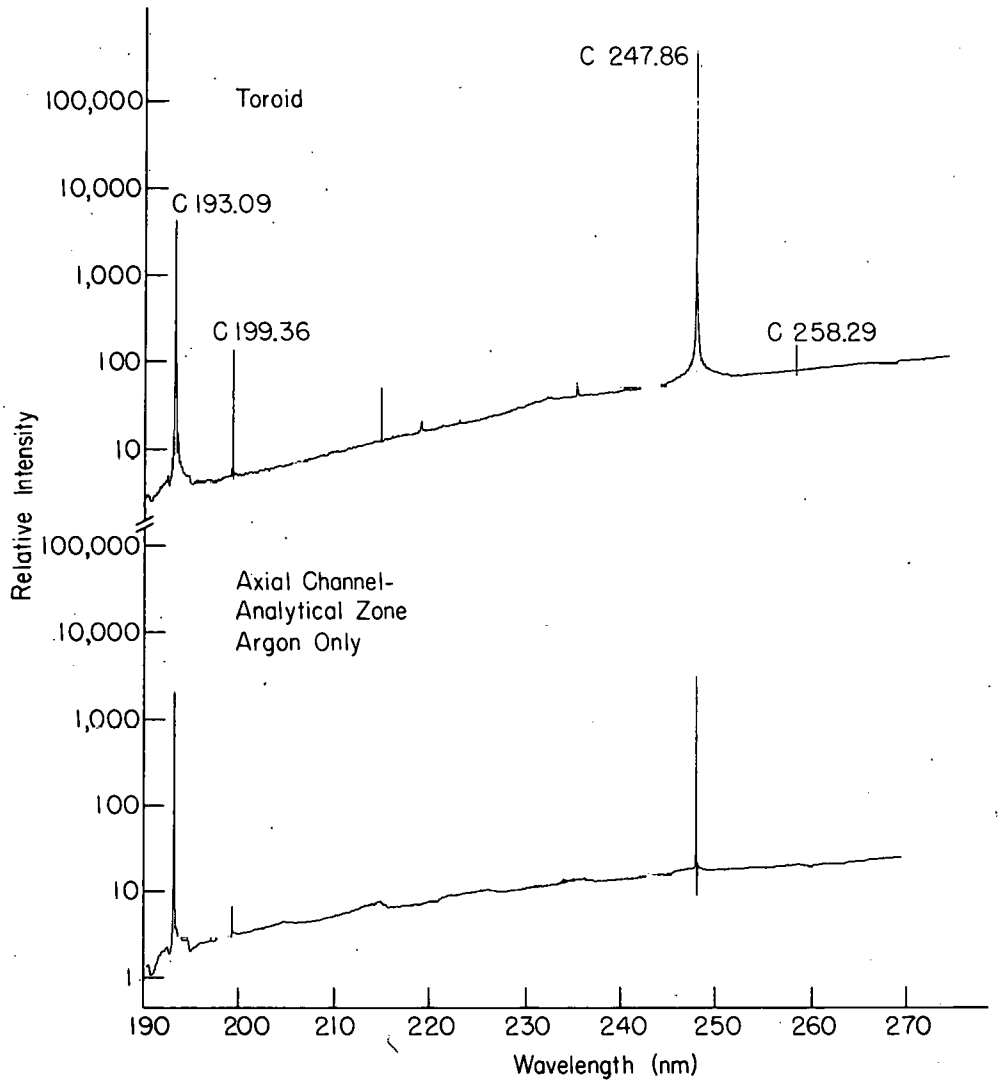

Figure 5. Wavelength scans from 190.0 to 520.0 nm for the toroid region (point D in Figure 3) under the same conditions as Figure 4 and for the analytical zone (point B in Figure 3) with no solution being nebulized, i.e., with only argon in the aerosol carrier gas.

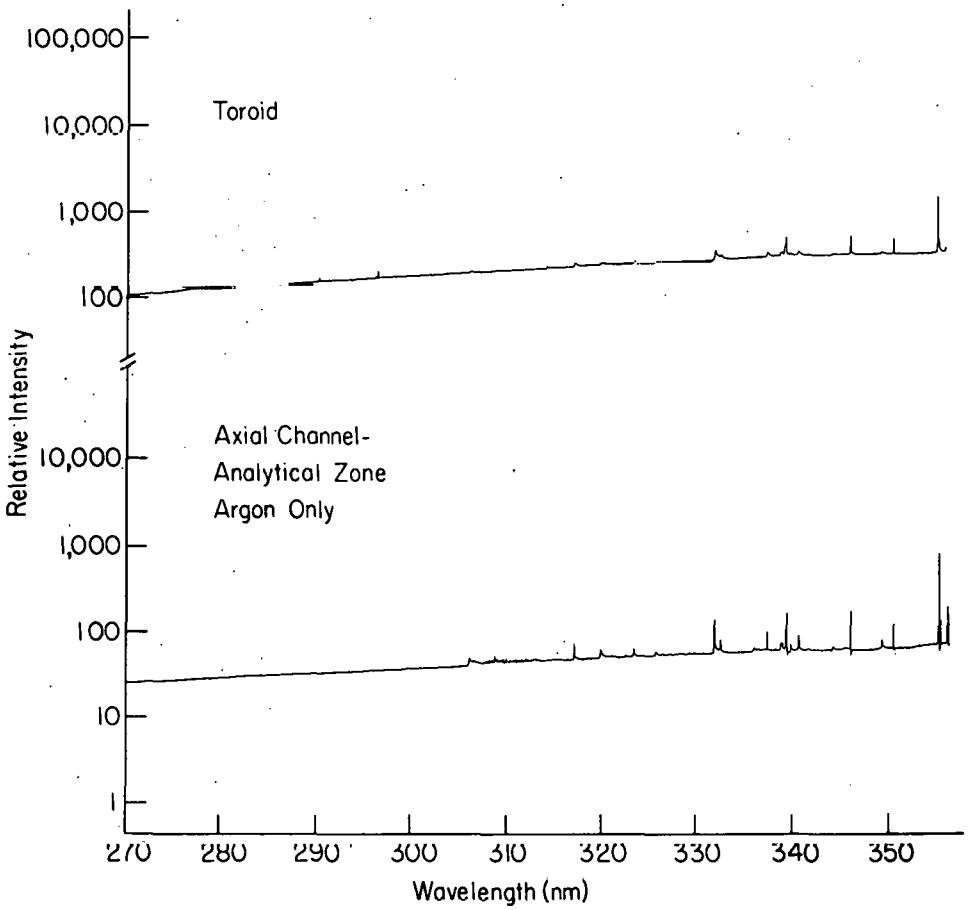

Figure 5. (Continued)

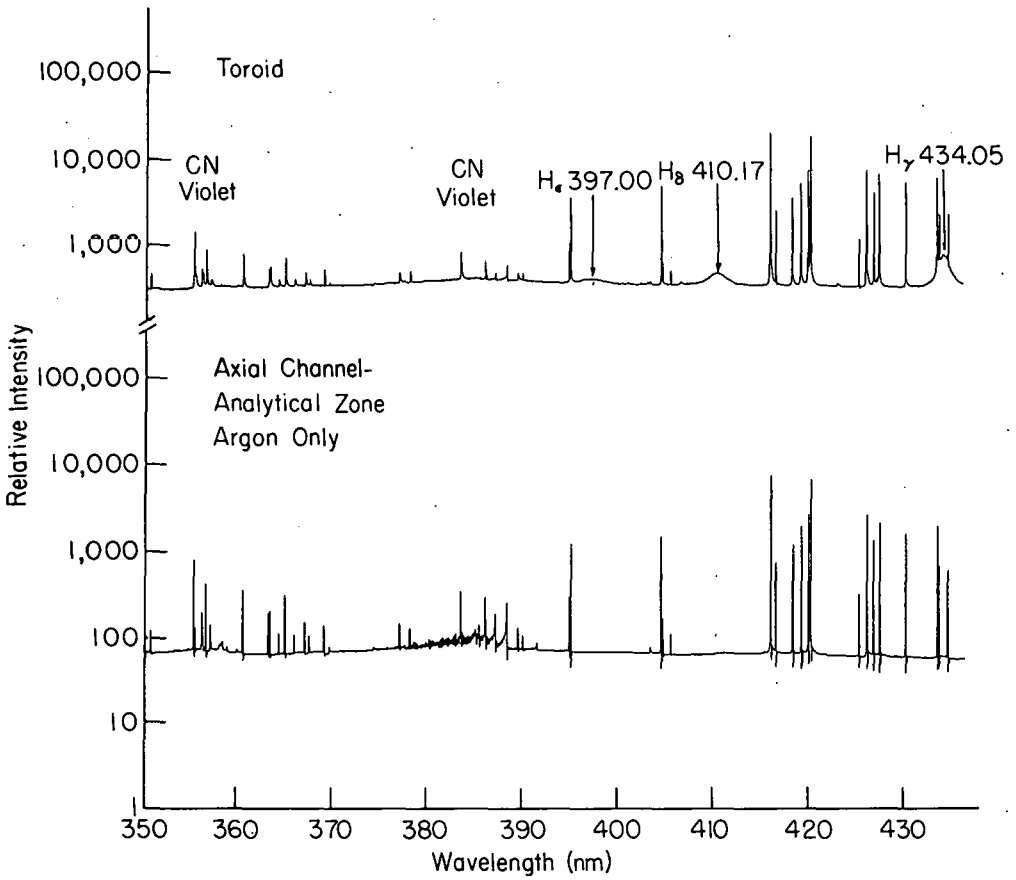

Figure 5. (Continued)

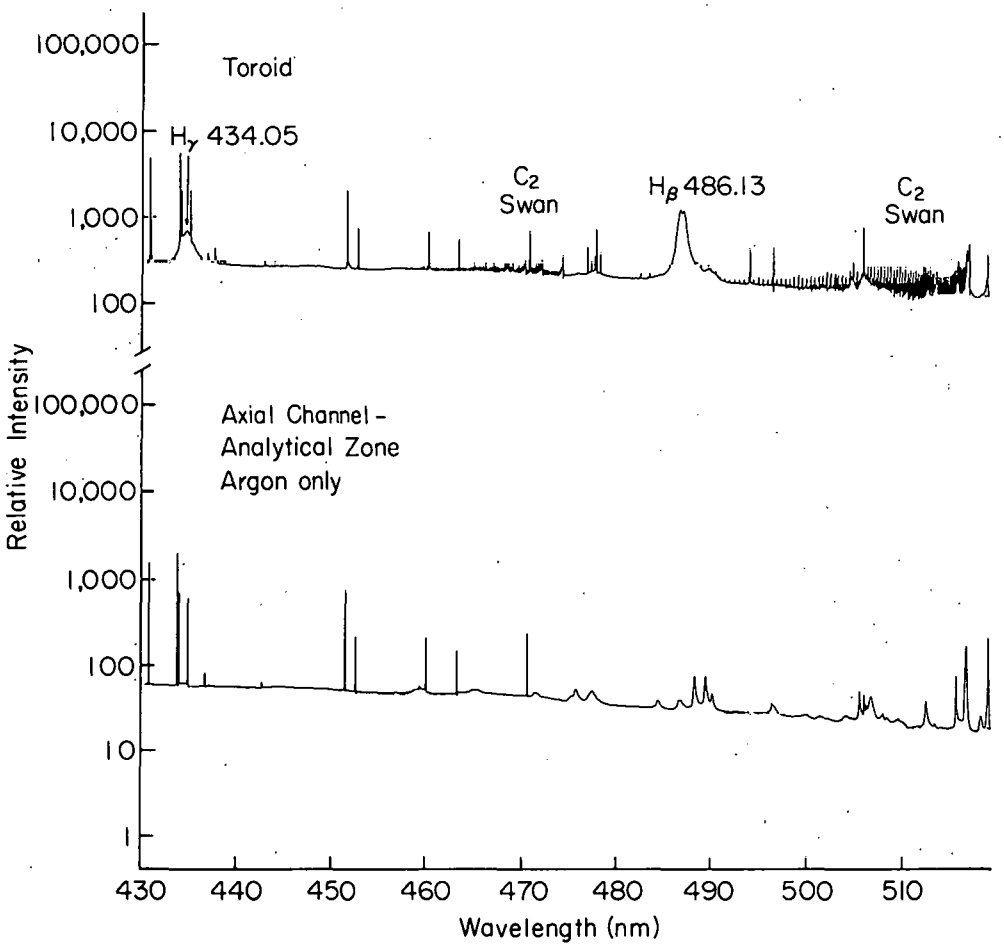

Figure 5. (Continued)

values in the wavelength scans in Figures 4 and 5 are all intercomparable, i.e., a relative intensity of 100 corresponds to the same photocurrent in all scans.

In the toroid region (D in Figure 3), the main spectral features are similar to those of Ar only and include the atomic lines of C, H, and Ar; the carbon and hydrogen species are believed to arise from impurities in the argon. As expected, CN emission is relatively nonexistent in the toroid, but does appear in the other regions. More air is entrained with increased height in the plasma and the intensity of the CN emission increases accordingly, as illustrated in Figure 4, p.28. Emission from C_2 is evident in all four regions. The CO fourth positive system is visible in the 190-230 nm region in the spectra of the tail flame and analytical zone. The continuum emission from the tail flame and the analytical zone is essentially the same in magnitude and remains essentially constant in the wavelength region studied. Low in the axial channel and in the toroid on the other hand, the magnitude of the continuum emission increases with wavelength from 190 nm to 390-400 nm and then begins to decrease. On the low wavelength end, the background emission from the axial channel low in the plasma and from the toroid is approximately a factor of two lower than that from the tail flame and analytical zone. However, at the continuum peak (390-400 nm), the emission from the axial

channel and toroid is approximately one and a half orders of magnitude greater than that from the tail flame and analytical zone. Thus, over most of the wavelength region of interest, the spectral background is much lower at the height normally used for analytical measurements than in the hotter regions low in the axial channel.

The intensity of several analytical lines relative to the background in the analytical zone is illustrated in Figure 6, a wavelength scan of the 190-350 nm region obtained while a 4.5 μg/g 1:10 solution of Conostan D-20 reference sample in MIBK was being nebulized. The conditions were slightly different from those used to obtain the scans in Figures 4 and 5.

Detection limits

The detection limits measured in oil/MIBK (1:10) solutions for the elements studied are given in Table IV. These values represent the concentration of the analyte that will yield an emission intensity three times the standard deviation of the blank signal. This definition is in accordance with IUPAC recommendations (43). It should be emphasized that these detection limits refer to the concentration of the element in the oil before dilution. Thus, the concentration in the aspirated solution is an order of magnitude lower. If the reasonable assumption is made that reliable quantitative measurements require a signal/noise ratio of 10, then the

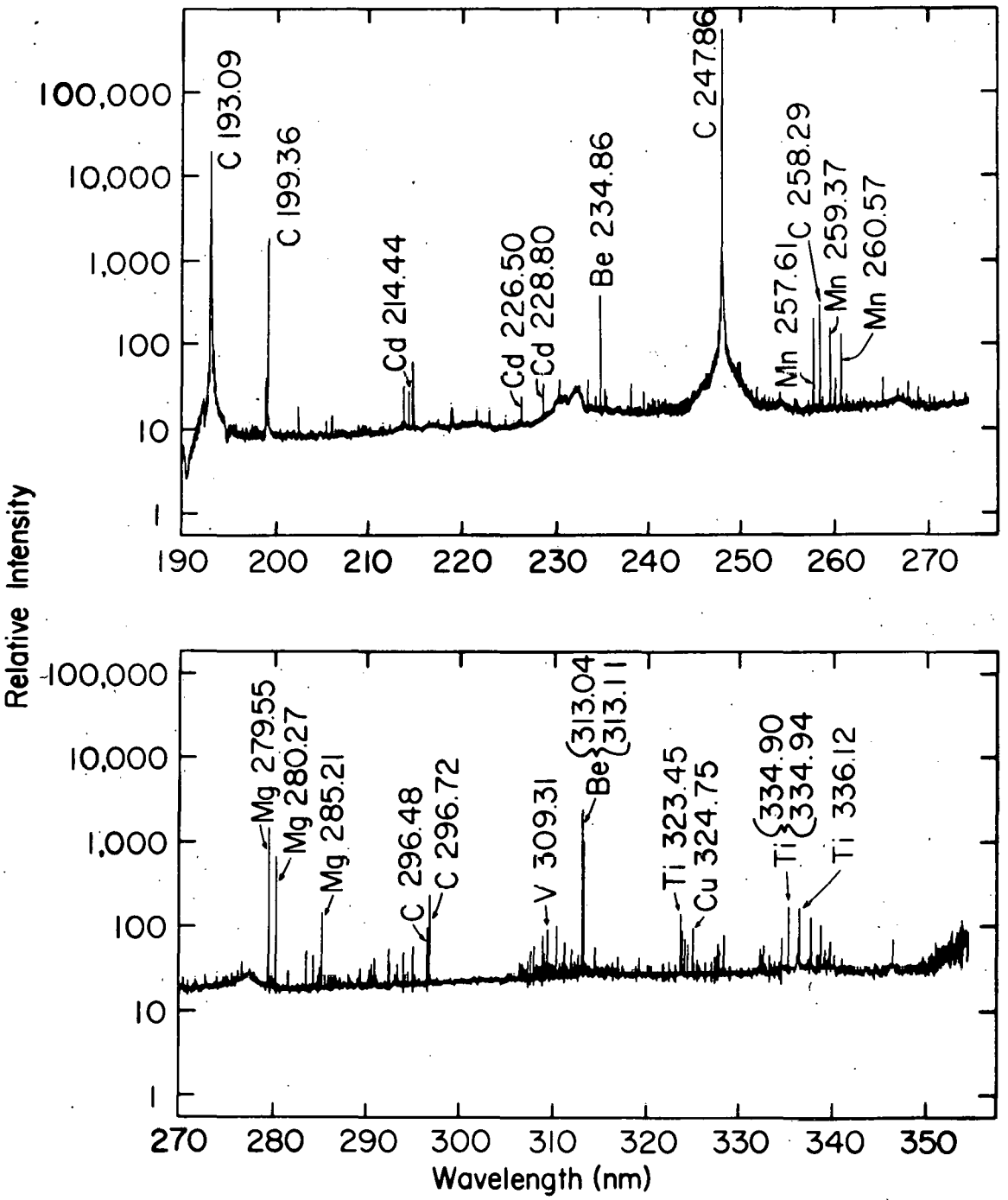

Figure 6. Wavelength scan for the analytical zone from 190.0 to 350.0 nm obtained while a 4.5 µg/g 1:10 solution of Conostan D-20 reference sample in MIBK was being nebulized.

Table IV. Detection limits of elements in oil

Element	Wavelength (nm)	Detection Limit (μg/g of oil)
Ag	328.07	0.02
Al	308.22	0.06
As	234.98[a]	2.
B	249.68	0.2
Ba	233.53	0.03
Be	313.04	0.004
Bi	223.06	0.4
Ca	393.37	0.0006
Cd	226.50	0.09
Co	238.89	0.06
Cr	283.56	0.03
Cu	324.75	0.009
Fe	259.94[a]	0.06
Hg	253.65	0.3
Mg	279.55	0.01
Mn	257.61	0.006
Mo	386.41	4.
Ni	341.48	0.1
P	255.33	9.
Pb	283.31[a]	0.5
Sb	217.59	0.6
Se	196.03	2.
Si	288.16	0.07
Sn	284.00[a]	0.05
Ti	334.94	0.01
V	309.31	0.05
Y	371.03	0.02
Zn	213.86	0.03

[a]For these elements, the 0.5 m Ebert monochromator was used in conjunction with Infotronics CRS80 Digital Readout System (Infotronics, Houston, TX) operated in the linear mode with 8-s signal integration. Detection limits for all other elements were determined with multichannel spectrometer B.

concentration level that would provide this signal (i.e., the lowest determinable concentration) will be ~3 times the detection limit. Detection limits were also determined for some alternate analytical lines that were available on multichannel spectrometer B. These lines and their detection limits are given in Table V. When xylene was used as the diluent, the detection limits generally did not vary by more than a factor of two or three from those obtained when MIBK was used. For toluene as the diluent, the detection limits generally varied randomly within a factor of four or those obtained for MIBK.

Analytical calibration curves

Figures 7 and 8 show a number of analytical calibration curves obtained simultaneously from Conostan D-20 organometallic reference samples when multichannel spectrometer B was used. The data points for these curves represent emission intensities (not intensity ratios) of one 10-second signal averaging interval. It is important to note that the curves are linear with concentration for a minimum of two orders of magnitude, and in the case of chromium, silver, copper and titanium this linearity extends over 4.5 orders of magnitude.

Wear Metals in Lubricating Oil

Table VI shows the analytical results obtained on six low viscosity jet engine oils (labeled A) and six high

Table V. Detection limits of alternate analytical lines available on multichannel spectrometer B

Element	Wavelength (nm)	Detection Limit (µg/g of oil)
Al	396.15	0.1
As	193.76	3.
Cd	228.80	0.1
Co	345.35	0.09
Fe	261.19	0.1
Mn	403.08	0.4
Ni	351.51	1.
Pb	405.78	2.
Sb	206.84	2.
Sn	303.41	1.
V	311.07	0.09
Y	242.2	0.2
Zn	202.55	1.

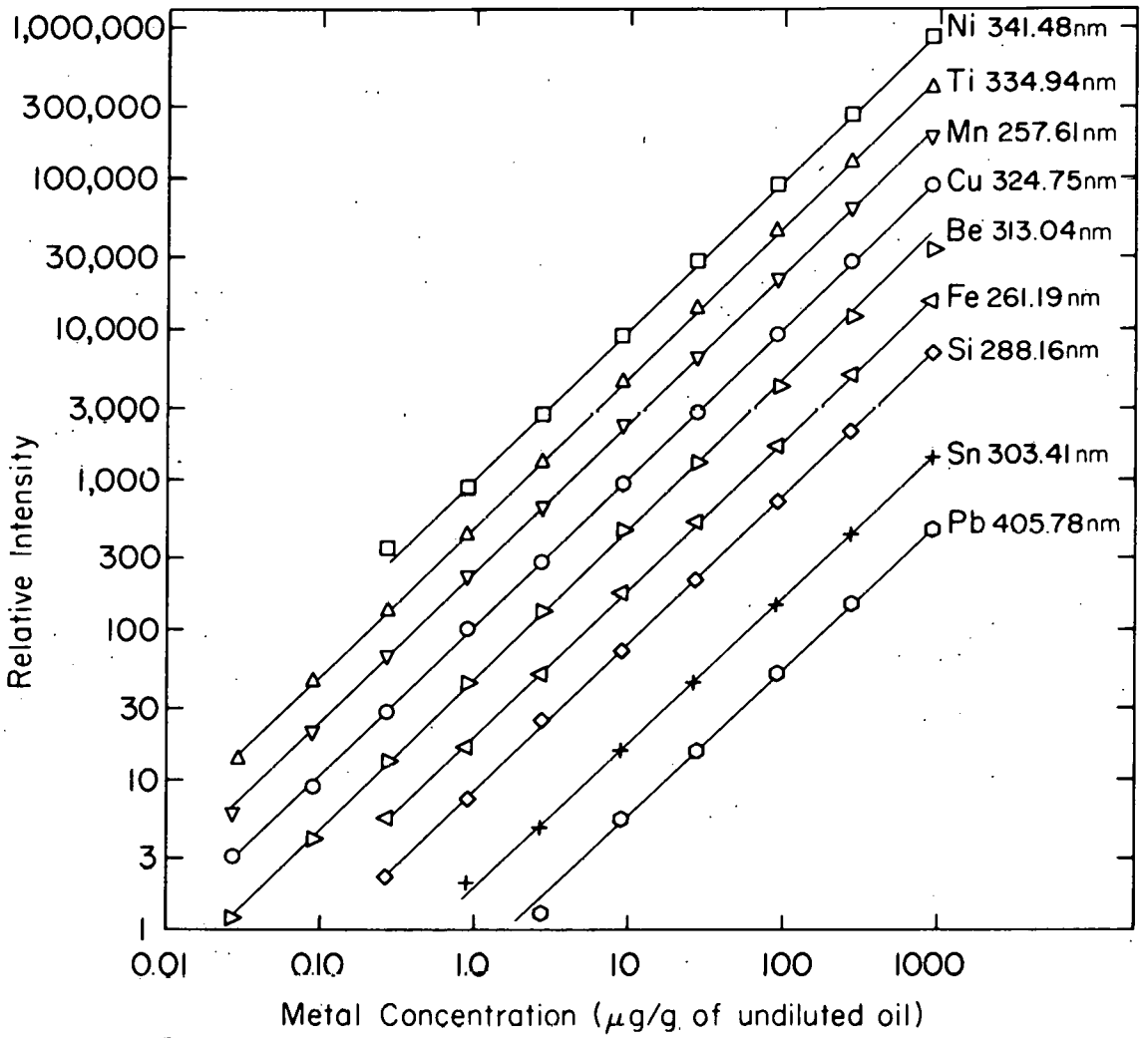

Figure 7. Sample analytical calibration curves.

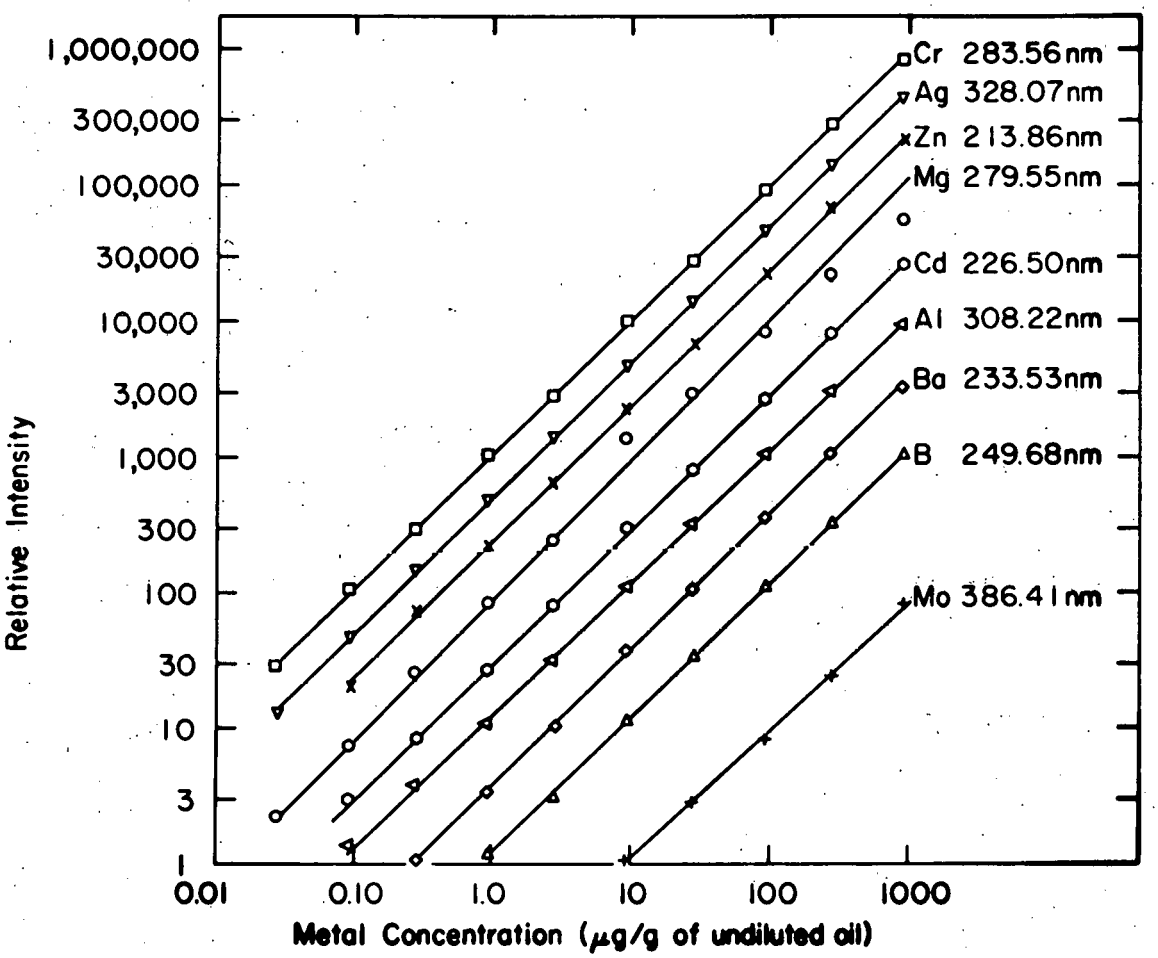

Figure 8. Sample analytical calibration curves.

Table VI. Comparison of results with USAF correlation program

Sample	Cr(μg/g) This Work[b]	Cr Rel. Std. Dev. (%)	Cr AF[c]	Fe(μg/g)[a] This Work	Fe Rel. Std. Dev. (%)	Fe AF
71-10A[d]	1.8±0.1	7.2	1.6±0.5	21.2±0.5	2.3	20.7±4.0
71-12A	4.3±0.2	4.0	3.1±1.3	18.7±0.5	2.6	18.9±5.0
72-1A	2.4±0.1	5.6	2.4±0.8	17.7±0.6	3.5	18.6±4.6
72-2A	3.5±0.1	3.3	2.9±1.1	12.6±0.3	2.7	14.1±3.4
72-3A	3.2±0.1	4.5	2.5±1.4	13.7±0.4	2.6	16.6±5.4
73-1A	1.2±0.1	8.3	1.1±0.4	31.8±1.1	3.5	31.8±6.5
71-10B[e]	5.1±0.2	4.3	3.0±0.9	29.2±0.9	3.1	22.1±2.9
71-12B	4.7±0.2	4.4	3.4±1.1	22.7±0.8	3.5	19.7±3.8
72-1B	4.0±0.2	5.7	2.5±0.9	25.8±0.9	3.3	18.8±2.8
72-2B	7.5±0.2	2.8	6.3±1.4	14.7±0.4	3.0	13.7±2.8
72-3B[f]	37.7±1.4	3.8	25.2±6.6	18.9±0.4	2.1	16.6±2.3
73-1B	3.2±0.2	5.6	1.9±0.8	46.0±1.4	3.1	29.2±6.1

Sample	Mg(μg/g)			Cu(μg/g)		
71-10A[d]	2.0±0.1	4.4	2.5±0.6	7.8±0.2	2.4	8.1±0.7
71-12A	6.1±0.2	2.7	5.7±1.6	3.3±0.2	6.0	3.5±0.6
72-1A	3.0±0.1	3.5	3.5±0.6	6.5±0.2	3.5	7.2±0.8
72-2A	4.8±0.2	3.2	5.2±1.5	2.9±0.2	5.6	3.4±1.2
72-3A	4.6±0.1	2.5	5.4±2.4	2.4±0.2	7.3	3.1±1.5
73-1A	2.2±0.1	4.5	2.7±0.5	3.6±0.2	5.9	3.9±0.4
71-10B[e]	2.9±0.2	5.6	2.9±0.7	8.6±0.2	2.2	8.5±0.9
71-12B	2.9±0.2	6.1	2.8±0.5	7.9±0.2	1.9	8.0±1.3
72-1B	2.1±0.1	6.3	1.8±0.9	8.0±0.2	2.5	7.4±0.7
72-2B	6.1±0.2	4.0	5.9±1.1	8.3±0.2	1.9	8.6±0.9
72-3B[f]	1.3±0.1	5.4	1.3±0.4	4.6±0.2	3.5	5.1±0.7
73-1B	1.9±0.1	7.0	1.9±0.4	7.7±0.3	3.4	7.8±0.9

	Ag(μg/g)			Al(μg/g)[g]		
Sample	This Work[b]	Rel. Std. Dev. (%)	AF[c]	This Work	Rel. Std. Dev. (%)	AF
71-10A[d]	0.4±0.1	34.4	0.48±.15	1.4±0.3	18.0	1.6±0.6
71-12A	0.7±0.1	20.8	0.82±.19	1.1±0.2	21.4	1.8±1.2
72-1A	0.5±0.1	26.7	0.7±0.3	1.6±0.2	14.5	2.1±1.3
72-2A	0.4±0.1	32.3	0.5±0.3	1.6±0.3	17.8	2.2±0.8
72-3A	0.5±0.1	18.7	0.7±0.6	0.9±0.3	32.5	1.1±0.8
73-1A	0.6±0.1	18.3	0.7±0.3	<0.7	--	0.8±0.6
71-10B[e]	1.8±0.1	7.2	1.9±1.0	10.3±0.5	4.4	9.2±2.5
71-12B	1.8±0.1	5.6	2.0±0.5	8.2±0.4	5.1	7.7±1.8
72-1B	1.4±0.1	9.5	1.3±0.3	9.0±0.4	4.4	7.9±1.5
72-2B	5.5±0.2	2.9	5.5±0.6	9.8±0.7	7.2	8.5±1.7
72-3B[f]	n.d.		0.1±0.1	6.2±0.4	6.4	5.1±1.6
73-1B	2.0±0.1	6.2	2.0±0.5	14.9±0.7	4.9	13.4±3.0

[a]Determined with the Fe 261.1 nm line programmed on multichannel spectrometer A.

[b]Mean values, standard deviations and relative standard deviations are determined from analyses repeated on ten different days.

[c]AF-U.S. Air Force mean values and standard deviations are derived from atomic absorption determinations by the laboratories participating in SOAP.

[d]A samples are jet engine oils.

[e]B samples are reciprocating engine oils.

[f]In this sample, a thin film formed on the bottom of the volumetric flask which would not go into suspension with shaking.

[g]These determinations were performed using plasma power supply 2 with the 0.5 monochromator and a strip chart recorder rather than integrating the signal.

viscosity reciprocating engine oils (labeled B) supplied by the USAF-SOAP. All of these results, except the Al determinations, were obtained simultaneously with multichannel spectrometer A and plasma power supply 1. The Al determinations were performed with plasma power supply 2 and the 0.5 m spectrometer. In this instance, peak height measurements on strip chart recordings were related to concentration levels. Because viscosity effects were shown to be negligible (33), a single set of reference solutions sufficed for both the jet engine oils and reciprocating engine oils. It is seen that all concentration values determined for the jet engine oils ranged within one standard deviation of the USAF mean which was derived from atomic absorption analyses performed by the laboratories participating in SOAP. For the reciprocating engine oils, significantly higher values were obtained for Cr and Fe by the plasma emission technique. The reciprocating engine oil samples were visually "dirty" and sedimentation of particulate matter was observed after prolonged standing. The important subject of the effect of particulate matter on the analytical results for these sample types will be discussed in the next section.

Metal Particles in Oil

Introduction

It is well known that actual used lubricating oils may contain suspended microscopic or submicroscopic particles,

indicative of gradual wear or erosion, or larger macroscopic particles, indicative of rapid failure of an oil wetted part. The tacit assumption is generally made that the atomizing source, i.e., the spark discharge or flame, will possess the same atomizing efficiency for particles and for dissolved, oil-soluble organometallic compounds from which reference samples have generally been prepared. Unfortunately, definitive data justifying these assumptions do not exist. There have, in fact, been repeated literature reports that these assumptions are invalid. As early as 1965, Means and Ratcliffe (44) and Burrows, et al. (45) called attention to the fact that low atomic absorption (AAS) results were likely to result if samples contained appreciable sludge or sufficiently large particles. One year later, Slavin and Slavin (46), though admitting too few samples were run to draw positive conclusions, noted that their results indicated "that the actual metal content of the used oils is often somewhat greater than is shown by direct atomic absorption, and much greater than is shown by emission methods. This would indicate that the direct atomic absorption method does not reduce quite all of the metal particles to an atomic vapor, while emission reduces an even smaller fraction to vapor." A series of four papers published in 1970 called further attention to this problem. Bartels and Slater (47) showed that iron metal particles in the 1.2 to 3 μm range were

detectable by both the standard AAS and optical emission (OES) techniques, but that the actual "recoveries" ranged from only 1 to 4% for AAS and from 10 to 28% by OES. In another paper from the same laboratory, Kriss and Bartels (48) reported that the "recovery" of iron particles was enhanced considerably if the solvent was changed from pure MIBK to acidified MIBK. The third paper in the 1970 series, consisted of a report by Kahn et al. (49) on the AAS determination of the Cr and Fe content of twenty used lubricating oils. Kahn et al. consistently found higher results in the hotter, lean air-C_2H_2 and N_2O-C_2H_2 flames than in the cooler normal air-C_2H_2 flame, suggesting a higher degree of atomization of these elements in the hotter flames. These investigators concluded that "if the problem of recoveries is considered important, considerably more work remains to be done before it is successfully solved." The fourth 1970 paper paid considerable attention to the presence of airborne silicon species in the lubricating oil (50). Although Jackson et al. concluded that the total silicon present in railway diesel oil as silicone, silica, or silicates can be determined satisfactorily by AAS, it is worth noting that the silicon contents of one sample run ten times by AAS and OES for reproducibility assessment purposes differed by over a factor of two, with the OES values showing the higher results.

That the metal particle problem is destined to remain live for some time is evidenced by the succession of papers appearing at regular intervals in recent years. Taylor, Bartels, and Crump's study (51) supported the view that if particulate matter is present, the efficiency of atomization of the total metal content of used oils in the flame is dependent on the particle size. According to Taylor et al. and Golden (52), the size of actual wear particles is typically <10 μm in diameter, but most often less than 1.5 μm in diameter. Golden also supported the earlier observations of Kriss and Bartels (48) that AAS results obtained when an acidified solvent is used are higher than those obtained with the neutral diluent or by the OES method. Reeves et al. (53) have noted that "further work (on the effect of temperature and chemical environment on the atomization of particles of different sizes) is needed to provide an understanding of the mechanism of gaseous atom production from metal and alloy particles." Thus it is apparent that the particle problem is recognized by an increasing number of analysts.

Wear metal particles in oil

Plasma emission-MIBK diluent vs. atomic absorption-acidified diluent As mentioned above, one method that has been utilized to minimize the particle problem is the use of an acidified diluent. It is presumed that the acid dissolves

at least a portion of the particles. In a procedure developed at Pratt & Whitney Aircraft by Robert Morgan, the sample is diluted with an acid-alcohol-MIBK mixture and analyzed by atomic absorption (54). Quantitative results obtained with this procedure are compared with ICP results in Table VII. Simple dilution with MIBK was used for preparing the sample for ICP analysis. In most cases the agreement between ICP and AAS results was as good as the agreement between duplicate AAS results. In those cases where there was disagreement, neither the AAS values nor the ICP values were consistently high. The poor reproducibility exhibited by the AAS results may have been due to sampling difficulties. The ICP results were obtained with one aliquot of sample, i.e. duplicate dilutions were not made.

In a recently reported atomic absorption procedure for determining titanium in aircraft lubricating oils, a small amount of an acid mixture (HF/HCl) was added to an MIBK-diluted oil sample, after which the sample was shaken for 10 s and then analyzed (55). Analytical results obtained for several used aircraft lubricating oil samples by this atomic absorption method with both titanium powder (325 mesh) and Conostan organometallic titanium used as the reference samples are shown in Table VIII. These results agree well with the ICP results also given in the table.

In neither of these studies were the ICP results con-

Table VII. Pratt & Whitney Aircraft samples[a] (μg/g of oil)

Sample	Mg	Fe		Cr	
	This work[b]	This work	P&WA,FRDC[c]	This work	P&WA,FRDC
A-847	0.07	1.7	2.3, 1.6	0.7	<1.0,<1.0
A-849	0.08	1.9	2.2, 2.0	0.9	<1.0,<1.0
A-854[d]	0.08	4.8	4.2, 5.0	1.5	1.4, 1.1
A-858[d]	0.08	5.0	4.7, 5.1	1.2	1.1, 1.3
A-867[d]	0.05	6.5	5.6, 7.0	1.8	2.0, 1.4
C-239[d]	0.12	0.6	2.0, 2.9	<0.1[e]	<1.0, 1.0
A-903[d]	0.10	31	23.2,20.4	2.6	2.5, 1.9
A-935	0.20	2.0	3.0, 2.3	0.9	1.0, 1.1
A-979	0.09	0.6	<1.0, 1.0	0.2	<1.0,<1.0
A-1079	0.08	1.5	1.9, 1.7	0.4	<1.0,<1.0
A-1083	0.10	1.8	1.9, 2.1	0.6	1.0, 1.0
A-1091	0.12	1.7	1.8, 2.1	0.4	1.0,<1.0
A-1094	0.80	4.1	4.2, 4.5	0.8	1.0, 1.0
A-1095[d]	0.41	4.5	5.4, 5.5	0.8	1.0, 1.0
A-1096[d]	0.40	190	840, >1000	20	6.5, 7.7

[a]Samples supplied by J. Y. Marks, Pratt & Whitney Aircraft, East Hartford, CT.

[b]Multichannel spectrometer B and plasma power supply 2 were used with Conostan D-12 reference solutions.

[c]Sample analyzed at Pratt & Whitney Aircraft, Florida Research and Development Center using a mixed solvent acidification procedure and atomic absorption spectrometry.

[d]Samples contained a sediment.

[e]Values designated < for this work represent concentrations less than the lowest determinable concentration (see p.38) on the day of analysis.

Table VII. (Continued)

Sample	Sn	Ti		Al	
	This work[b]	This work	P&WA,FRDC[c]	This work	P&WA,FRDC
A-847	<0.5[e]	1.6	1.2	0.7	<1.0,<1.0
A-849	<0.5	1.8	<1.0	0.8	<1.0,<1.0
A-854[d]	54	0.2	---	0.6	---,<1.0
A-858	<0.5	0.3	<1.0	0.8	1.2,<1.0
A-867[d]	42	0.2	---	0.4	---,<1.0
C-239	<0.5	0.2	<1.0	2.4	7.5,10.0
A-903[d]	58	0.3	---	1.0	---,<1.0
A-935	<0.5	0.4	<1.0	0.8	<1.0,<1.0
A-979	<0.5	<0.1	<1.0,<2.0	<0.4	<1.0,<1.0
A-1079	<0.5	1.3	<1.0, 2.3	0.5	<1.0,<1.0
A-1083	<0.5	1.8	1.6,<2.0	0.7	<1.0,<1.0
A-1091	<0.5	1.8	2.0, 2.0	0.5	<1.0,<1.0
A-1094	<0.5	6.3	4.9, 5.6	0.6	<1.0,<1.0
A-1095	<0.5	6.5	7.1, 7.9	0.8	<1.0,<1.0
A-1096[d]	3.6	16	12.0,12.3	2.7	<1.0, 2.8

Table VII. (Continued)

Sample	Cu		Ag	
	This work[b]	P&WA,FRDC[c]	This work	P&WA,FRDC
A-847	<0.05[e]		<0.1	<0.5,<0.5
A-849	<0.05		<0.1	<0.5,<0.5
A-854[d]	0.12	0.1	0.2	<0.5, 1.0
A-858	<0.05		0.1	<0.5, 1.0
A-867[d]	0.23	<0.1	0.3	<0.5, 1.0
C-239	0.14		<0.1	<0.5, 1.0
A-903[d]	0.24	0.3	0.5	0.7, 1.0
A-935	0.14		0.2	<0.5, 0.6
A-979	0.6		0.1	<0.5,<0.5
A-1079	<0.05		0.2	<0.5,<0.5
A-1083	0.071		0.3	<0.5,<0.5
A-1091	0.6		0.2	<0.5,<0.5
A-1094	0.7		0.3	<0.5,<0.5
A-1095	0.7		0.3	<0.5,<0.5
A-1096[d]	0.59		15	13.6,14.3

Table VIII. Comparison of Ti analytical data

Sample[a]	Analytical Results (μg Ti/g of oil) ICP-AES[b]	Atomic Absorption[c] Ti Powder[d]	Organometallic[e]
Dover #1	1.5	1.6	1.4
Dover #2	1.5	1.8	1.6
Dover #3	2.7	3.2	2.8
Dover #4	1.4	1.4	1.1
Dover #5	5.7	5.5	4.6
Dover #6	4.9	5.1	4.4
TF-39 #1[f]	17	20.2	19.5
McConnell #1	4.3	4.9	4.2

[a]Samples supplied by K. J. Eisentraut, Wright-Patterson Air Force Base, OH.

[b]Multichannel spectrometer B and plasma power supply 2 were used with Conostan D-12 reference solutions.

[c]These analyses were performed by C. S. Saba and K. J. Eisentraut, Wright-Patterson Air Force Base, OH (55).

[d]325 mesh titanium powder in oil used as the reference sample.

[e]Conostan organometallic titanium used as the reference sample.

[f]This sample is labeled Kelly No.1 in reference 55.

sistently low relative to results obtained by the AAS procedure for which the acidified diluent was used. This would indicate that a particle problem did not exist in the ICP procedure for the samples examined.

Chemical oxidation vs. dilution A method of circumventing the potential particle problem is to destroy the organic matrix by chemical oxidation and determine the metal content of the resulting aqueous solution. If aqueous reference samples are used, the metals in samples and reference samples are in the same chemical form. Chemical oxidation of three used lubricating oils was accomplished by the procedure described in Chapter II (p.23) and the resultant solutions were analyzed against the aqueous standards described on p.23. Multichannel spectrometer B and plasma power supply 3 were used. The results of this analysis are compared with results obtained by the MIBK dilution technique in Table IX. In general, the results obtained by the two methods are in agreement. The chemical oxidation values for chromium have been corrected to account for contamination by the perchloric acid, which was found to contain ~0.3 μg Cr/ml. As mentioned in Chapter II, the aqueous reference solutions and blank were prepared to contain an acid concentration approximately equal to the final acid concentration of the samples. In this way, differences in nebulization caused by variation in acid concentration (40) were avoided. During

Table IX. Comparison of chemical oxidation and dilution

Sample	Mg(μg/g)		Fe(μg/g)		Cr(μg/g)	
	Oxidation[a]	Dilution[b]	Oxidation	Dilution	Oxidation[c]	Dilution
72-2B[d]	5.5, 5.4	6.1	14,14	14.7	6.9,5.0	7.5
A-854[e]	<0.1,<0.1	0.077	4.1,4.3	4.8	1.3,1.5	1.5
A-867[e]	<0.1,<0.1	0.053	6.0,6.5	6.5	1.8,1.5	1.8

Sample	Ni(μg/g)		Al(μg/g)		Ti(μg/g)	
72-2B[d]			8.9, 9.4	9.8		
A-854[e]	2.4, 2.4	2.2	<1.1,<1.4	0.63	0.20,<0.2	0.19
A-867[e]	3.2, 2.8	2.1	<1.2,<1.1	0.41	0.27, 0.21	0.20

Sample	Cu(μg/g)	
72-2B[d]	8.4, 8.4	8.3
A-854[e]	0.19,0.29	0.12
A-867[e]	0.31,0.37	0.23

[a]Sample prepared by chemical oxidation technique described in Chapter II.

[b]Sample prepared by diluting 1:10 with MIBK as described in Chapter II.

[c]The perchloric acid used in the oxidation contained chromium contaminant. To correct for this contamination, 1.5 μg/g was subtracted from the measured values. The corrected values are given above. See text for more complete explanation.

[d]Sample supplied by U.S. Air Force (see Table XI). Sample was "dirty" and contained a sediment.

[e]Sample supplied by Pratt and Whitney Aircraft (see Table VII). Sample contained a sediment.

the wet oxidation of the samples, approximately half of the perchloric acid was consumed. Thus, in order for the final acid concentrations to be equal, twice as much acid was used to prepare the samples as was used to prepare the reference solutions and blank. This difference in the amount of acid used would account for ~1.5 μg of chromium, the amount subtracted from the measured values to obtain the values in Table IX. The reason for the large discrepancy in chromium values between the two 72-2B oxidation samples has not been determined.

Behavior of synthetic suspensions of iron particles in oil

Even though the results of the last section indicate that the presence of particles is not a problem in the analysis of the used oil samples examined, no conclusions can be drawn concerning larger metal particles. A series of experiments were conducted to determine the analytical behavior of larger iron particles in oil in the ICP system.

Particle decomposition and vaporization behavior in various plasmas have been examined by others. Theoretical analyses of heat transfer to particles, particle decomposition, and vaporization have been given for plasma jets (56,57), radio-frequency augmented flames (58), and inductively coupled plasmas (59). A discussion of this subject can be found in the Appendix. Barnes and Schleicher (60) predicted the

decomposition of Al_2O_3 particles with height in an ICP. Borgianni et al. (59) measured the decomposition of CuO, TiO_2, NiO and Al_2O_3 particles as a function of distance traveled in an argon ICP, while Capitelli et al. (61) studied the decomposition of Al_2O_3 particles injected into argon-nitrogen ICPs containing 0, 4, and 8% N_2. None of these authors used a plasma configuration similar to the one used in the present investigation, i.e., a toroidal ICP with tangential plasma argon introduction. In addition, these analyses considered the particle behavior only from the time the particle entered the plasma.

Experimental equipment and sample preparation Oil samples were prepared containing -325 mesh iron particles which had a mean diameter of approximately 3.0 μm according to the manufacturer (CERAC Corp., Butler, WI). As can be seen in Figure 9, however, the particles included agglomerates as well as spheres and covered a size range from less than 0.5 μm in diameter to greater than 4.0 μm. (Attempts to determine the size range of wear metal particles for comparison were unsuccessful.) The particle-containing oil samples were diluted with MIBK as before.

Plasma power supply 1 was used to obtain the data summarized in Table X and Figure 10, whereas plasma power supply 2 was used to obtain the data summarized in Figure 11 and Tables XI and XII.

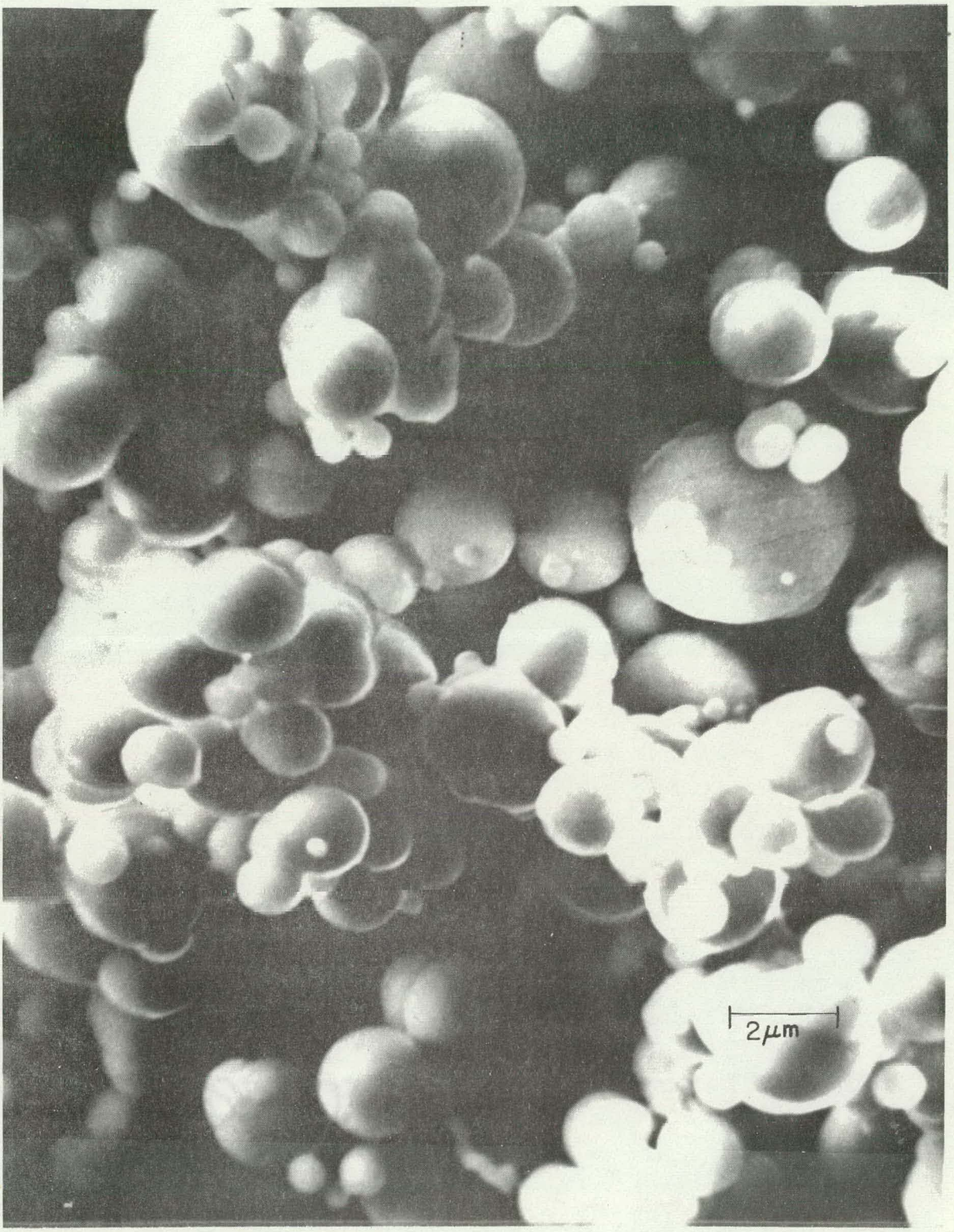

Figure 9. Iron used to prepare samples. Photomicrograph taken at 3750X magnification.

Results and discussion As can be seen in Figure 10, the noise level for the iron particle suspensions is high and the recovery is roughly 10-20 percent. To determine if the high noise level was due to continuum emission from the particles, the 0.5 m Ebert spectrometer was set at ~259.84 nm, a wavelength displacement approximately 0.1 nm from the 259.94 nm Fe line, and the particle suspensions were nebulized into the plasma. Compared to a Conostan blank solution and a 10 μg/g organometallic iron solution, there was no significant increase in either the signal or the noise levels observed when particle suspensions were nebulized. Thus, the high noise level could not have been due to continuum emission from the particles. Although the recovery for the particle suspensions was low, the values compared very favorably with AAS results obtained by Bartels and Slater (47) for "3.0 μm" particles (0.7 to 1.9%) and were within the range of their OES values (10 to 28%).

Loss of particles from suspension A number of factors could have influenced the low recovery of the particle suspensions and several of these were investigated. It was noticed that when particle suspensions were left undisturbed, particle deposits became visible on the bottom of the flasks. This observation raised concern over the extent of settling during the relatively short period needed to aspirate the sample. A simple experiment was conducted in which the

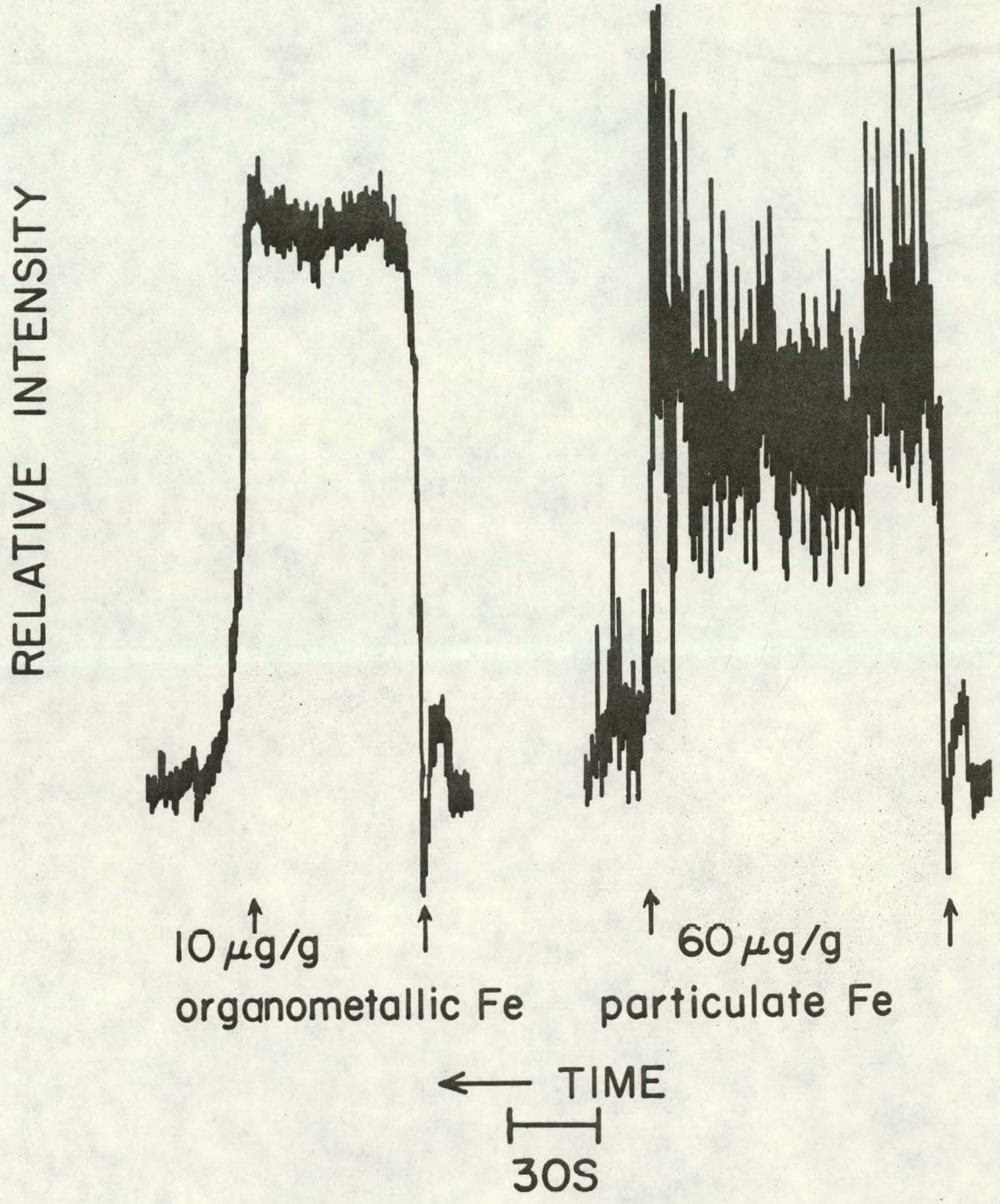

Figure 10. Noise of a particle containing solution relative to an organometallic reference solution. Arrows indicate when uptake tube was changed from blank to sample or from sample to blank.

nebulizer uptake tube was positioned near the top and near the bottom of the sample flask. Increased recovery when sampling lower in the flask, as shown in Table X, indicated particle buildup due to settling.

Table X. Effect of position of uptake tube

Particulate Iron added (μg/g)	Iron Found (μg/g)		% Recovery	
	Top[a]	Bottom[a]	Top[a]	Bottom[a]
21	2.3	3.1	11	15
60	5.5	6.3	9.2	11

[a]Refers to uptake tube being near the top or bottom of the flask.

Obviously, because of the noise associated with the sample signal there is a substantial uncertainty on an absolute basis in the values given in Table X as well as Tables XI and XII presented below. However, these values can be used to establish differences in recovery under various conditions.

During the course of this study, the nebulizer uptake tube was shortened from 81 to 42 cm. When this was done, the clean out time, i.e., the time required for the analytical signal to return to the base line value after the uptake tube was switched to the blank, was shortened for the particle suspensions and the recovery improved markedly. These changes are illustrated in Figure 11. This suggested that the particles were forming a deposit in the long tube as well as

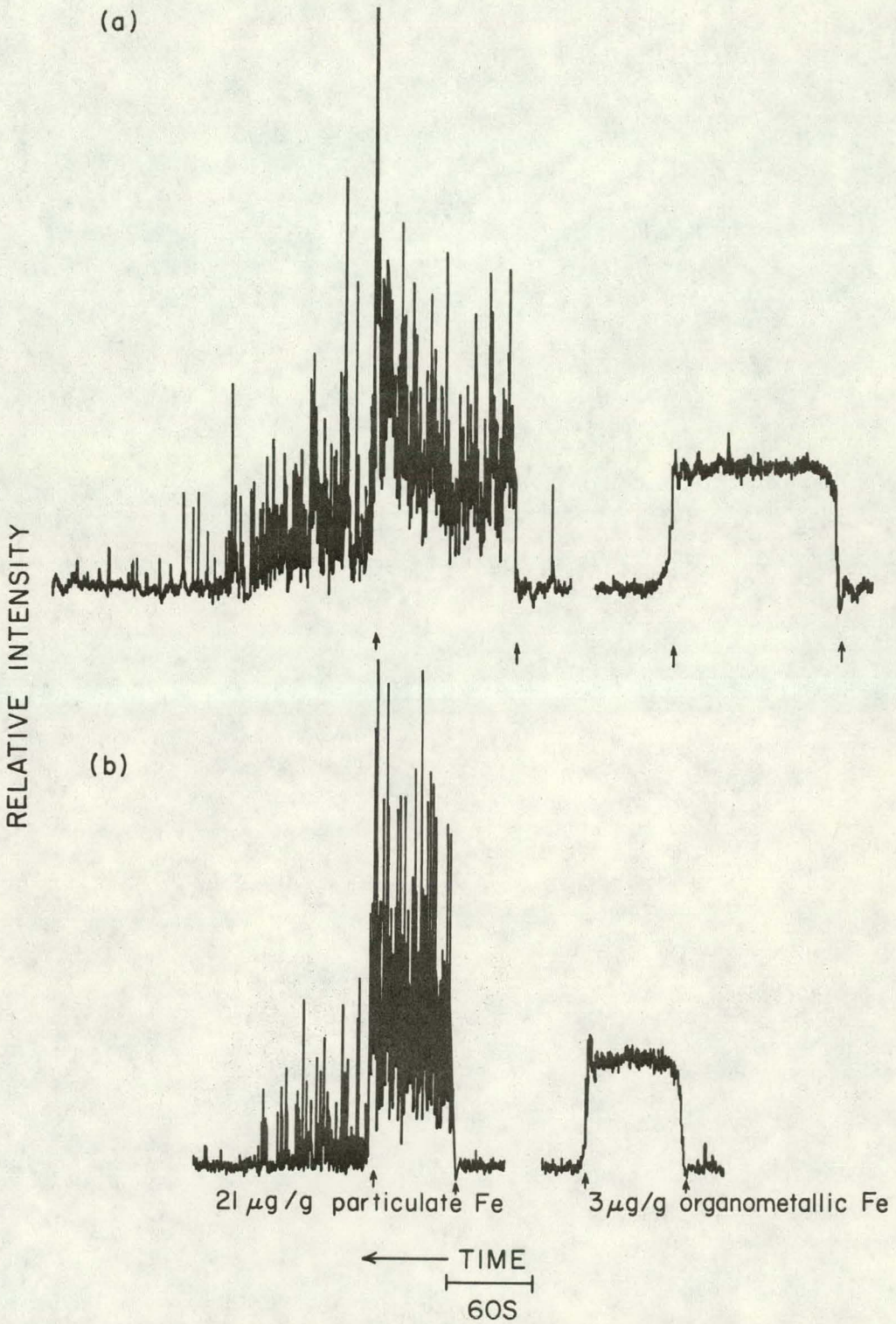

Figure 11. Effect of length of uptake tube; (a) 81 cm uptake tube, (b) 42 cm uptake tube. Arrows indicate when uptake tube was changed from blank to sample or from sample to blank.

in the solution flask.

Particle settling, though significant, could not by itself account for the overall low recovery observed for particle suspensions.

Loss of particles in spray chamber Taylor et al. (51) reported the efficiency of nebulization, ε_n, i.e., the ratio of the amount of analyte entering the flame (or plasma) to the amount of analyte aspirated (62), in their apparatus was less for "3.0 μm" iron particle suspensions (ε_n = 0.078) than for organometallic solutions (ε_n = 0.313). Willis (63) came to similar conclusions for mineral suspensions and aqueous solutions. It was reasonable to expect that similar results would be obtained with the apparatus and suspensions used in the present investigation. The efficiency of nebulization for the iron particle suspensions and for organometallic solutions was determined by nebulizing 25 ml of solution (or suspension) with a normal aerosol carrier gas flow of ~1 ℓ/min. The aerosol emanating from the plasma torch was directed via polyvinylchloride tubing to an impinger set in a cold bath of toluene to which had been added sufficient liquid nitrogen to form a slush. Five milliliter aliquots of the stock organometallic solution and the stock particle suspension were collected so that the concentration of iron in the solution (or suspension) before

nebulization could be determined. After 25 ml of the particle suspension were nebulized, 7 ml of the original 32 ml remained in the graduate; the 7 ml aliquot was also treated as a sample. As suggested by Milner (4), 5 ml of concentrated H_2SO_4 were added to each sample and the mixture was then slowly heated on a hot plate until only a dry carbonaceous ash remained. The samples were then placed in a muffle furnace at 500°C until the carbon was completely oxidized. The residue was dissolved in 5 ml of redistilled HCl and diluted to 25 ml with deionized water. These solutions were then analyzed (with multichannel spectrometer B and plasma power supply 4). The reference solutions and the blank contained 20% by volume of HCl.

Nebulization efficiencies of 0.024 and 0.020 were found for organometallic solutions and particle suspensions, respectively. Consequently, for the ratio ε_n (particles)/ε_n (organometallic) a value of 0.83 was obtained. This ratio indicated that another significant reason for the low recovery obtained for particle suspensions was loss of particles in the spray chamber.

The preceding values are even somewhat optimistic. Because of the length of time required to nebulize 25 ml (~25 min), extensive settling of the particles occurred in the suspension. From the concentration of iron in the stock suspension (as determined from the 5 ml aliquot), it was

calculated that 1600 μg of iron were contained in 32 ml of suspension in the graduated cylinder. After nebulizing 25 ml, 1200 μg of iron were found to be in the 7 ml that remained. Thus, after nebulizing more than 3/4 of the suspension volume, 3/4 of the particles remained. It is reasonable to assume that the larger particles settled out of suspension faster than the smaller ones. Therefore, the ε_n determined for the particle suspension would be weighted in favor of the ε_n of the smaller particles because they remained suspended longer. Because aerosol droplets containing smaller particles would probably weigh less than droplets containing larger particles, it is reasonable to assume that the ε_n for smaller particles would be greater than the ε_n for larger particles. Thus, the value given above for the ε_n of the particle suspension is probably greater than the true value. In that case, the loss of particles in the spray chamber would also have been greater.

Incomplete particle vaporization It was, of course, also possible that the particles were not completely vaporized at the height of observation. The longer an imcompletely vaporized particle experiences the high temperature environment of the plasma, the more complete should be its vaporization (see the Appendix). Thus, for incompletely vaporized particles greater percentage recovery should be observed at increasing heights in the plasma. To test for

incomplete vaporization, the particle suspensions were analyzed at several observation heights after organometallic reference solutions had been used to establish analytical calibration curves at these heights. The results of this study, summarized in Table XI, indicate that there was, indeed, incomplete vaporization of the particles studied at the height used for most analytical observations (20 mm).

Table XI. Effect of observation height on recovery

Concentration added (μg/g)	Concentration Found (μg/g)					
	20 mm[a]	25 mm	30 mm	35 mm	40 mm	45 mm
21	2.9	3.7	3.5	4.2	4.7	_[b]
60	8.9	9.0	8.3	10.5	10.9	10.2

[a]Refers to height above the load coil.

[b]For this suspension at 45 mm the signal wandered from a signal level corresponding to 3.8 μg/g to a signal level corresponding to 7.7 μg/g.

Since the recovery vs. height study indicated incomplete vaporization of the particles, several parameters which might influence the vaporization process were studied. Temperature measurements of the ICP at two power levels had shown an increase in temperature with power (64). Although particle vaporization would be expected to vary with temperature, variation of the forward power did not yield a definite trend as the results summarized in Table XII show.

Table XII. Effect of forward power on recovery

Concentration added (μg/g)	Concentration Found (μg/g) 1700 W	1800 W	1900 W	2000 W	2100 W	2200 W
21	5.9	6.4	6.3	5.8	6.9	5.9
60	16	14	14	15	14	14

The effect of extending the outer tube of the plasma torch was also examined. Extension of the tube should lengthen the high temperature zones by inhibiting air entrainment and subsequent cooling. Although it appeared that recovery decreased rather than increased as extensions of 1.0, 2.0, and 2.5 cm were added, no definite trend could be established because the noise level for the particle suspensions increased considerably as the extension height increased.

Summary Several factors contributed to the incomplete recovery for the iron particle suspensions examined in this study: 1) particles were lost from suspension by settling in the flask and in the uptake tube, 2) the efficiency of nebulization for the particle suspensions was lower than for the organometallic reference solutions, and 3) there were indications of incomplete vaporization of particles at the normal height of observation in the plasma.

Trace Metals in Fuel Oil

The National Bureau of Standards (NBS) has certified the concentrations of a number of trace elements in what is essentially a "No. 6 Fuel Oil" (65), Standard Reference Material (SRM) 1634. This SRM was obtained and analyzed to determine the applicability of the ICP procedure to fuel oil analysis.

Because fuel oil has characteristics different than lubricating oil, it is reasonable to expect the dissolution behavior of the two matrices to differ. When MIBK was used as the solvent for SRM 1634, a portion of the oil appeared not to dissolve and left a grainy residue on the glassware and a precipitate in the flask. Most of the precipitate could be suspended with shaking. The use of toluene or xylene as the solvent alleviated these problems and the oil appeared to dissolve completely. Wavelength profiles for SRM 1634, Conostan 245 base oil and Conostan D-20 reference samples diluted with each of the three solvents were obtained as described in Chapter II (p.23) with multichannel spectrometer B. The only problem that these profiles revealed was a small increase of the background of SRM 1634 with respect to Conostan 245 base oil in the vicinity of the chromium line when either MIBK or xylene was used as the solvent.

The results obtained for all three solvents are compared with the NBS values in Table XIII. Also included are results

Table XIII. Trace metals in SRM 1634

Technique/solvent	Concentration (μg/g) Cr	Fe	Mn	Ni	V	Zn
Plasma/MIBK[a]	0.16	20	0.22	29	290	0.20
Plasma/xylene[a]	0.17	19	0.23	38		
Plasma/toluene[a]	<0.3	21	0.22	37	290	
Neutron activation[b]	0.14±0.01	37±1	0.25±0.01		300±14	0.40±0.02
NBS values	(0.09)[c]	13.5±1.0	(0.12)[c]	36±4	320±15	0.23±0.05

[a]Multichannel spectrometer B was used; the analyses were based on analytical calibration curves obtained from Conostan D-20 organometallic reference solutions.

[b]Analysis performed by K. Malaby at Ames Laboratory Research Reactor. The standard counting error is given, not the standard deviation for the method.

[c]Values in parentheses are not certified, but are listed by NBS for information only (65).

obtained by neutron activation analysis at the Ames Laboratory Research Reactor. There is general agreement among the plasma values, except in the case of nickel for which the value is significantly lower when MIBK is used as a solvent. This discrepancy is not surprising when the fact that some nickel is associated with the heavier petroleum fractions (66) is considered along with the behavior of MIBK as a solvent (see above).

Agreement between the plasma values and the NBS certified values is element dependent. For nickel (with the exception of MIBK as a solvent) and zinc, the plasma results are within one standard deviation of the NBS certified value. The plasma value for vanadium is two standard deviations from the NBS value, whereas the neutron activation value falls between these two. In the case of iron, the plasma values for all three solvents are significantly higher than the NBS certified value, with the neutron activation value being even higher. Wavelength scans in the vicinity of the iron line produced no evidence of spectral interference and no other reason for the disagreement has been ascertained. The NBS "information only" values for chromium and manganese are also markedly lower than the plasma and neutron activation values. The higher plasma values for chromium with either MIBK or xylene as the solvent may in part be due to the background shift discussed above.

CHAPTER IV. DETERMINATION OF TRACE ELEMENTS IN A CENTRIFUGED COAL LIQUEFACTION PRODUCT

Introduction

As mentioned in Chapter I, there has recently been an increasing interest in coal liquefaction and with this has come an interest in the trace element content of coal liquefaction products. The analytical effort that has been reported is limited. Three liquefaction product samples from the catalytic hydrogenation process of Gulf Research and Development Co. were analyzed by d.c. arc emission spectroscopy (67). The results of these analyses, considered by the authors to be approximate, are given in columns 2, 3 and 4 of Table XIV. In the sample preparation, the liquid product was distilled at a pressure of 1 torr until approximately one third of the product remained. The undistilled residue was oxidized by an oxygen plasma without external heat in a low temperature asher. The use of low temperature oxidation has been shown to reduce substantially losses of some volatile inorganic compounds in comparison to oxidation at high temperatures in a muffle furnace (73,74). However, studies have also shown appreciable losses of some elements, including silver, gold, mercury, selenium and arsenic even under low temperature oxidation conditions (73-77). In addition, as suggested by Koppenaal and Manahan (78)

Table XIV. Concentration of trace elements in coal liquefaction products

Reference	67			68
Liquefaction Process	Gulf Catalytic Hydrogenation			COED
Units	PPM			PPM
Analytical Method	d.c. arc emission			SSMS
Sample Designation	PSOC-239	PSOC-284	PSOC-221	12130
Al				90
As				2
B	0.15	0.12	0.03	4
Ba				1
Be	0.0004	0.01	0.0009	
Bi	N.D.[a]	N.D.	N.D.	<0.3
Br				<0.1
Ca				30
Cd				<0.3
Ce				
Cl				3
Co	0.12	0.01	0.004	0.1
Cr	0.05	0.12	0.05	0.7
Cs				0.2
Cu	0.02	0.03	0.01	0.3
Er				
Eu				
F				1
Fe				400
Ga	N.D.[a]	N.D.	N.D.	0.2
Gd				
Ge	N.D.	N.D.	N.D.	<0.7
Hf				
Hg				
Ho				
K				
La				1
Lu				

[a]N.D. - not detected

[b]The highest concentration reference solution was 900 µg/g Conostan D-20.

69		70	71,72	This Work
Solvent Refined Coal		SYNTHOIL	SYNTHOIL	SYNTHOIL
PPM		PPM	µg/g	µg/g
NAA	XRF	?	AAS	ICP
			FB55 Batch 67	FB55 Batch 67
		29.1		870
2.1	1.8			
				0.81
0.14				9.0
4.7	4.8			
		2.3		
			0.077	
0.4				
0.26		<0.1		
7.5	6.0		7.6	9.0
0.12				
	0.6		2.7	1.7
0.065				
0.025				
270	300	67.4		>900[b]
	0.4			
0.14				
0.054				
0.02				
0.030				
		5.0		
0.10				
0.014				

Table XIV. (Continued)

Reference	67			68
Liquefaction Process	Gulf Catalytic Hydrogenation			COED
Units	PPM			PPM
Analytical Method	d.c. arc emission			SSMS
Sample Designation	PSOC-239	PSOC-284	PSOC-221	12130
Mg				20
Mn	0.05	0.12	0.05	0.4
Mo	0.08	0.01	N.D.	0.7
Na	5	2.5	0.9	10
Nb				0.3
Nd				1
Ni	0.15	0.08	0.03	4
P				3
Pb	0.02	N.D.	N.D.	1
Pr				0.4
Rb				0.2
Sb				<0.1
Sc				0.4
Se				≤0.1
Si				1,000
Sm				
Sn				<0.3
Sr				10
Ta				≤0.5
Tb				
Te				<0.5
Th				0.8
Ti	5	6	0.5	20
Tl	N.D.	N.D.	N.D.	0.5
Tm				
U				1
V	0.06	0.25	0.004	2
W				0.4
Y				1
Yb				
Zn	0.12	0.12	0.05	2
Zr				2

69		70	71,72	This Work
Solvent Refined Coal		SYNTHOIL	SYNTHOIL	SYNTHOIL
PPM		PPM	µg/g	µg/g
NAA	XRF	?	AAS	ICP
			FB55 Batch 67	FB55 Batch 67
		2.2		130
			11	7.0
		<0.2		
8.8		2.9		
0.27				
<6	2.1		6.6	~6
	<1		1.1	
0.045				
	<0.4			
0.066				
0.45				
0.17				
		135.5		>900[b]
0.11				
0.96				
0.043				
0.026				
0.19				
				210
0.016				
0.54				
				7.2
0.094				
8.1	7.2			9.5

trace metals may be present in coal liquefaction products as organometallic compounds. In fact, Given et al. (67) reported titanium was enriched relative to other elements in two liquefaction product samples compared to the original coals. They reasoned that this might have been because titanium was present in these samples in organometallic combination. These compounds may also vaporize at the reduced pressure used for distillation and under low temperature oxidation. To the author's knowledge, full recovery of metals present as organometallic compounds has not been demonstrated for either reduced pressure distillation or low temperature oxidation.

Spark source mass spectrometry was used to analyze the liquefaction product from the COED process (68). The product oil was dissolved in acetone and erbium was added as a reference element. A small aliquot of the solution was placed on a graphite electrode and dried at ~450°C for ten minutes. The electrode was then sparked. The results are shown in column 5 of Table XIV. In this procedure loss of organometallic and volatile inorganic species could have occured because of the elevated temperatures used. Hence, the reported values may be low.

A solvent refined coal sample was examined by instrumental and radiochemical neutron activation analysis and by X-ray fluorescence spectroscopy (69). The neutron activation

analysis involved four sequential irradiations with decay intervals ranging from 15 minutes to 50 days. A radiochemical group separation of the rare earth elements after irradiation was also employed. For X-ray fluorescence, the sample was absorbed on cellulose powder and dried. The powder was then pulverized and pressed into a pellet. The results of these analyses are given in columns 6 and 7 of Table XIV. The long time lag required before results were available for some elements was a distinct disadvantage of the neutron activation method.

Yavorsky and Akhtar (70) have reported the quantitative results for trace metals in a SYNTHOIL sample shown in column 8 of Table XIV. The product oil was ashed at 550°C and the resulting ash was analyzed. No further details of the analytical procedure were given. Once again, the heating of the sample to a relatively high temperature may have led to loss of analyte.

The centrifuged liquefaction product sample used in the present research was also analyzed at the Pittsburgh Energy Research Center (PERC) (71,72). At PERC, concentrated H_2SO_4 was added to the sample and the mixture was then heated on a hot plate until a coke-like material remained. This residue was placed in an oven and ashed at 450°C until all carbonaceous material appeared to be removed. A test of this procedure showed satisfactory recoveries of oil

soluble organometallic reference samples. Two or three days were required for complete ashing, after which the ash was dissolved in HCl. Chromium, copper, manganese, and nickel were then determined by atomic absorption with calibration by the method of analyte additions. A separate analyte additions procedure was used for the determination of lead and cadmium. After additions of analyte had been made to a series of aliquots, ascorbic acid, potassium iodide and MIBK were also added. The iodides of lead and cadmium were extracted into the MIBK and this layer was subsequently analyzed by atomic absorption. The results of these analyses are given in column 9 of Table XIV. Because atomic absorption is a single element technique and an analyte addition method was used, a minimum of 24 analyses (6 elements x 4 aliquots) had to be performed.

The lengthy and elaborate sample preparation schemes for the methods noted above are in marked contrast to the simple dilution used to obtain the preliminary results reported here. As noted previously, many of the methods also involve sample preparation steps which may result in loss of analyte.

Experimental Conditions and Procedures

Centrifuged liquefaction product sample

The centrifuged liquefaction product that was used in

this research was labeled FB55, Batch 67. It was obtained from the Pittsburgh Energy Research Center, USERDA and was made by the SYNTHOIL process. A brief description of this process may be found in reference (9). The sample was taken during an experimental production run in which the sulfur and ash levels of the centrifuged liquid product (0.8% and 2.7%, respectively) were much higher than the levels anticipated in commercial practice. The viscosity of the black, tar-like sample was reported as 172SSF at 180°F (71, 72) (~3.6 x 10^{-4} m^2s^{-1}). The sample had an odor similar to that of road tar or asphalt. A discussion of the general nature of coal liquefaction products may be found in reference (79).

Dilution procedure and reference samples

The sample, reference and blank oils were all diluted 1:10 w/v with 4-methyl-2-pentanone (MIBK), i.e., 1.00 g of oil was diluted to 10 ml with MIBK. The reference oils were prepared from 900 ppm Conostan D-20 (Conostan Division, Continental Oil Company, Ponca City, OK), a hydrocarbon oil that contains equal concentrations (900 µg/g) of twenty elements as organometallic compounds (see Chapter II, p.22), by appropriate serial dilutions with Conostan 245 base oil.

Experimental conditions

The experimental conditions were as described in Table I

(p.15). Multichannel spectrometer B and plasma power supply 3 were used.

Results and Discussion

Sample dilution

The particular centrifuged liquid product under study did not completely dissolve in MIBK but left an adherent, opaque, grainy coating on the glassware and a precipitate in the flask which could be suspended to some extent with shaking. The coating was thicker than the one left by fuel oil (Chapter III, p.67). Subsequent to this investigation, F. Grabau IV of this Laboratory found a solvent that appeared to dissolve the sample completely (80). The solvent, a 50:50 mixture of pyridine and MIBK, also dissolved the reference samples and caused no apparent problems in nebulization or plasma operation.

Wavelength profiles

The wavelength profiles in Figures 12 and 13 were obtained as described in Chapter II (p.23). The spectral line of interest should be located approximately in the center of the wavelength region plotted. When the profiles are plotted, the computer expands or reduces the vertical scale so that the profile will utilize the available space. Because of this feature and the high concentration of certain

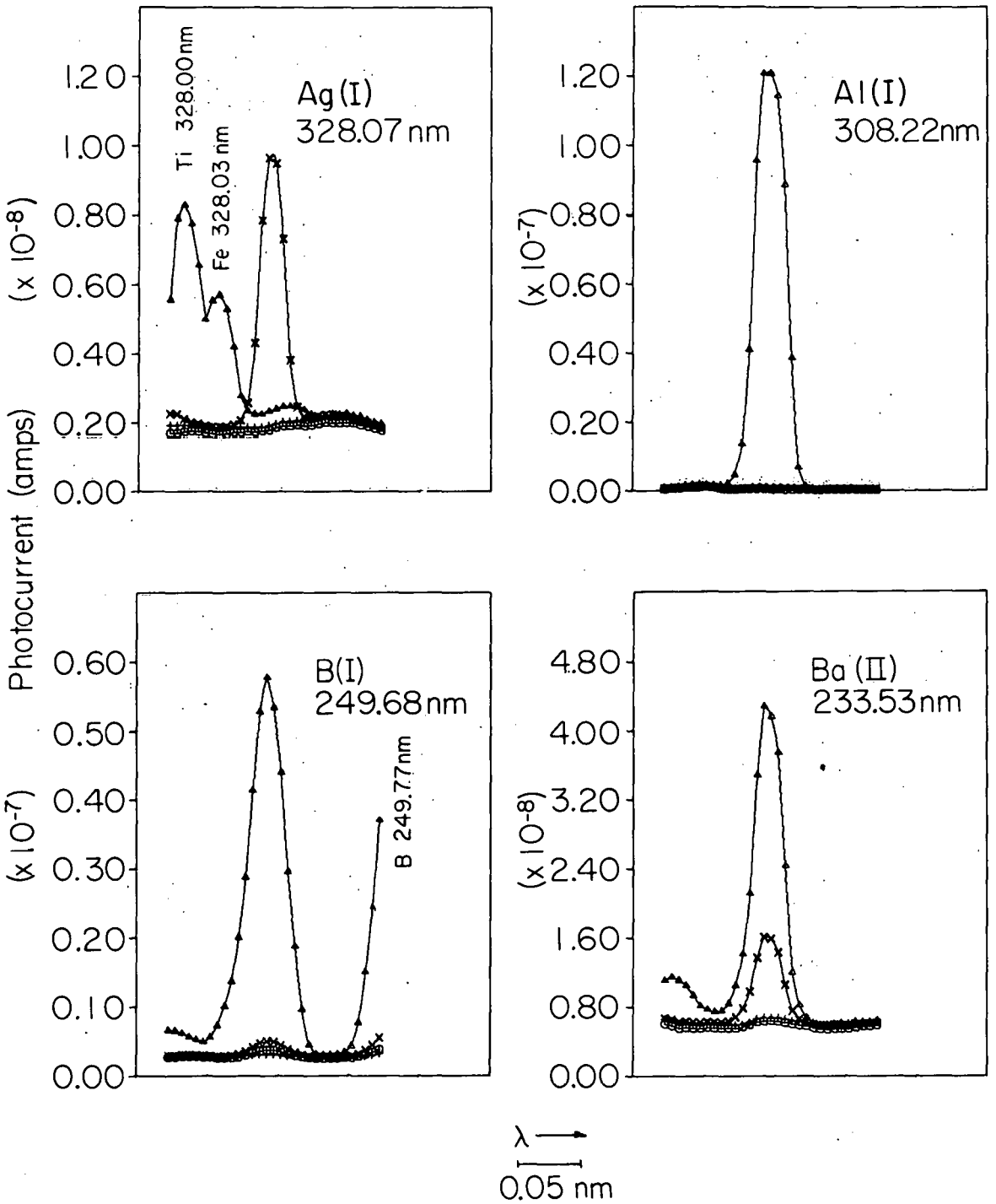

Figure 12. Wavelength profiles of centrifuged liquefaction product FB55, Batch 67 (—Δ—), Conostan 245 blank oil (—O—, —+—), and 2.7 µg/g Conostan D-20 reference sample (—X—).

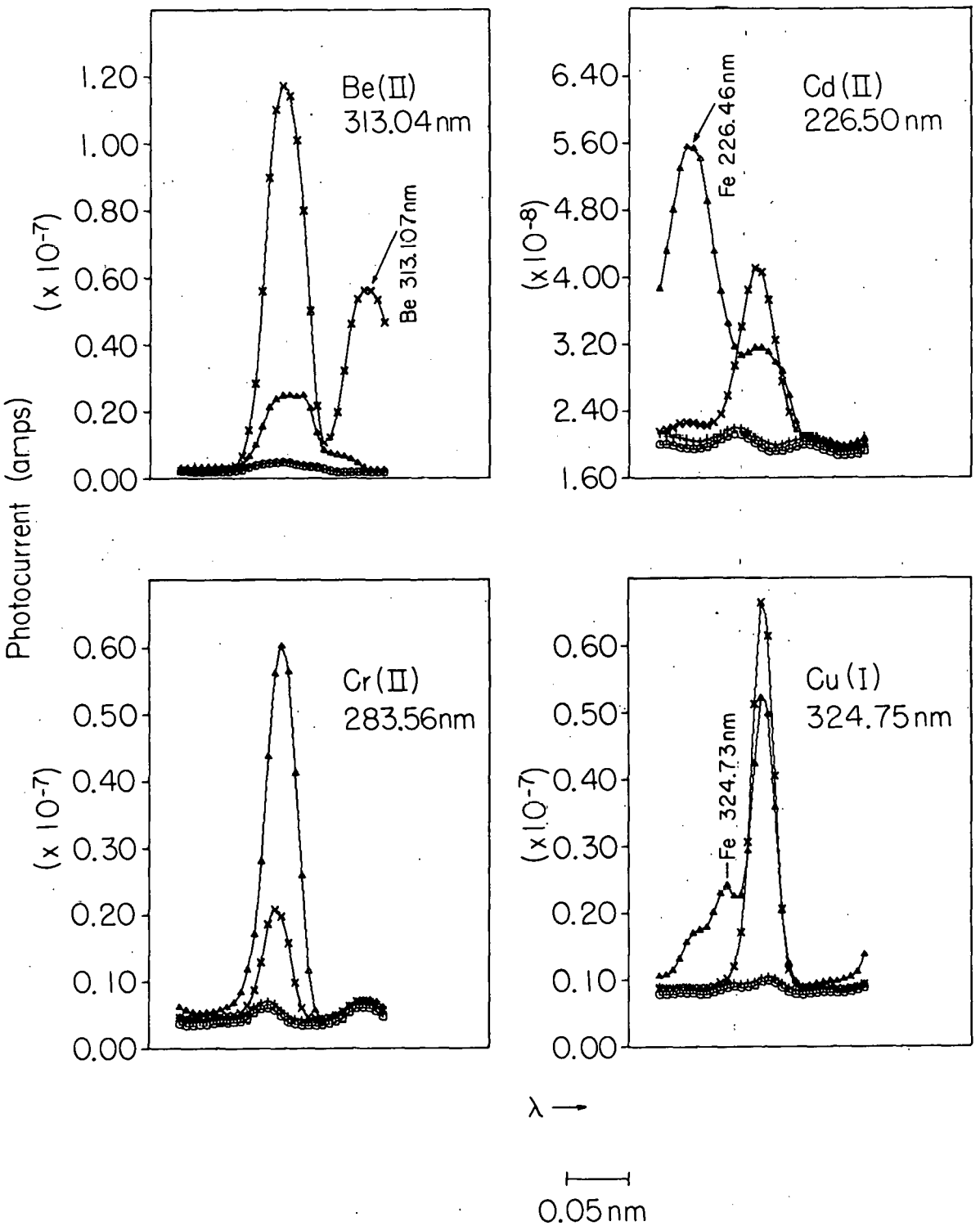

Figure 12. (Continued)

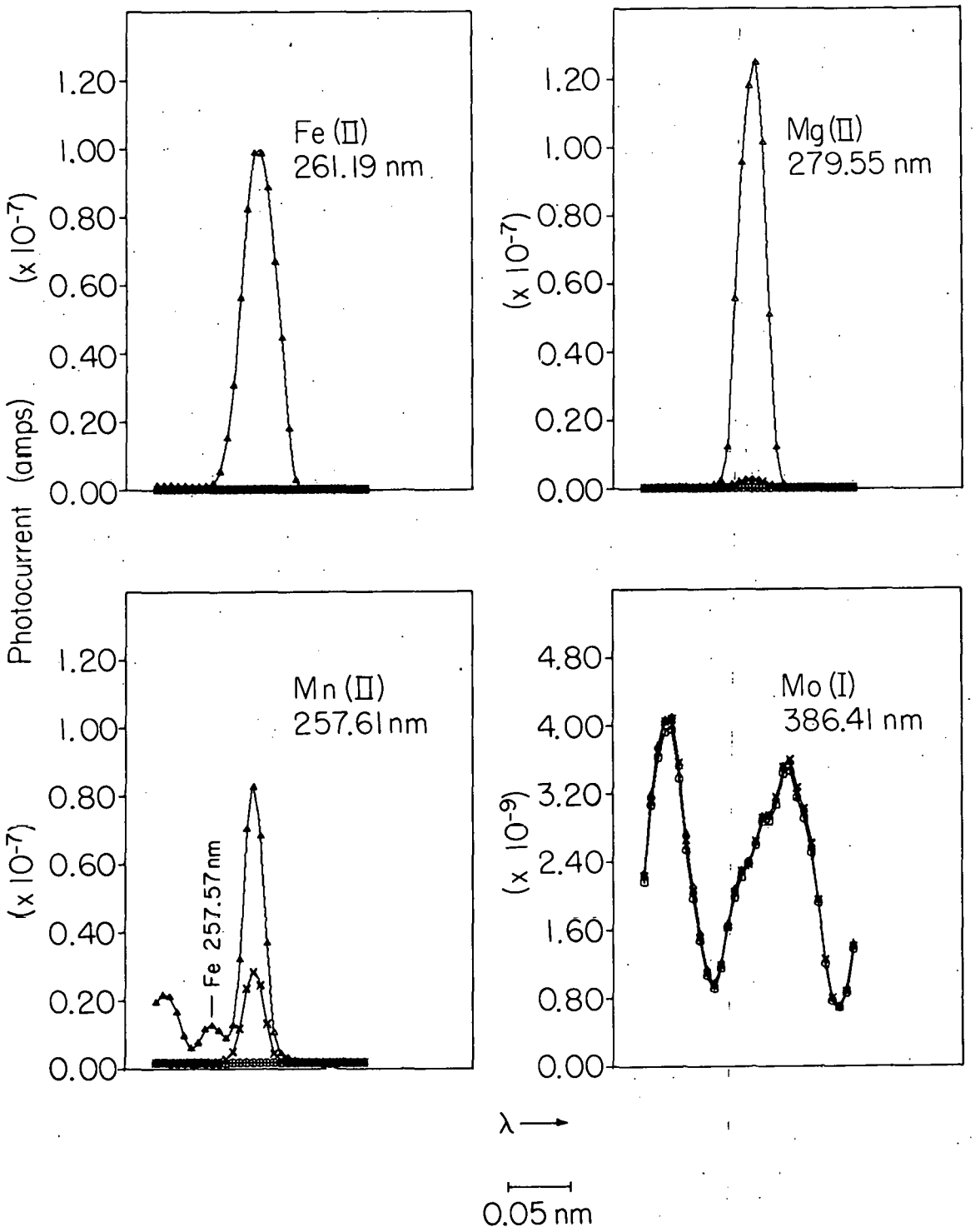

Figure 12. (Continued)

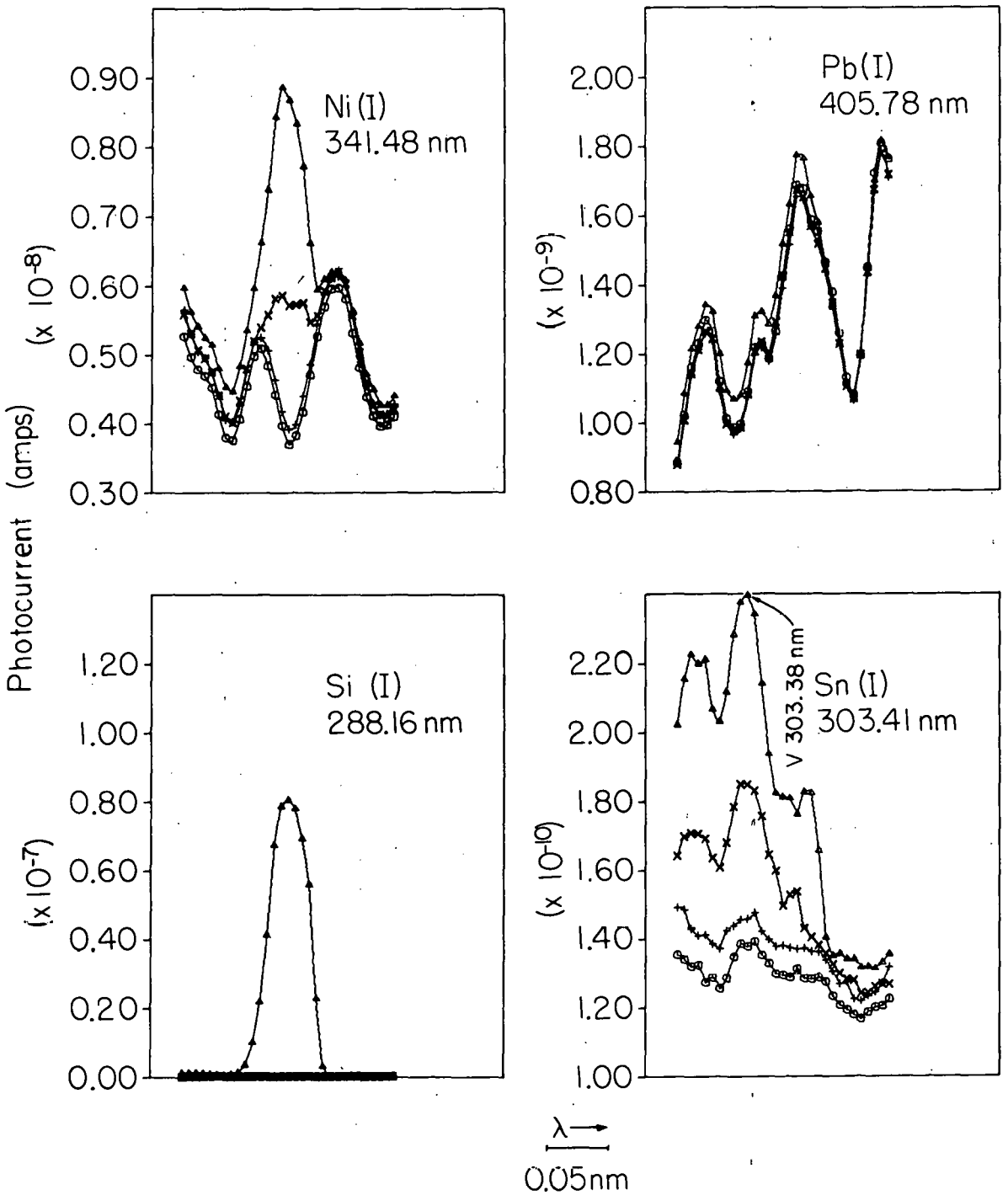

Figure 12. (Continued)

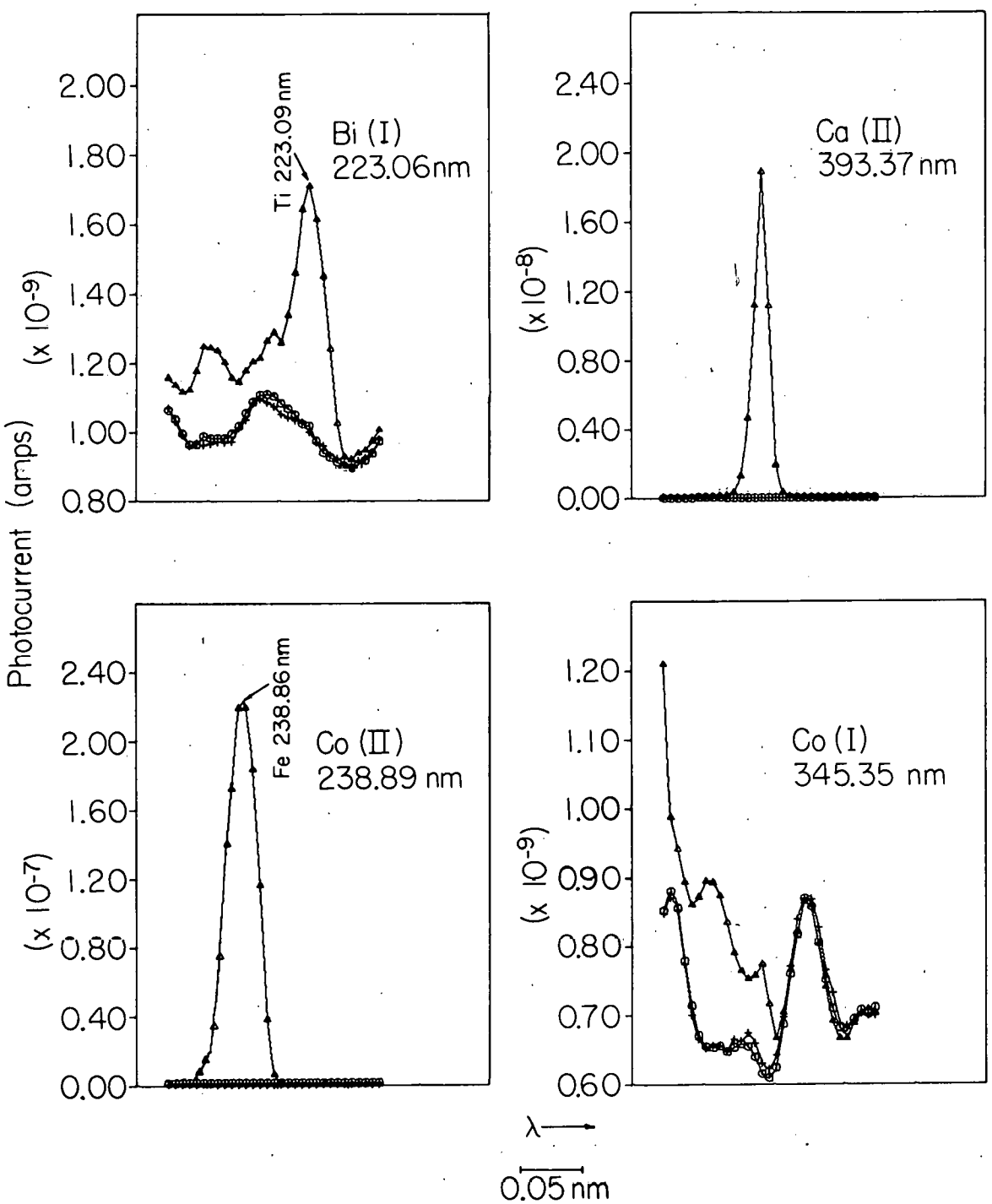

Figure 13. Wavelength profiles of centrifuged liquefaction product FB 55, Batch 67 (—Δ—) and Conostan 245 blank oil (—O—, —+—)

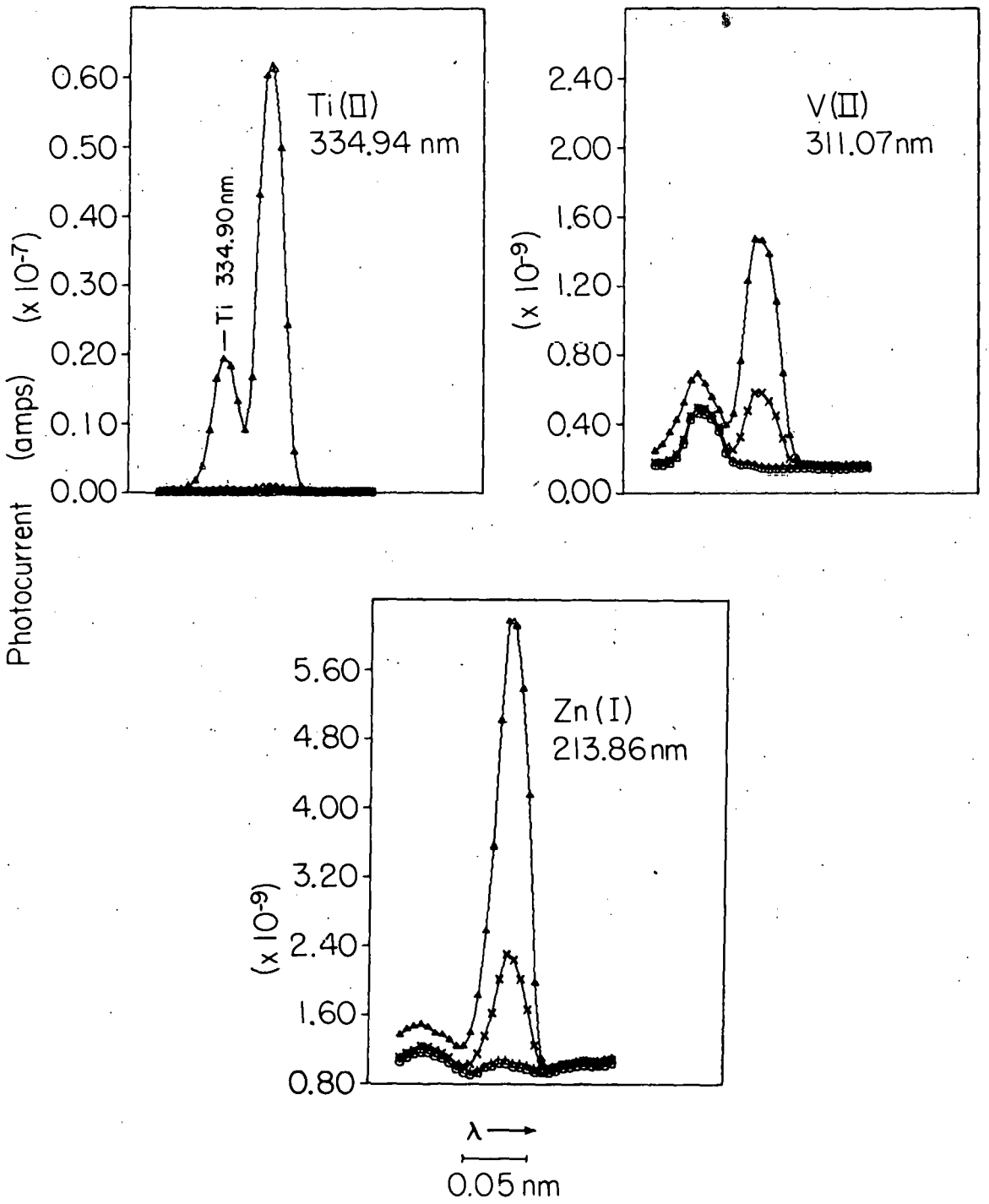

Figure 12. (Continued)

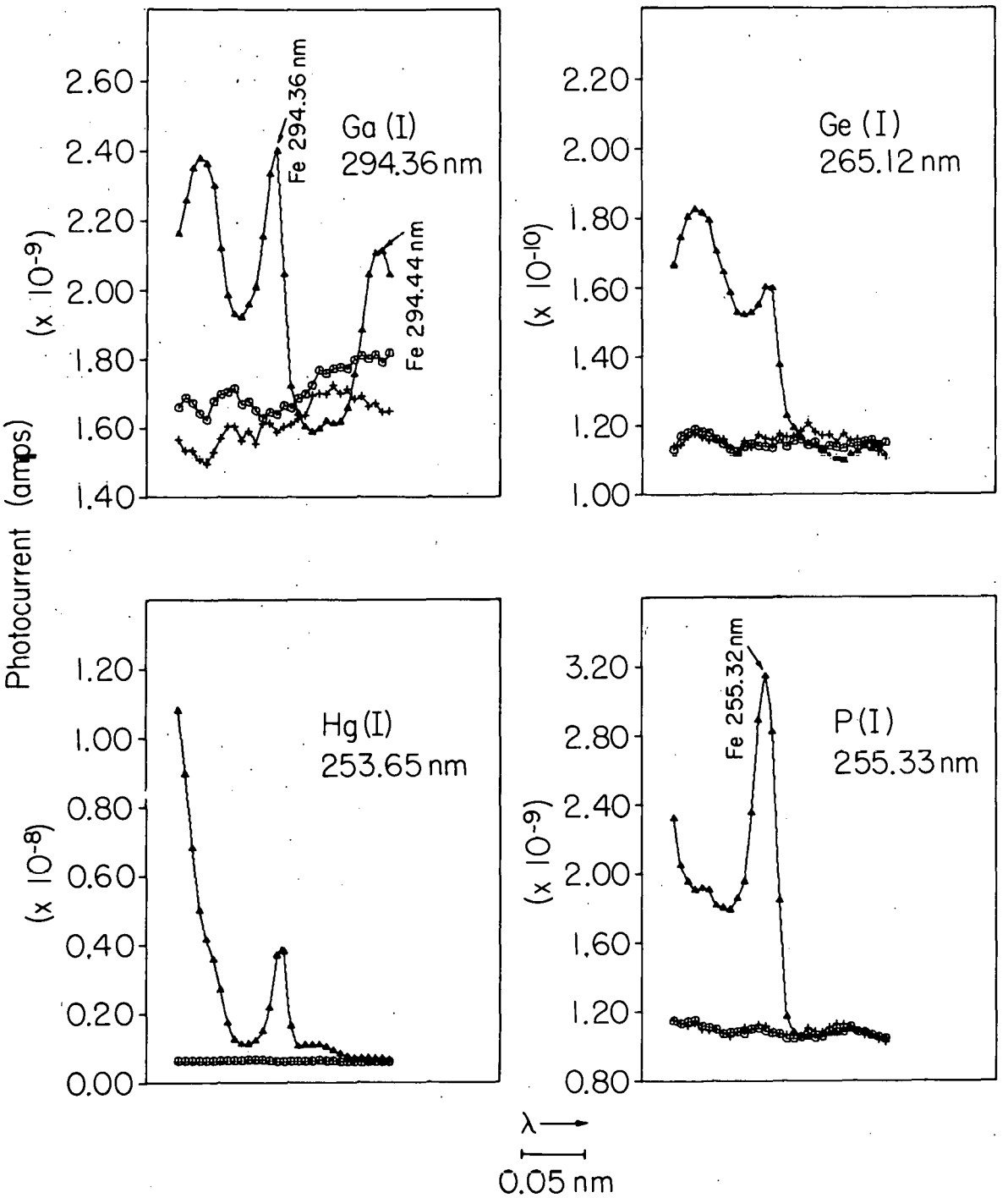

Figure 13. (Continued)

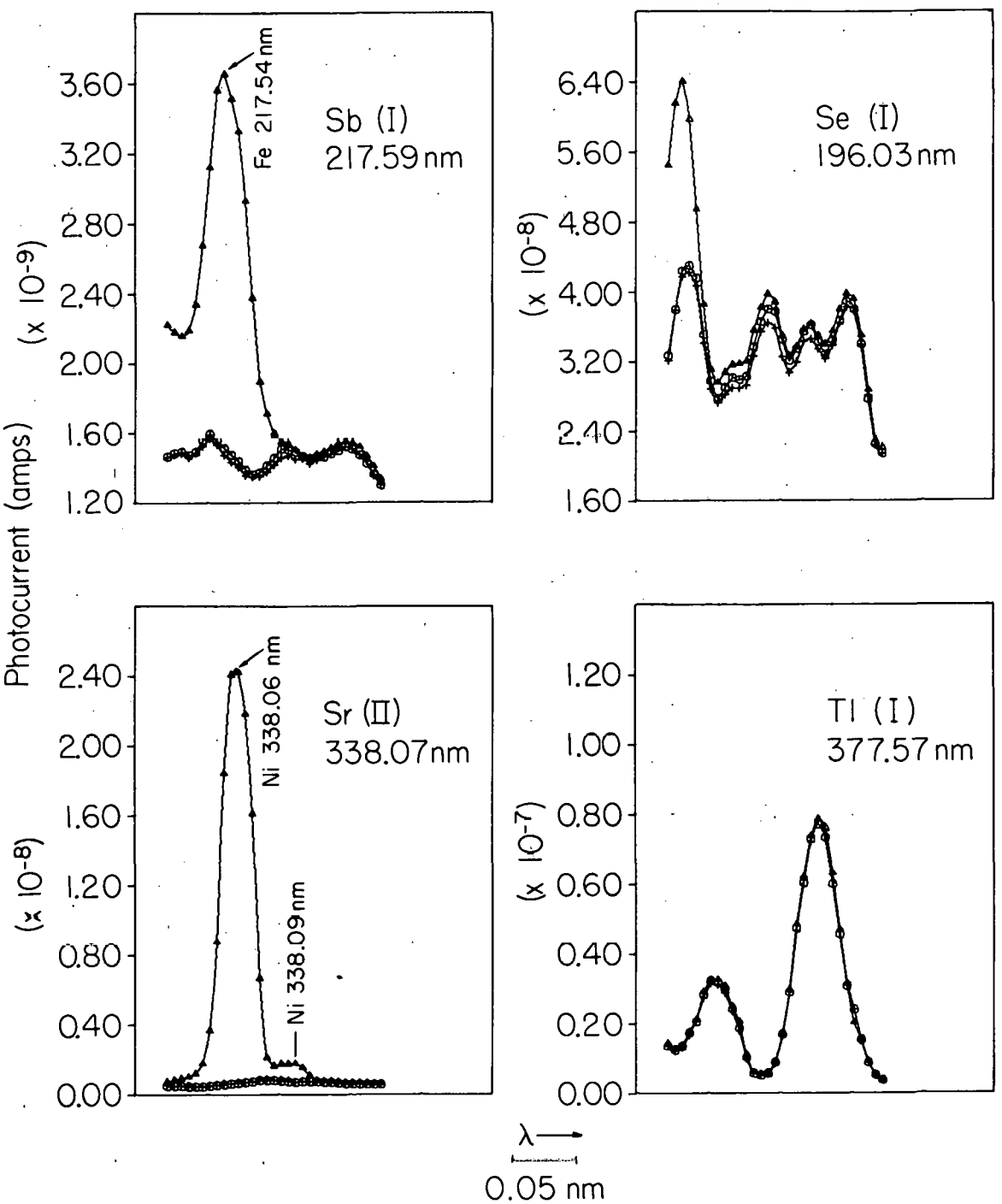

Figure 13. (Continued)

elements in the centrifuged liquefaction product, the signal of the 2.7 μg/g reference sample cannot be differentiated from that of the blank in the profiles of Al, Fe, Si, and Ti in Figure 12 and can scarcely be differentiated from the blank in the profiles of B and Mg. When only the blank and the reference sample are plotted, the signal from the 2.7 μg/g reference sample is readily evident. In the case of Mo and Pb in Figure 12, the wavelength profile of the reference sample cannot be differentiated from that of the blank because the concentration of the reference sample was below the Mo detection limit (4 μg/g) and near the Pb detection limit (2 μg/g). The Pb line in Figure 12 is not the recommended line (see Chapter III, p.37), but is the best line available on multichannel spectrometer B.

A number of spectral interferences are evident in Figures 12 and 13. Because many of the interfering lines are iron lines (see for example the Cd profile in Figure 12, and the Co 238.89 nm, Ga, P, and Sb profiles in Figure 13), the problem is aggravated by the high concentration of iron in the sample. Other line interferences include the interference of Ti on Bi in Figure 12, the interference of Ni on Sr in Figure 13 and the interference of V, as well as other unidentified lines, on Sn in Figure 13. Also apparent in some profiles (e.g., Co 345.35 nm, Ge, Hg, and Se in Figure 13) are unexplained differences in spectral features between

the centrifuged liquefaction product solution and the blank and reference solutions. Whether these differences are unidentified spectral line interferences or actual differences in the spectral background features has not been determined. Areas of research that should be explored to circumvent these problems are discussed in the future research section below.

Analytical results

The analytical results obtained for centrifuged liquefaction product FB55, Batch 67 are summarized in column 10 of Table XIV. The analysis was performed for those elements contained in the reference sample for which no spectral interferences were evident in the wavelength profiles. When these values were reported to personnel at PERC, they confirmed that the results were reasonable for this particular sample. Column 9 of Table XIV contains values obtained on the sample at PERC as described on p.76. The differences in copper and manganese values may be due to the fact that the sample did not completely dissolve in MIBK.

In addition to the elements in Table XIV, it is evident from Figure 13 (p.85) that there is also a substantial amount of calcium in the sample.

Future Research

It is obvious from the wavelength profiles in Figures 12 and 13 that more research is needed before this technique

becomes applicable to routine analysis of centrifuged liquefaction products for elements other than those listed in Table XIV. A study of spectral interferences by various elements should be undertaken; the effects of iron, silicon, aluminum, titanium and magnesium should expecially be examined because of the high concentration of these elements in the sample. Alternate analytical lines should be sought for those lines that are interfered with and/or do not possess the desired sensitivity. In cases where there are differences in the spectral background features between the sample and blank and reference solutions, the use of dynamic background correction should be explored. The use of alternate solvents should also be examined. Research in these areas is currently being performed in this laboratory.

CHAPTER V. DETERMINATION OF TRACE ELEMENTS IN EDIBLE OILS

As mentioned in Chapter I, these are a number of elements of interest in edible oils. The quantitative study described here is confined to the three elements, iron, magnesium, and calcium for which comparative analytical data were available and for which analytical lines were programmed on multichannel spectrometer B.

Experimental Conditions and Procedures

Samples, dilution procedures, and reference samples

Three crude soybean oil samples labeled Ill., Ark., and S.C. that had previously been analyzed (81) were obtained from L.T. Black of the USDA Agriculture Research Service, Northern Regional Research Laboratory, Peoria, IL. In addition, three commercial oils were purchased; namely, Mazola corn oil, Planters peanut oil, and Wesson vegetable oil.

The samples, reference and blank oils were all diluted 1:4 w/v with 4-methyl-2-pentanone (MIBK), i.e., 1.00 g of oil was diluted to 4 ml with MIBK. The reference oils for calibrating the spectrometer were prepared from experimental organometallic reference corn oil samples (ArRo Laboratories, Joliet, IL) by appropriate dilution with a low metal content corn oil blank (also supplied by ArRo Laboratories). The

experimental organometallic corn oil sample was formulated by ArRo to contain 500 μg/g of each of the following elements: iron, calcium, magnesium, sodium, and potassium. Within experimental error, neutron activation analysis performed at the Ames Laboratory Research Reactor confirmed these concentration levels, except for iron. In the case of iron, neutron activation analysis gave a concentration value of 620 μg/g when either of two gamma lines were used. After consultation with the supplier (82), it was determined that 620 μg/g should be considered the correct concentration of iron in the reference sample.

Plasma torch placement

When corn oils were nebulized, a solid, yellow deposit formed on the tip of the aerosol tube, as shown in Figure 14. This deposit deflected the aerosol, which caused the plasma to become unstable and to extinguish eventually. This buildup could be avoided by positioning the torch in the coil so that the top of the intermediate tube of the torch was approximately even with or slightly above the bottom of the coil.

Other experimental conditions

The aerosol carrier-gas flow rate was ~0.8 ℓ/min. All other conditions were as described in Table I (p.15).

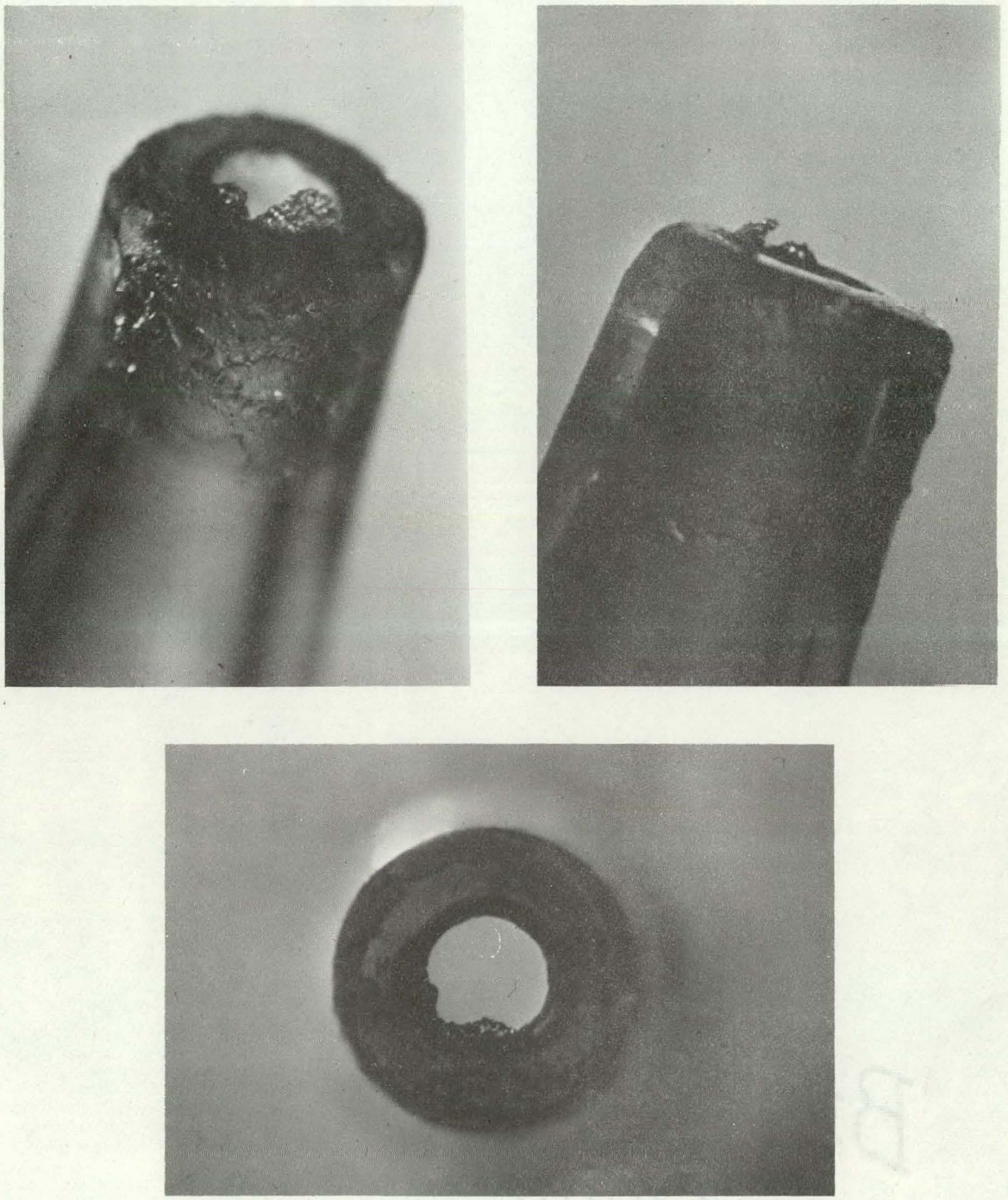

Figure 14 Deposit on tip of aerosol tube.

Multichannel spectrometer B and plasma power supply 3 were used.

Results and Discussion

Detection limits and analytical calibration curves

Detection limits measured for the elements studied are shown in Table XV. In accordance with IUPAC recommendations (43), these values represent the concentration of analyte that will yield an emission intensity three times the standard deviation of the blank signal. It should be emphasized that these values refer to the concentration of the element in the oil before the 1:4 dilution.

Analytical calibration curves obtained simultaneously on multichannel spectrometer B are shown in Figure 15. Each data point represents a relative emission intensity measure of one 10-s signal averaging interval. The lowest data points on the magnesium and iron curves represent concentrations approaching the detection limit. It is important to note that the calcium and magnesium curves are linear with concentration over four orders of magnitude and the iron curve is linear over at least three orders of magnitude.

Wavelength profiles

It was important to determine whether differences in protein content and other organic constituents among the various oils that were studied affected the nebulization or

Table XV. Detection limits of elements in corn oil

Element	Wavelength (nm)	Detection Limit (μg/g of oil)
Ca	393.37[a]	0.002
	315.89	0.06
Fe	261.19	0.06
Mg	279.55	0.008

[a]Recommended line

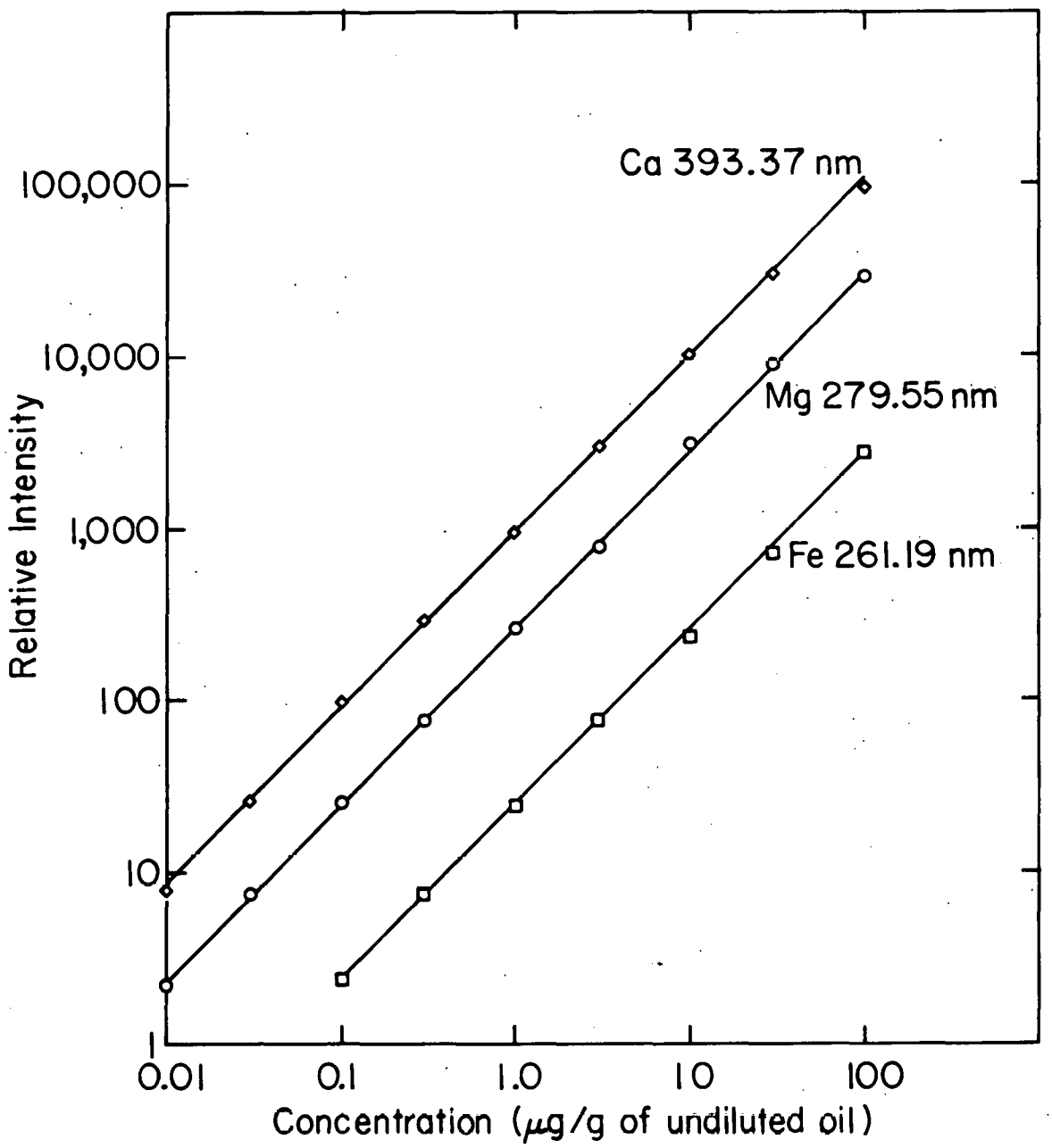

Figure 15. Analytical calibration curves for corn oil.

spectral features and, thus, caused a difference in spectral background. Early in the investigation, wavelength profiles of the oils were obtained as described in Chapter II (p.23) for 19 of the 32 elements programmed on multichannel spectrometer B. A few of these profiles are shown in Figures 16, 17 and 18. No substantial differences in spectral features or background shifts were evident among the soybean oils, commercial edible oils, and the corn oil blank. At low analyte concentrations, the structure of the background becomes evident as can be seen in the Fe profile in Figure 16, the Cu profile in Figure 17, and the Mn profile in Figure 18. Even though the Cu line coincides with a background feature and the Mn line occurs on the side of a background peak, these lines have been found to be the preferred analytical lines.

Because the characteristics and chemical components of edible oils differ from those of lubricating oils, it was not surprising to find that the Conostan 245 and Condor 105 hydrocarbon dilution oils showed background shifts relative to the corn oil blank in several profiles. Of the 20 spectral lines profiled, the background from Condor 105 was shifted higher in 13 cases, whereas the background from Conostan 245 was higher in three cases and lower in two cases. These background shifts may arise from the differences in nebuli-

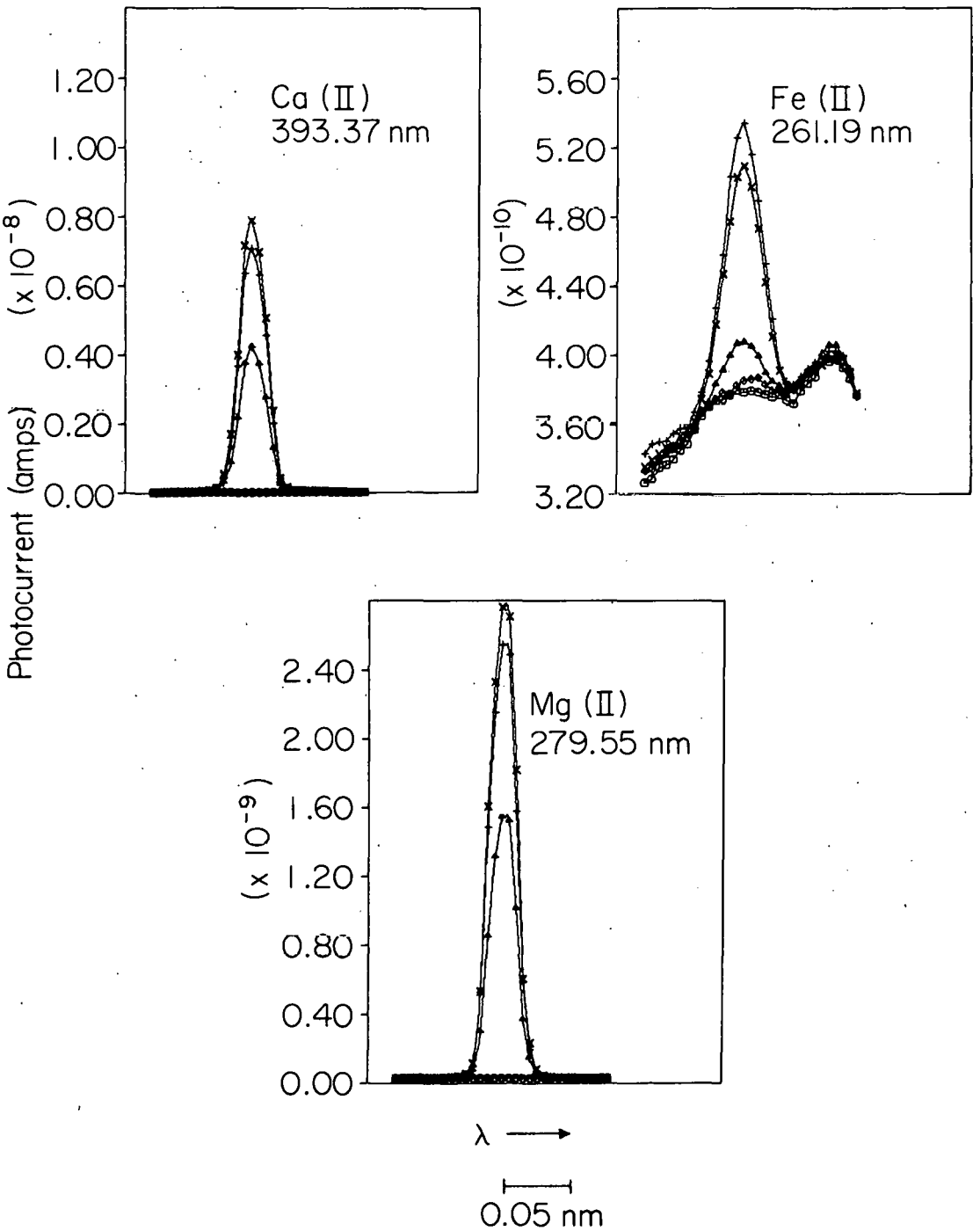

Figure 16. Wavelength profiles of corn oil blank (—O—, —◇—), 30 µg/g reference sample (—†—) for Ca and Mg, 0.3 µg/g reference sample (—Δ—) for Fe, and crude soybean oil samples Ill. (—+—) and Ark. (—X—).

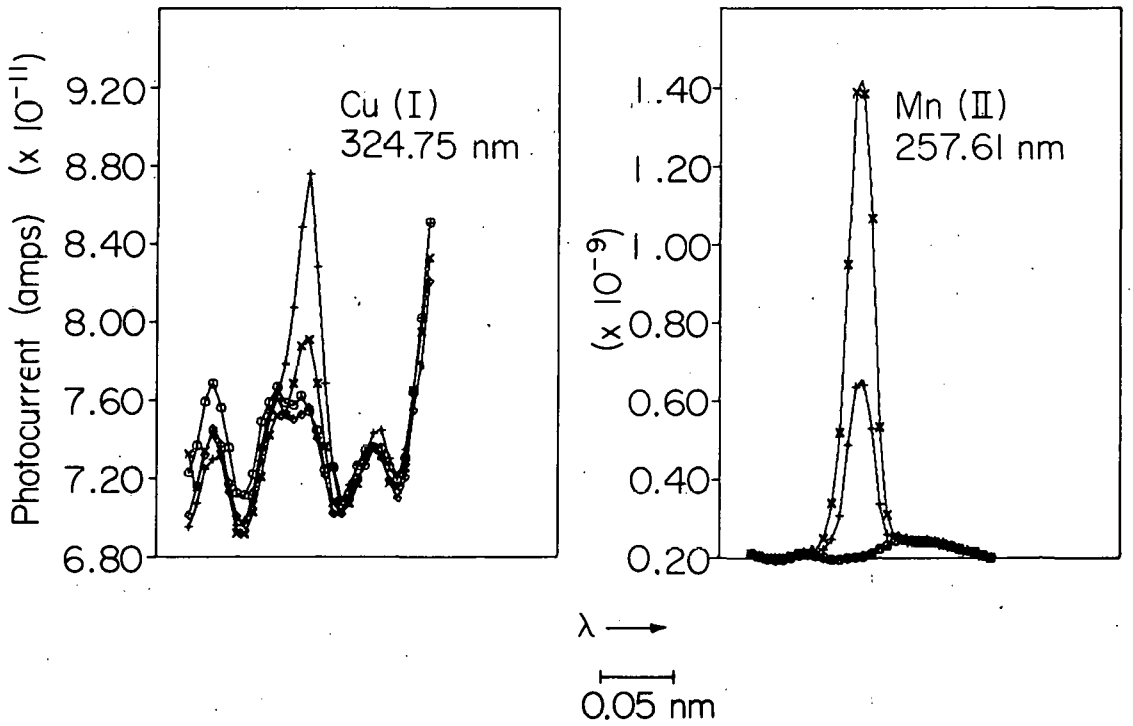

Figure 17. Wavelength profiles of corn oil blank (—o—, —◊—) and crude soybean oil samples Ill. (—+—) and Ark. (—X—).

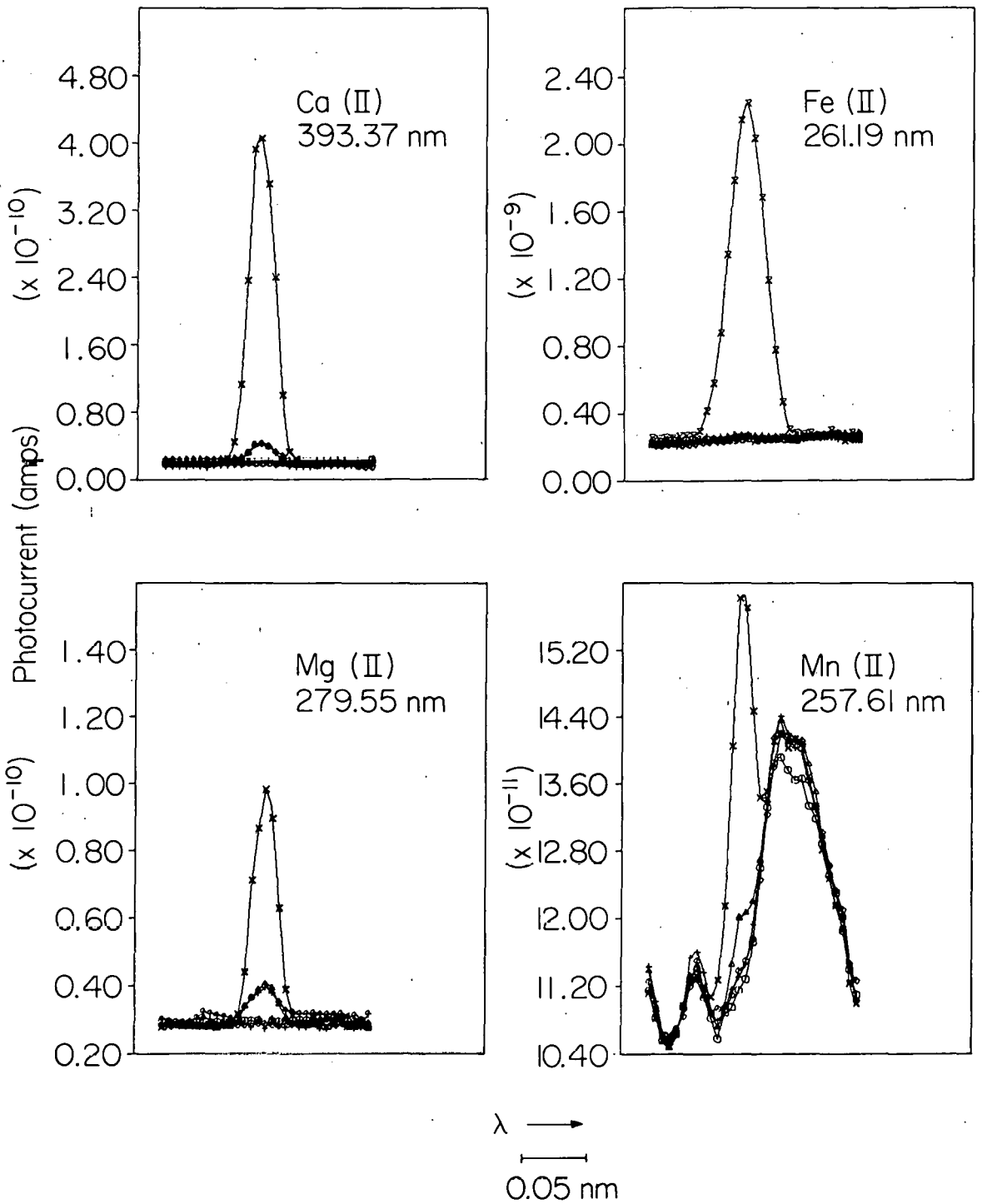

Figure 18. Wavelength profiles of corn oil blank (— O —, —◊—), 30 µg/g reference sample (—X̄—) for Fe, 0.3 µg/g reference sample (—†—) for Ca and Mg, Mazola corn oil (—Δ—), Wesson oil (—+—), and Planters peanut oil (—X—).

zation characteristics of the solutions; uptake rates for the 1:4 oil/MIBK solutions at an aerosol carrier-gas flow rate of ~0.8 ℓ/min were 0.49 ml/min for the corn oil blank, 0.48 ml/min for the Conostan 245 oil, and 0.67 ml/min for the Condor 105 oil.

Approximately nine months after the above wavelength profiles were obtained, multichannel spectrometer B was used to profile analytical lines of the 13 elements that had not been profiled previously. Two of these profiles are shown in Figure 19. In a number of profiles, sample Ill. exhibited a background shift relative to the other edible oils as is shown in the Ba profile in Figure 19. During the nine month period between sets of profiles, a precipitate had formed in the sample Ill. solution, and the background shift is believed to result from this deterioration of the sample. With the exception of sample Ill., no substantial differences in spectral features or background shifts were evident among soybean oil sample Ark., the commercial edible oils, and the corn oil blank. (Conostan 245 and Condor 105 were not profiled.)

Analysis of soybean oil samples

The analytical results for the crude soybean oil samples obtained by the ICP method are shown in Table XVI along with the results obtained by three atomic absorption methods (81).

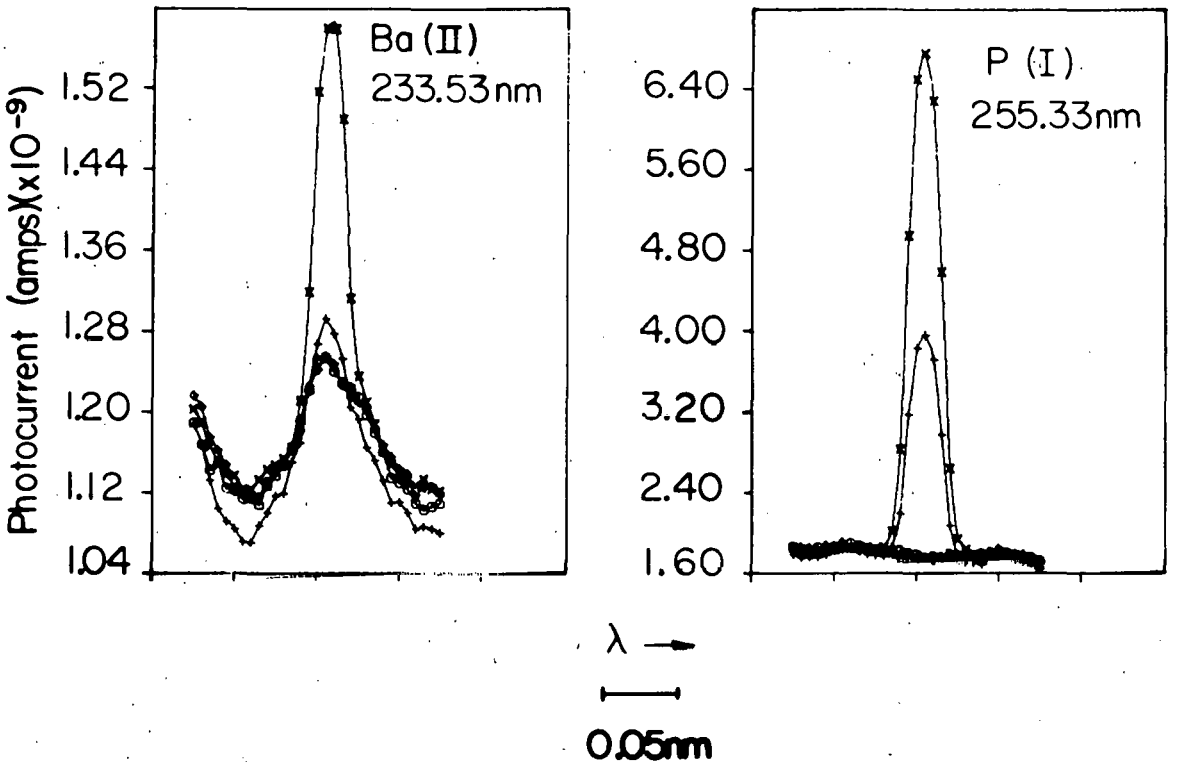

Figure 19. Wavelength profiles of corn oil blank (— o —, —◊—) and crude soybean oil samples Ill. (—+—) and Ark. (—X—).

Table XVI. Comparison of results for crude soybean oil samples

Sample[a]	Element	Concentration (μg/g)			
		Atomic absorption[b]			This Work
		Char Ash	Direct Aspiration	Carbon Rod	
Ark.	Ca	10.0	20.5	31.4	55
	Mg	47.0	47.5	46.3	49
	Fe	1.57	1.63	1.62	1.7
Ill.[c]	Ca	9.1	19.2	27.5	48
	Mg	44.3	45.0	40.0	45
	Fe	1.78	1.73	1.78	1.6
S.C.[d]	Ca	11.4	21.2	28.7	57
	Mg	49.7	49.5	40.1	48
	Fe	6.54	6.68	6.61	5.6

[a]Samples supplied by L. T. Black, Northern Regional Research Laboratory, ARS, USDA, Peoria, IL.

[b]Reference 81.

[c]Sample contained some sediment.

[d]Sample contained an appreciable amount of sediment; therefore only the supernatant liquid was aspirated.

The results for magnesium show reasonable agreement as do the results for iron in samples Ark. and Ill. The lower result obtained for iron in sample S.C. by the ICP method may reflect the fact that this sample originated from field-damaged beans (81) and the MIBK-diluted solution contained an appreciable amount of sediment. Because this sediment tended to clog the nebulizer, only the supernatant liquid was aspirated. Thus, iron that was contained in or adsorbed on the sediment was not detected.

The results for calcium vary appreciably among the four methods with the ICP results being higher than the others. Black (81) accounts for the disparity in calcium results among the atomic absorption techniques by noting that crude soybean oil contains high concentrations of phosphorous (see Figure 19). The depressing effect of phosphorous on calcium in flame atomic spectroscopy is well-known. Some depression has also been observed with a carbon rod volatilization system (83). The plasma used in this study however, has been shown to be essentially free from this interference (29).

Wavelength profiles described in the last section were obtained for sample Ill. and Ark.; a satisfactory profile was not obtained for sample S.C. because of the tendency of the sample to clog the nebulizer. Of the 32 elements profiled, only copper, manganese, phosphorous and barium

were evident in addition to the elements for which reference data were available. The profiles of these elements are shown in Figures 17 and 19. In agreement with earlier reported atomic absorption results (81), the profiles showed more copper and less manganese in sample Ill. than in sample Ark. Sample Ill. also contained less barium and phosphorous than sample Ark.

Analysis of commercial edible oils

The analytical results obtained for the three commercial edible oils are shown in Table XVII. As mentioned above, wavelength profiles of these oils were obtained for 32 elements. Profiles for four of these elements are shown in Figure 18. In addition to the elements in Table XVII, the only elements evident in the profiles were silicon in Mazola corn oil, and manganese in Planters peanut oil and Mazola corn oil. The concentration of manganese in the peanut oil was considerably greater than in the corn oil.

Table XVII. Analytical results for commercial edible oils

Sample	Concentration (μg/g)		
	Mg	Fe	Ca
Wesson vegetable oil	<0.05	<0.3	<0.05
Planters peanut oil	2.6	<0.3	4.2
Mazola corn oil	0.66	0.5	0.37

CHAPTER VI. PARTICLE VELOCITY AS DETERMINED BY HIGH FRAMING SPEED MOVIES

In Chapter III, the determination of elements present in oils as wear metal particles and iron particles was explored. One of the potential problems discussed was incomplete vaporization of particles in the plasma. One of the important factors influencing the extent of particle vaporization is the length of time the particle experiences the high temperature environment of the plasma, i.e., the residence time of the particle. (A discussion of vaporization theory can be found in the Appendix.) In this study, undertaken with G. F. Larson, high framing speed photography was used to determine the effects of two parameters, aerosol carrier-gas flow rate and aerosol tube geometry, on the particle velocity and, thus, on the residence time.

Experimental Facilities and Operating Conditions

The experimental facilities and operating conditions are summarized in Table XVIII. As shown in the table, three different aerosol tube designs were used with the plasma torch. An aerosol carrier-gas flow rate of 1.0 ℓ/min was used with each torch. The standard torch design was used when aerosol carrier-gas flow rates of 1.0, 1.3 and 1.6 ℓ/min were compared.

Table XVIII. Experimental facilities and operating conditions

Plasma power supply	International Plasma Corporation generator, 27.12 MHz with coupling circuit as described in (84) operated at 1200 W.
Sample introduction device	Fluidized bed apparatus similar to that of Dagnall et al. (85). A small vibrator was used to vibrate the bed if needed.
Plasma torch assembly	All fused quartz assembly. With the exception of the aerosol tube, the torch is described in Table I and shown in Figure 2. Three types of aerosol tubes were used: a. Standard tapered tip with a 1.5 mm i.d. orifice as shown in Figure 2. b. Same as (a) with a 2 mm i.d. orifice. c. Capillary aerosol tube, the upper 50 mm of the aerosol tube consisted of 1.5 mm i.d. capillary tubing.
Gas flows	Plasma argon: 14 ℓ/min Auxiliary plasma argon: 0.0 ℓ/min Aerosol carrier argon: varied, see text.
Particles	Al_2O_3 sieved to -325 mesh (44 μm).
Camera and associated equipment	Wollensak Fastax Model WF3 16 mm high framing speed camera with a Wollensak WF 301 Fastax Control unit. Operated at ~8000 frames/s. A Wollensak Pulse Generator operated at 1000 CPS was used for obtaining timing marks on the film.
Film	Eastman Plus-X Negative 7231.

For each of these conditions, high framing speed movies (~8000 frames/s) were obtained while aluminum oxide particles were being carried through the plasma. Selected film sequences of particles traversing the plasma were printed. In the sequence shown in Figure 20, the top of the load coil can be seen at the bottom of frame 2. The faint dark horizontal line across the center of the plasma is the top of the plasma torch. The luminous spots observed in the films were either similar in size to the one in Figure 20 or much dimmer and smaller. Sequences of this second type of luminous spot did not reproduce well and, therefore, a sample is not included. From the printed sequences, measurements were made of the particle position vs. frame number. With these measurements and the film speed as determined from timing marks on the film, the particle velocities could be determined. Similar methods have been used by others (24, 86, 87) to determine particle velocities in inductively coupled plasmas. Instead of movies, Gold (88) has used a "Plasmascope" for particle velocity determination.

Results and Discussion

It was expected that as the gas velocity at the tip of the aerosol tube increased, the particle velocity would also increase. In the case of aerosol carrier-gas flow rate

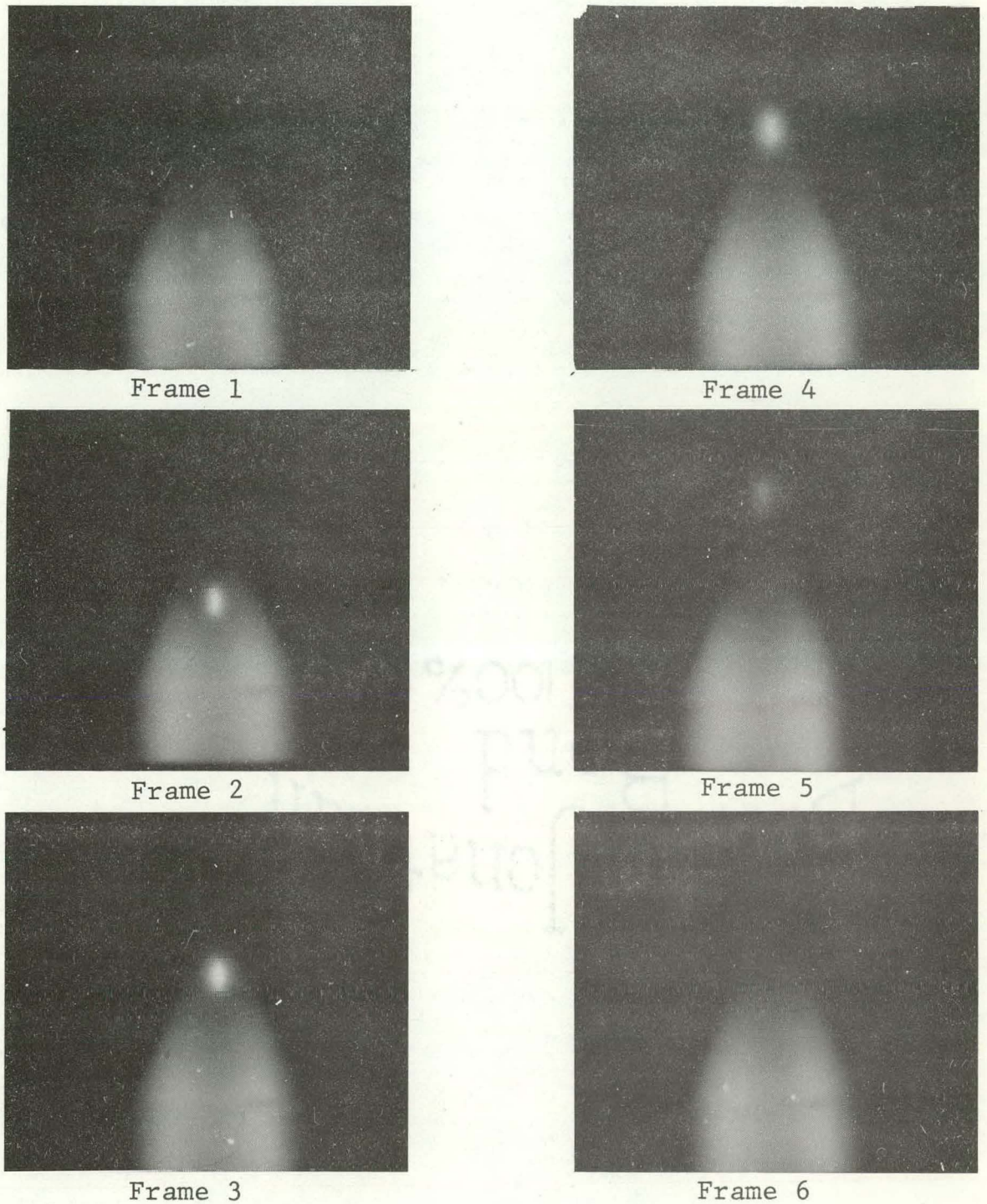

Figure 20. Film sequence of an apparently large particle traversing the plasma. Film speed ~7800 frames/s.

changes, the gas velocity at the tip of the aerosol tube should be directly proportional to the flow rate. For the different aerosol tube tip geometries, the velocity dependence is slightly more complicated. When the capillary tube tip is used, the initial vertical velocity component should be higher because less turbulence should be developed at the exit. On the other hand, the exit velocity of the gas for the tube with the 2 mm i.d., tip should be lower because of the greater cross-sectional area. Despite expectations, it is seen in Table XIX that no correlation was found between aerosol carrier-gas flow rates or aerosol tube geometry and particle velocity in the plasma.

It was also expected that the vertical coordinate at which emission from the particle, believed to be due to a sodium impurity, was first observed would be inversely correlated with the aerosol carrier-gas velocity at the tip of the aerosol tube. Table XX indicates such a correlation for differing gas flows, but this correlation does not extend to the set of differing torch geometries.

One explanation for the unexpected results is that the effects of other forces at work in the plasma such as expansion thrust (see Chapter I), overwhelmed any differences caused by varying the initial velocities. It is also possible that the observed particles varied significantly in size.

Table XIX. Effect of aerosol carrier-gas flow rate and aerosol tube geometry on particle velocity

Torch	Flow Rate (ℓ/min)	Calculated Velocity at Tip (m/s)[a]	Velocity from Photos (m/s)[b]
Standard	1.6	15.1	18.5, 20.2
	1.3	12.3	16.4, 17.2
	1.0	9.4	17.9, 17.1
	1.0	9.4	24.2
Capillary tip	1.0	9.4	19.9, 22.1
	1.0	9.4	25.8, 27.6
2 mm i.e. tip	1.0	5.3	21.5, 23.2
	1.0	5.3	24.1

[a]Calculated velocity assuming that the particles travel at the same velocity as a laminar flow of argon through a column of the same diameter as the aerosol tube tip.

[b]The first velocity was calculated using the top of the streak on each photograph, the second was calculated using the bottom of the streak. If only one value is given, the center of the spot or streak was used.

Table XX. Effect of flow rate on position of first appearance of emission from particle

Aerosol Carrier-Gas Flow Rate	Position Above Load Coil of First Appearance[a]
1.0 ℓ/min	8 mm, 7 mm
1.0 ℓ/min	11 mm
1.3 ℓ/min	15 mm, 14 mm
1.6 ℓ/min	20 mm, 18 mm

[a]The first value refers to the top of the streak on each photograph, the second refers to the bottom of the streak. If only one value is given, the center of the spot or streak was used.

Although the initial mean diameter of the Al_2O_3 particles in the fluidized bed as determined by optical microscopy was 42 μm, those remaining after the flow rate experiments had a mean diameter of 64 μm. These observations imply either a selective removal of the smaller particles from the bed, or agglomerization (89). Since the particles were not observed until they were fairly high in the plasma, the possibility still exists that the variables examined have a definite effect on particle velocity lower in the plasma. These explanations are, of course, speculation. The actual reason for the particle behavior is unknown.

CHAPTER VII. OBSERVATIONS ON PLASMA MOTION

Introduction

Visually, the inductively coupled plasma appears to be a very spatially steady source, especially when compared to many flame, arc, and spark emission sources. However, it was discovered in the course of investigations reported in previous chapters that when viewed in "slow motion," the plasma exhibited definite fluctuations of shape and intensity. Although this area of research was not directly related to the determination of trace elements in oil, it was deemed worthy of investigation. Studies involving high framing speed photography have been conducted by others (23,24,86,89, 90), but few details concerning changes in the plasma structure have been reported to date. Greenfield et al., (89,90) reported a growth and decay cycle of their plasma along with the apparent cause (see below). Other investigations (23,24,86) have used high framing speed photography to track particles in a plasma, as was discussed in Chapter VI.

Experimental Facilities

To study the plasma fluctuations, a Wollensak Fastax Model WF3 16 mm high framing speed camera operated at 5200-

5600 frames/s was used to photograph the plasmas formed by three plasma systems under various experimental conditions. Table XXI summarizes some of the electrical characteristics of the plasma power supplies.

Results and Discussion

Lepel generator system

The most dramatic differences in fluctuation patterns were those among the plasma systems. A plasma generated by the Lepel generator system was filmed as an oil/MIBK (1:10) solution was being nebulized. The presence of the organic aerosol accented the various regions of the plasma. A sequence of this film is not shown because the film contrast was not great enough to obtain good printed copies that clearly displayed the plasma fluctuations. It was apparent from the film that the main body of the plasma (the pink region and the green region in the axial channel in Figure 3, p.25) was moderately steady, but the outer envelope (the outer green region in Figure 3) and the tail flame (the violet region in Figure 3) oscillated regularly at a frequence of ~220 Hz. An up and down motion of the luminous zone low in the axial channel was irregular and did not appear to have a definite period.

Plasma-Therm generator system

A sequence from a high framing speed movie taken of

Table XXI. Characteristics of Generators

Manufacturer	Lepel	Plasma Therm	
Where described	Table I, p.15, supply 1	Table I, p.16, supply 2	
Type	Free running	Crystal controlled	
Frequency	~30 MHz	27.12 MHz	
Other qualifying conditions		As first received	With low ripple option
Filtering network capacitor			
Power			
a. shown on instrument panel meter	45%	2300 W	2100 W
b. measured with Bird wattmeter			1945 W
Output voltage ripple[a]			
a. Magnitude	0.5-0.9%	~4-6%	<0.5%
b. Frequency	120 Hz+360 Hz	360 Hz	60 Hz
Predominant frequency of oscillation in films	~220 Hz	360 Hz	
Film sequence	Not shown	Figure 21	Figure 22

[a]Measured with G. Holland, Ames Laboratory.

Table XXI. (Continued)

Manufacturer	International Plasma Corporation			
Where described	Table XVIII, p.108			
Type	Crystal controlled			
Frequency	27.12 MHz			
Other qualifying conditions	a.c. on filament		d.c. on filament	
Filtering network capacitor	4 μf	4 μf	4 μf	12 μf
Power				
a. shown on instrument panel meter	1100 W		1400 W	1010 W
b. measured with Bird wattmeter	955 W	955 W	1270 W	955 W
Output voltage ripple[a]				
a. Magnitude	19-25%	2.7-3.7%	4.4-6.4%	1.5-2.0%
b. Frequency	60 Hz+120 Hz + higher order	120 Hz + higher order	120 Hz + higher order	120 Hz
Predominant frequency of oscillation in films	60 Hz	_b	120 Hz	
Film Sequence	Figure 23	_b	Figure 24	Not shown

[b]Data are included for comparison purposes only.

the plasma formed by the Plasma-Therm generator system as first received in this laboratory is shown in Figure 21. The faint horizontal line approximately 2 mm from the bottom of the t = 3.33 ms frame is the top of the plasma torch. The plasma contracted radially forming an indention as can be seen along the right side of the t = 1.85 ms frame and then expanded forming a bulge as can be seen in the t = 3.33 ms frame. This sequence was repeated at frequency of ~360 Hz, which corresponds to the frequency of the ripple on the output voltage. As was the case for the Lepel system, the luminous zone seen in some of the frames (eg. t = 2.22 ms) low in the axial channel moved up and down and fluttered with no set frequency.

Figure 22 shows a film sequence of the plasma formed by the Plasma-Therm system after a low ripple option (Plasma-Therm) which reduced the 360 Hz ripple on the output power, had been installed. Although the 360 Hz oscillation was not apparent, this may be due to the geometrical perspective of the figure, as well as any changes in the plasma. This figure clearly shows the type of activity in the tail flame of the plasma. These oscillations were not of a set frequency, but appeared to be randomly spaced movements of the same basic character.

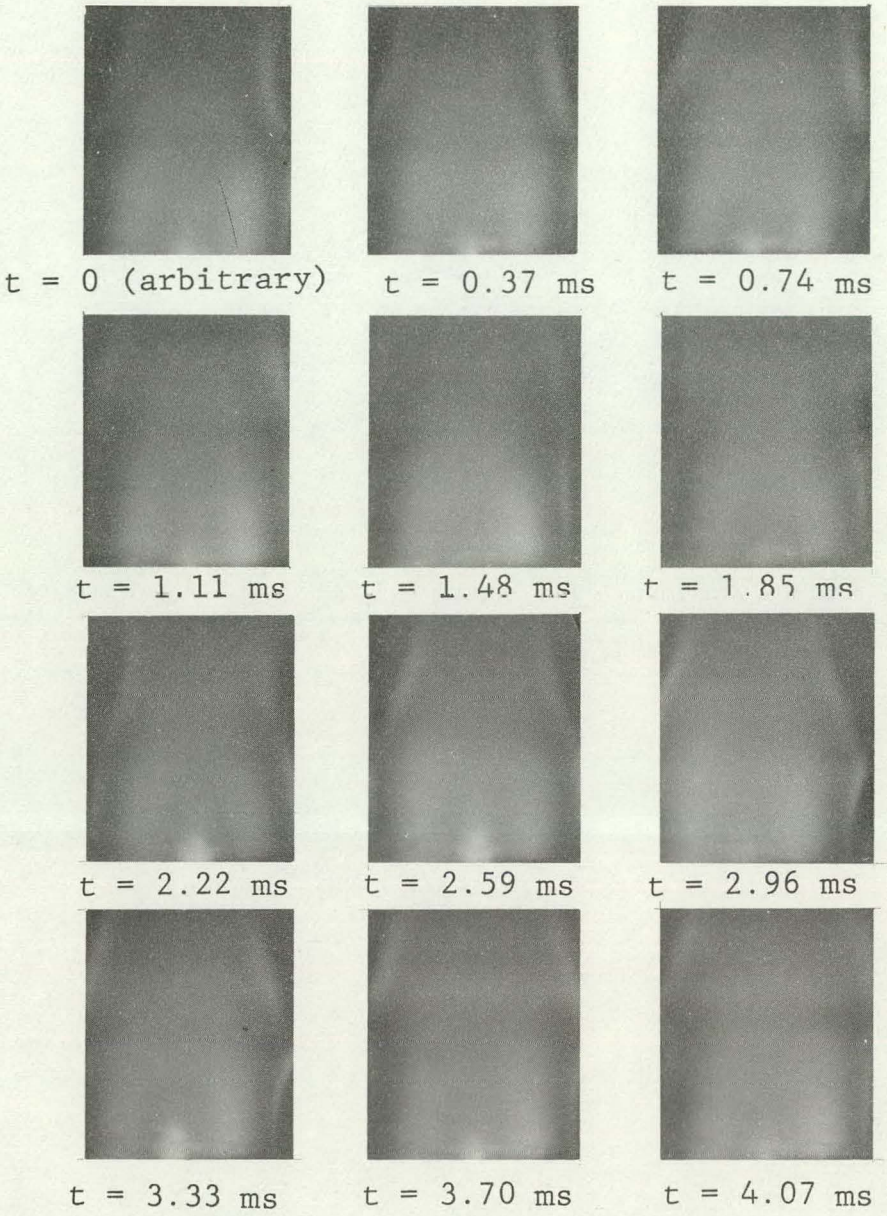

Figure 21. Plasma formed using Plasma Therm generator (plasma power supply 2 in Table I) as first received. Generator was operated at 2300 W forward power with a 1:10 Conostan base oil/MIBK solution being nebulized. Film sequence was taken at 5400 frames/s. Every second frame is shown.

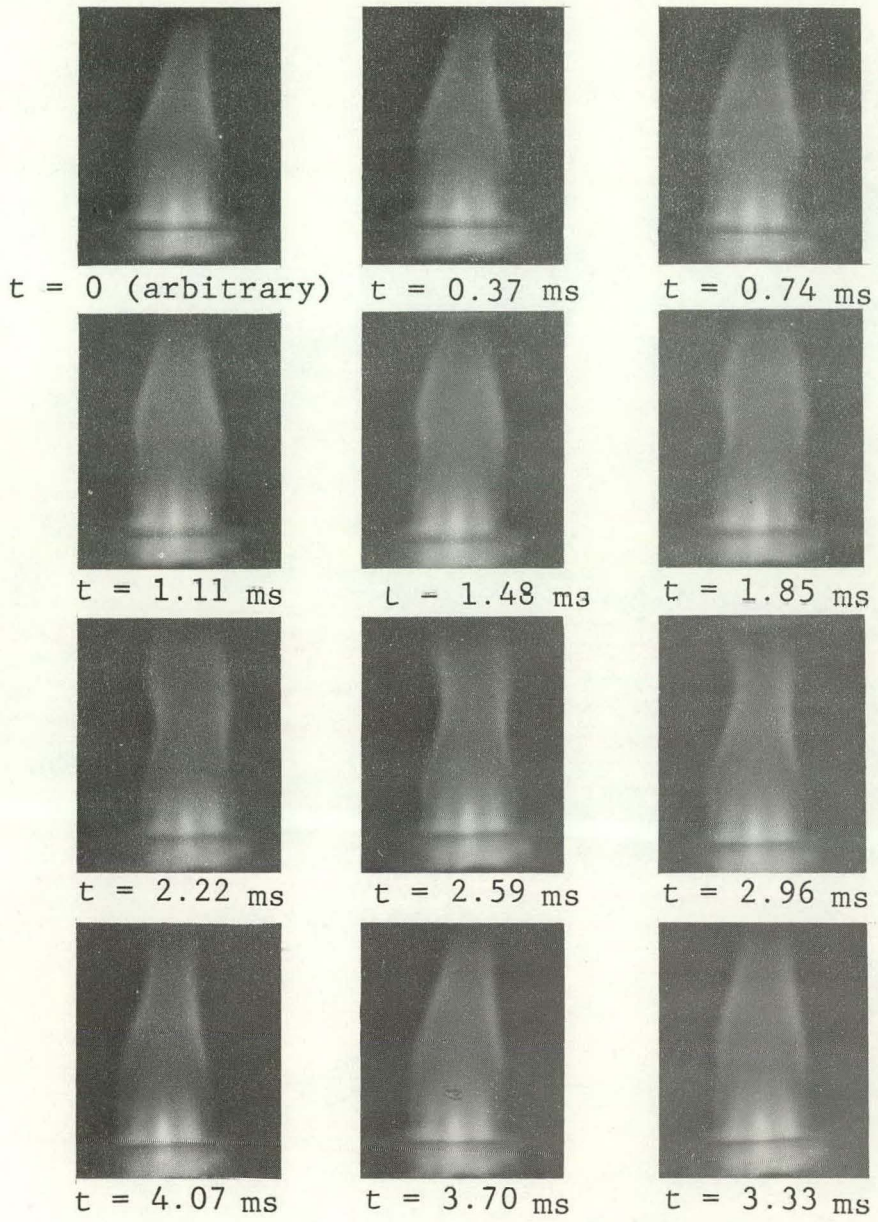

Figure 22. Plasma formed using the Plasma Therm generator (see Figure 21) after the low ripple option was installed. Generator was operated at 2100 W forward power with a 1:10 Conostan base oil/MIBK solution being nebulized. Film sequence was taken at ~5400 frames/s. Every second frame is shown.

International Plasma Corporation generator system

Observations on the International Plasma Corporation generator system illustrate the influence of the RF envelope features on plasma behavior. A 60 Hz sinusoidal ripple on the output power of the generator, produced by the a.c. voltage on the filament of the power amplifier tube, has been reported by Larson (91) and Kalnicky et al. (92). Recent measurements have shown that at the forward power level used in the present work the magnitude of the ripple on the output voltage was 19-25% (see Table XXI). The 60 Hz plasma growth and decay sequence caused by this ripple can be seen in Figure 23. Although the plasma luminosity is greatly reduced during the decay portion of the sequence, the impression that the plasma is almost extinguished is probably due to the exposure level of the film.

Some features apparent in the film cannot be seen in the sequence shown in Figure 23. In addition to the principal growth and decay sequence, the main body of the plasma, especially the pointed top, underwent two smaller oscillations during the high intensity portion of every second cycle. For a brief period, these minor oscillations became more subdued, but occurred during every cycle. The cause of these minor oscillations is probably traceable to disturbances on the mains, but the exact cause is unknown.

Larson (91) and Kalnicky et al. (92) have reported that

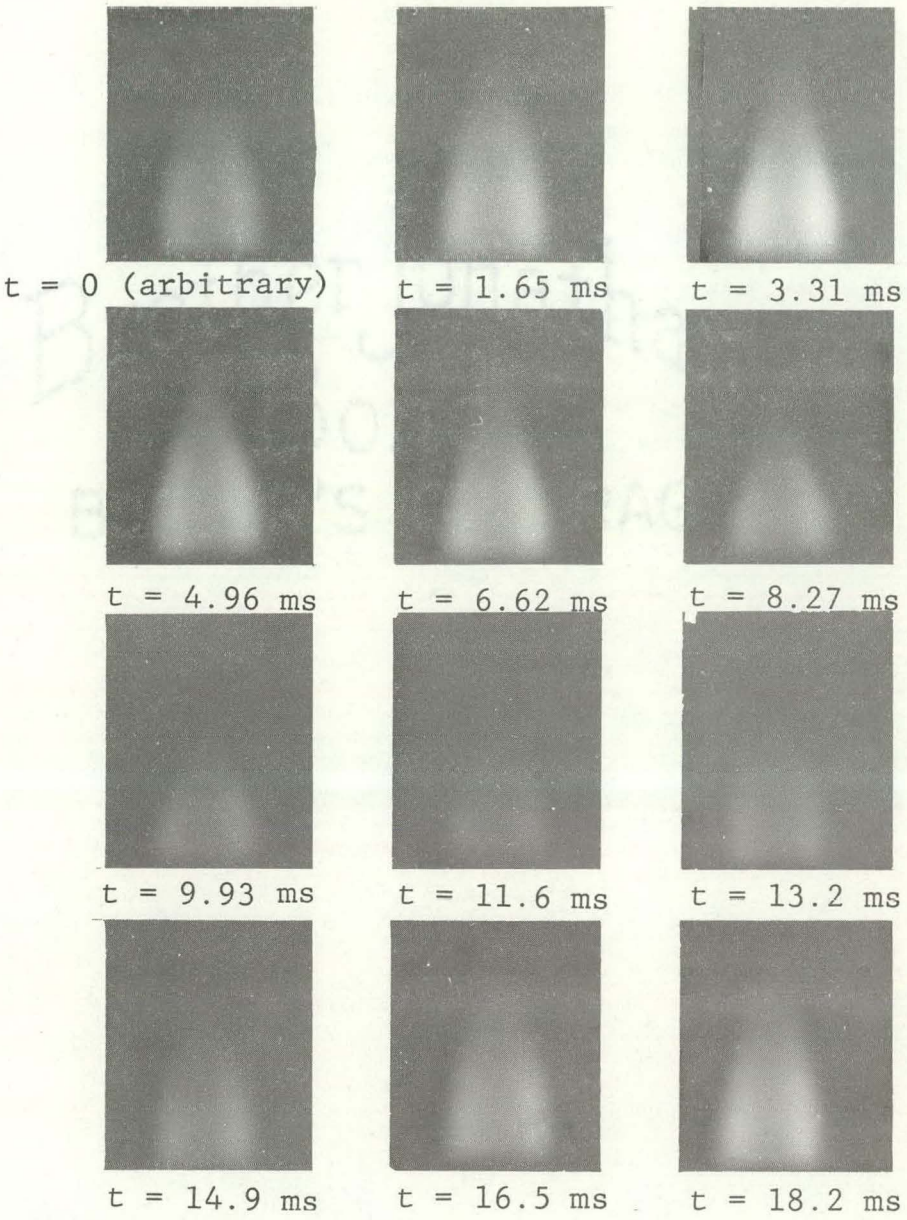

Figure 23. Plasma formed using the International Plasma Corporation generator with a 60 Hz ripple on the output power of the generator. Generator was operated at 1100 W forward power with deionized water being nebulized. Film sequence was taken at 5440 frames/s. Every ninth frame is shown.

when the 60 Hz ripple was eliminated by using a d.c. supply for the filament, a 120 Hz sawtooth ripple was seen in the RF voltage envelope. At the power level used in the present work, the magnitude of this ripple was found to be 4.4-6.4% and the power pulse resulting from this ripple could readily be seen in movies taken of the plasma. When the plasma regions were accented by nebulizing an aqueous sodium chloride solution, it could be seen that the toroidal region of the plasma became brighter and dimmer, while the main body of the plasma expanded and contracted. In addition, the luminous zone low in the axial channel moved up slowly as the plasma contracted and moved down quickly as the plasma expanded. Unfortunately, these phenomena cannot be readily distinguished in the film sequence of this plasma shown in Figure 24. The activity in the tail flame, however, is visible in the sequence. During each power cycle, the tail flame underwent two unevenly spaced oscillations. In frames t = 0 through t = 2.91 ms the tail flame expands radially. This is followed in frames t = 3.64 ms and t = 4.36 ms by a radial contraction. In frame t = 5.09, a bulge begins to form along the outer envelope in approximately the middle of the frame. This bulge expands and rises until it is almost out of view in frame t = 8.00 ms. While these oscillations were most evident in the tail flame, it appeared in the films as if the entire plasma may have undergone these

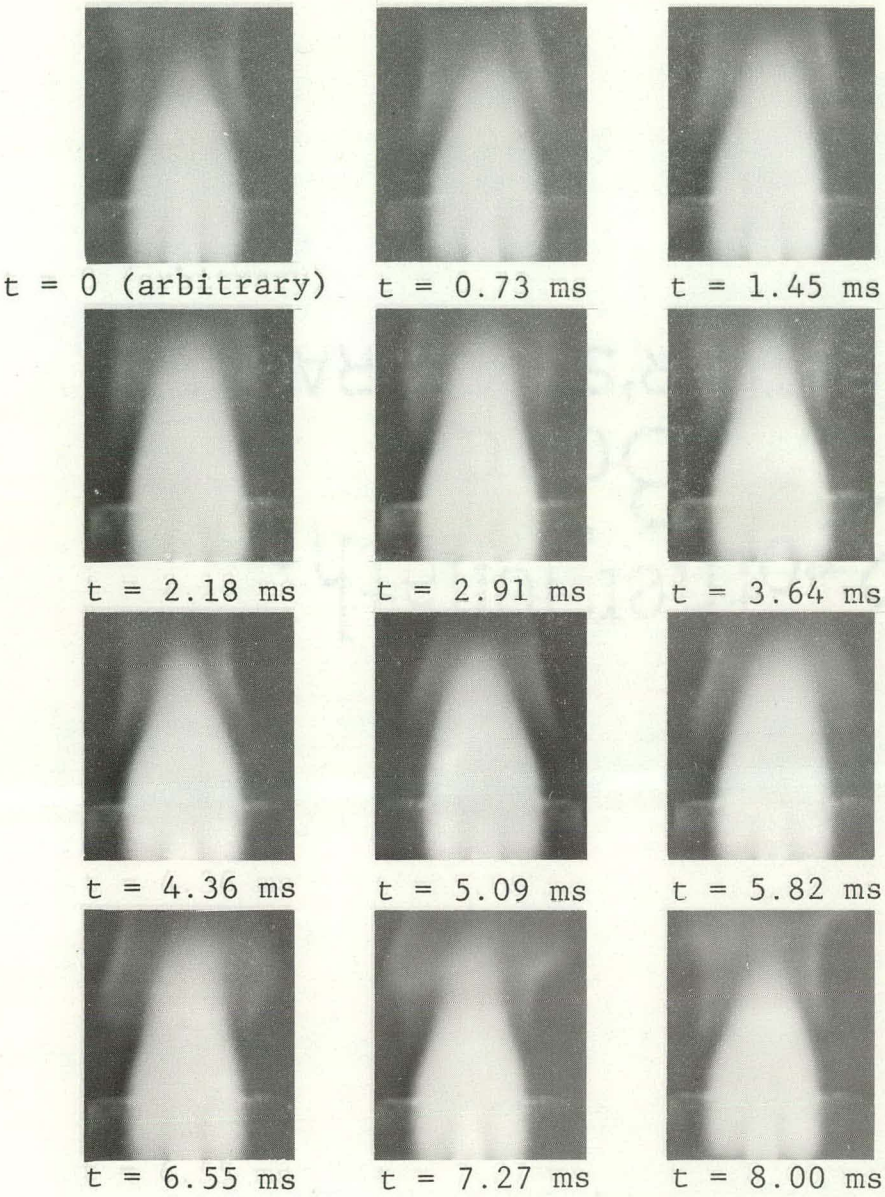

Figure 24. Plasma formed using the International Plasma Corporation generator with a d.c. supply for the filament. Generator was operated at 1400 W forward power with a solution of 6900 µg Na/ml in 10% (v/v) HCl being nebulized. Film sequence was taken at 5500 frames/s. Every fourth frame is shown.

pulses. These observations correlate with previous work (91) which noted two emission maxima during each period of the 120 Hz sawtooth ripple when the time resolved emission of several atomic and ionic spectral lines were observed.

Greenfield et al. (89,90) have also reported pulsations at twice the mains frequency in high framing speed movies of their plasma when the full-wave rectifier in their generator was not fully smoothed. The effect on their plasma was much more drastic than reported here. In fact, they have stated, "High-speed cine films of the plasma demonstrated that, without smoothing in the rectification circuit, the plasma was extinguished in every half-cycle of the mains frequency" (89). As can be seen in Figure 23, that did not happen in our system.

Gold (88) detected a regular disturbance in his plasma with the aid of a "Plasmascope." As in the present research, a ripple on the anode supply voltage (in Gold's case at 300 Hz) reportedly influenced the brightness of the plasma.

On the International Plasma Corporation system, the 120 Hz sawtooth ripple on the output voltage was reduced to 1.5-2.0% when the capacitance in the high voltage filtering network was increased from 4 μf to 12 μf in agreement with previous work (91,92). When the resultant plasma with a sodium chloride solution being nebulized was filmed, the 120 Hz oscillations were not evident. The pulses in the tail

flame appeared to be smoother and irregular rather than of a definite period.

Effects of torch geometry

The geometry of the plasma torch can noticeably affect the plasma shape. In the course of this research, an outer tube of 24 mm i.d. that extended 3 inches above the standard torch was fitted over the torch. With the added tube, the main body of the plasma was elongated and the luminous zone low in the axial channel extended higher in the plasma. Instead of being pronounced and pointed, the top boundary of the main body was more rounded and diffuse. The outer envelope was much less distinct, but it was faintly visible.

In many of the high framing speed movies taken of plasmas when oil/MIBK or aqueous sodium chloride solutions were being nebulized, small luminous pockets appeared to be released at the top of the luminous zone low in the axial channel and to rise a short distance in the plasma before disappearing. When the extended tube was used, these luminous pockets traveled higher in the plasma before disappearing.

Movies taken of the plasma formed with the capillary tipped aerosol delivery tube torch described in Table XVIII, revealed that the luminous zone low in the axial channel extended substantially higher in the plasma, giving the impression that the aerosol carrier-gas flow rate had been increased. The luminous pockets discussed above remained

visible higher in the plasma; a few even looked as if they traversed the plasma.

Future Research

Each of the plasma systems examined in this research displayed distinct behavior with respect to fluctuations of the plasma. Research is needed to determine what characteristics of the RF generator and impedance matching network influence this behavior and what effect these fluctuations have on the emission intensities of analyte species. The results of such an investigation could lead to improvements in design of the RF generator and/or impedance matching network, as well as improvements in the sampling and processing of the analytical signal.

BIBLIOGRAPHY

1. H. A. Laitinen, Anal. Chem., 46, 2073 (1974).

2. R. A. Hofstader, O. I. Milner, and J. H. Runnels, Eds., "Analysis of Petroleum for Trace Metals," Advances in Chemistry Series, No. 156, American Chemical Society, Washington, D.C., 1976.

3. B. B. Agrawal and I. B. Gulati, Petroleum & Hydrocarbons, 6, 193, 198 (1972).

4. O. I. Milner,"Analysis of Petroleum for Trace Elements," The Macmillan Company, New York, 1973.

5. T. F. Yen, Ed., "The Role of Trace Metals in Petroleum," Ann Arbor Science Publishers, Inc., Ann Arbor, MI, 1976.

6. H. A. Braier, Anal. Chem., 39, 175R (1967); 41, 169R (1969); 43, 185R (1971), 45, 196R (1973); 47, 199R (1975).

7. A. J. Mittledorf, The Spex Speaker, 13, No.1 (March) 1968).

8. D. Scott, W. W. Seifert, and V. C. Westcott, Scientific American, 230, 88 (1974).

9. D. L. Katz, D. E. Briggs, E. R. Lady, J. E. Powers, M. R. Tek, B. Williams, and W. E. Lobo, Electric Power Research Institute Report EPRI 206-0-0, Palo Alto, CA, 1974.

10. N. P. Cochran, Scientific American, 234(5), 24 (1976).

11. P. M. Yavorsky, presented at Ames Laboratory Coal Research Seminar, Ames, IA, April 17, 1974.

12. A. E. King, H. L. Roschen, and W. H. Irwin, Oil and Soap, 10, 204 (1933).

13. C. H. Lea,'Rancidity in Edible Fats," Chemical Publishing Co., New York, NY, 1939, pp. 154-161.

14. H. A. Braier and J. Eppolito, Preprints, Div. of Petrol. Chem., ACS, 18(4), 593 (1972).

15. H. A. Braier and J. Eppolito in "The Role of Trace Metals in Petroleum," T. F. Yen, Ed., Ann Arbor Science Publishers, Inc., Ann Arbor, MI., 1976, Chapter 4.

16. G. M. Gambrill, A. G. Gassmann, and W. R. O'Neill, Anal. Chem., 23, 1365 (1951).

17. V. A. Fassel and R. N. Kniseley, Anal. Chem., 46, 1110A, 1155A (1974).

18. V. A. Fassel, ASTM Spec. Tech. Pub. 618, American Society for Testing and Materials, Philadelphia, PA, 1977, pp. 22-42.

19. T. B. Reed, J. Appl. Phys., 32, 821 (1961).

20. T. B. Reed, Int. Science and Tech., June 1962, p.42.

21. V. A. Fassel, Proc. 16th Coll. Spectr. Int., Heidelberg, 1971, Adam Hilger, London, 1972, p.63.

22. J. D. Chase, J. Appl. Phys., 40, 318 (1969).

23. J. D. Chase, J. Appl. Phys., 42, 4870 (1971).

24. B. Waldie, Conference Proceedings International Round Table on the Study and Applications of Transport Phenomena in Thermal Plasmas, Odeillo-Fontromeu, France, Sept. 1975, IV-9.

25. M. I. Boulos, Conference Proceedings International Round Table on the Study and Applications of Transport Phenomena in Thermal Plasmas, Odeillo-Fontromeu, France, Sept. 1975, IV-7.

26. M. I. Boulos, IEEE Trans. Plasma Sci., PS-4, No. 1, 28 (1976).

27. B. M. Dymshits and Ya. P. Koretskii, Z. Tekhn. Fiz., 39, 1039 (1969); Sov. Phys.-Tech. Phys., 14, 779 (1969).

28. V. S. Klubnikin, Teplofiz. Vys. Temp., 13, 473 (1975); High Temp., 13, 439 (1975).

29. G. F. Larson, V. A. Fassel, R. H. Scott, and R. N. Kniseley, Anal. Chem., 47, 238 (1975).

30. G. Pforr, "Schmierstoffe und Schmierungstechnik," No. 25, Deutscher Verlag für Grundstoffindustrie, Leipzig.

31. G. Pforr and O. Aribot, Z. Chem., 10, 78 (1970).

32. S. Greenfield and P. B. Smith, Anal. Chim. Acta, 59, 341 (1972).

33. V. A. Fassel, C. A. Peterson, F. N. Abercrombie, and R. N. Kniseley, Anal. Chem., 48, 516 (1976).

34. F. N. Abercrombie, Ames Laboratory, USERDA, Iowa State University, Ames, IA, unpublished data.

35. S. E. Valente and W. G. Schrenk, Appl. Spectrosc., 24, 197 (1970).

36. C. C. Butler, R. N. Kniseley, and V. A. Fassel, Anal. Chem., 47, 825 (1975).

37. R. K. Winge, V. A. Fassel, R. N. Kniseley, E. L. DeKalb, and W. J. Haas, Spectrochim. Acta, in press.

38. A. Montaser and V. A. Fassel, Anal. Chem., 48, 1490 (1976).

39. R. N. Kniseley, H. Amenson, C. C. Butler, and V. A. Fassel, Appl. Spectrosc., 28, 285 (1974).

40. S. Greenfield, H. McD. McGeachin, and P. B. Smith, Anal. Chim. Acta, 84, 67 (1976).

41. E. C. Kuehner, R. Alvarez, P. J. Paulsen, and T. J. Murphy, Anal. Chem., 44, 2050 (1972).

42. W. J. Haas, R. K. Winge, V. A. Fassel, and R. N. Kniseley, Abstracts, 3rd Annual Meeting, Federation of Analytical Chemistry and Spectroscopy Societies, Philadelphia, PA, Nov. 1976, No. 79.

43. IUPAC Commission on Spectrochemical and Other Optical Procedures for Analysis, Pure Appl. Chem., 45, 99 (1976).

44. E. A. Means and D. Ratcliffe, At. Absorption Newslett., 4, 174 (1965).

45. J. A. Burrows, J. C. Heerdt, and J. B. Willis, Anal. Chem., 37, 579 (1965).

46. S. Slavin and W. Slavin, At. Absorption Newslett., 5, 106 (1966).

47. T. T. Bartels and M. P. Slater, At. Absorption Newslett., 9, 75 (1970).

48. R. H. Kriss and T. T. Bartels, At. Absorption Newslett., 9, 78 (1970).

49. H. L. Kahn, G. E. Peterson and D. C. Manning, At. Absorption Newslett., 9, 79 (1970).

50. D. R. Jackson, C. Salama, and R. Dunn, Can. Spectrosc., 15, 17 (1970).

51. J. H. Taylor, T. T. Bartels, and N. L. Crump, Anal. Chem., 43, 1780 (1971).

52. G. S. Golden, Appl. Spectrosc., 25, 668 (1971).

53. R. D. Reeves, C. J. Molnar, M. T. Glenn, J. R. Ahlstrom, and J. D. Winefordner, Anal. Chem., 44, 2205 (1972).

54. J. Y. Marks, Pratt & Whitney Aircraft, East Harford, CT, personal communication, 1975.

55. C. S. Saba and K. J. Eisentraut, Anal. Chem., 49, 454 (1977).

56. S. V. Dresvin, Ed., "Physics and Technology of Low Temperature Plasmas," Atomizdat, Moscow, 1972.

57. M. I. Boulos and W. H. Gauvin, Can. J. Chem. Eng., 52, 355 (1974).

58. P. D. Johnston, Combust. Flame, 18, 373 (1972).

59. C. Borgianni, M. Capitelli, F. Cramarossa, L. Triolo, and E. Molinari, Combust. Flame, 13, 181 (1968).

60. R. M. Barnes and R. G. Schleicher, Spectrochim. Acta, 30B, 109 (1975).

61. M. Capitelli, F. Cramarossa, L. Triolo, and E. Molinari, Combust. Flame, 15, 23 (1970).

62. IUPAC Commission on Spectrochemical and Other Optical Procedures for Analysis, Pure Appl. Chem., 45, 105 (1976).

63. J. B. Willis, Anal. Chem., 47, 1752 (1975).

64. D. J. Kalnicky, R. N. Kniseley, and V. A. Fassel, Spectrochim. Acta, 30B, 511 (1975).

65. Trace Elements in Fuel Oil, National Bureau of Standards Certificate of Analysis, Standard Reference Material 1634 (1975).

66. R. H. Filby in "The Role of Trace Metals in Petroleum," T. F. Yen, Ed., Ann Arbor Science Publishers, Inc., Ann Arbor, MI, 1976, Chapter 2.

67. P. H. Given, R. N. Miller, N. Suhr, and W. Spackman in "Trace Elements in Fuel," S. P. Babu, Ed., Advances in Chemistry Series, No. 141, American Chemical Society, Washington, D.C., 1975, Chapter 14.

68. J. A. Carter, J. C. Franklin, and L. Landau in "Preliminary Results: Chemical and Biological Examination of Coal-Derived Materials," W. D. Shults, Ed., USERDA Report ORNL/NSF/EATC-18, Oak Ridge, TN, March 1976.

69. J. S. Fruchter, J. C. Laul, M. R. Petersen, and P. W. Ryan, Preprints, Div. of Petrol. Chem., ACS, 22, 793 (1977).

70. P. M. Yavorsky and S. Akhtar, "Environmental Aspects of Coal Liquefaction," EPA Symposium on Environmental Aspects of Fuel Conversion Technology, May 13-16, 1974, St. Louis, MO.

71. H. Schultz, G. A. Gibbon, E. A. Hattman, H. B. Booher, and J. W. Adkins, "The Distribution of Some Trace Elements in the ½ Ton per Day SYNTHOIL Process Development Unit," USERDA Report PERC/RI-77/2, Pittsburgh, PA, February 1977.

72. H. Schultz, G. A. Gibbon, E. A. Hattman, H. B. Booher, and J. W. Adkins, Preprints, Div. Of Petrol. Chem., ACS, 22, 588 (1977).

73. C. E. Gleit and W. D. Holland, Anal. Chem., 34, 1454 (1962).

74. J. R. Hollahan in "Techniques and Applications of Plasma Chemistry," J. R. Hollahan and A. T. Bell, Eds., John Wiley and Sons, New York, NY, 1974, Chapter 7.

75. C. E. Gleit in "Chemical Reactions in Electrical Discharges," R. F. Gould, Ed., Advances in Chemistry Series, No. 80, American Chemical Society, Washington, D.C., 1969, Chapter 18.

76. P. R. Walsh, J. L. Fasching, and R. A. Duce, Anal. Chem., 48, 1012 (1976).

77. C. E. Mulford, At. Absorption Newslett., 5, 135 (1966).

78. D. W. Koppenaal and S. E. Manahan, Environ. Sci. Technol., 10, 1104 (1976).

79. H. W. Sternberg, R. Raymond, and F. K. Schweighardt, Preprints, Div. of Petrol. Chem., ACS, 21, 198 (1976).

80. F. Grabau IV, Ames Laboratory, USERDA, Iowa State University, Ames, IA, unpublished data.

81. L. T. Black, J. Amer. Oil Chem. Soc., 52, 88 (1975).

82. T. M. Laciak, ArRo Laboratories, Inc., Joliet, IL, personal communication, 1977.

83. M. Routh, Varian Instrument Division, Palo Alto, CA, personal communication, 1977.

84. R. H. Scott, V. A. Fassel, R. N. Kniseley, and D. E. Nixon, Anal. Chem., 46, 75 (1974).

85. R. M. Dagnall, D. J. Smith, T. S. West, and S. Greenfield, Anal. Chim. Acta, 54, 397 (1971).

86. R. G. Schleicher and R. M. Barnes, 2nd Annual Meeting of the Federation of Analytical Chemistry and Spectroscopy Societies, Indianapolis, IN, October 1975, No. 89.

87. S. V. Desai, E. S. Daniel, and W. H. Corcoran, Rev. Sci. Instr., 39, 612 (1968).

88. D. Gold, Conference Proceedings International Round Table on the Study and Applications of Transport Phenomena in Thermal Plasmas, Odeillo-Fontromeu, France, Sept. 1975, IV-8.

89. S. Greenfield, H. McD. McGeachin, and P. B. Smith, Talanta, 23, 1 (1976).

90. S. Greenfield, L. Ll. Jones, C. T. Berry, and L. G. Bunch, Proc. Soc. Anal. Chem., 2, 111 (1965).

91. G. F. Larson, Ames Laboratory Quarterly Report, 6/74-9/74.

92. D. J. Kalnicky, V. A. Fassel, and R. N. Kniseley, Appl. Spectrosc., 31, 137 (1977).

93. G. J. Bastiaans and G. M. Hieftje, Anal. Chem., 46, 901 (1974).

94. N. C. Clampitt and G. M. Hieftje, Anal. Chem., 44, 1211 (1972).

ACKNOWLEDGMENTS

I would like to thank Dr. Velmer A. Fassel and Dr. Richard N. Kniseley for their guidance and critical review of this work. My fellow graduate students and co-workers have also contributed to this research through numerous discussions.

The many hours spent by George Holland modifying, testing, and maintaining the plasma power supply systems used in this work are greatly appreciated. I would also like to thank a number of individuals and the organizations they represent for contributing samples, reference samples, and comparative data used in these investigations: J. L. Armstrong and T. M. Laciak of ArRo Laboratories, Inc.; T. T. Bartels of McDonnel-Douglas Corp.; L. T. Black of Northern Regional Research Laboratory, ARS, USDA; K. J. Eisentraut and C. S. Saba of the Air Force Materials Laboratory, Wright-Patterson Air Force Base; J. Y. Marks of Pratt & Whitney Aircraft Group, United Technologies; N. J. Mazzocco, H. Schultz, G. A. Gibbon, A. G. Sharkey, Jr., and R. G. Lett of the Pittsburgh Energy Research Center, USERDA; and the U.S. Air Force Spectrometric Oil Analysis Program.

The financial assistance granted by the Shell Companies Foundation is gratefully acknowledged.

I would like to express my appreciation for the love, guidance and encouragement my parents, Ernest and Arlene Peterson, have given me over the years. I would also like to

thank Richard and Dolores Hicks for the help they have given me since I met their daughter.

Above all, I am thankful for my wife Patricia, whose love, support, and patience helped immeasurably in the completion of this thesis. May I be able to repay her for all she has done and all she has given.

APPENDIX:

PARTICLE VAPORIZATION THEORY

The high temperature experienced by a particle in the plasma may transform all or part of it into a vapor. The mechanism by which this process occurs is dependent on the nature of the particle, the temperature of the plasma, and the particle size (93).[1] The process may be mass-transfer controlled, in which case the vaporization rate would depend on the diffusion coefficient of the vaporized species, the volatility of the particle substituents, and the temperature (93). Another possibility is heat-transfer controlled vaporization. According to Bastiaans and Hieftje, "If the boiling point of the molten material is appreciably lower than the flame (gas) temperature, conduction of heat from the flame gases to the surface of the molten particle will likely be the rate-limiting process for vaporization." This condition appears to hold for most substances in the hot regions of the plasma through which the particle passes. Thus, the favored mechanism in these regions would likely be heat-transfer control.

---

[1] In the case of aerosol droplets, the droplet must also be desolvated, a process which will not be discussed here. The mechanism of desolvation has been discussed in a recent article by Clampitt and Hieftje (94).

Theoretical analyses of heat transfer to particles have been given for an inductively coupled plasma (59) and for a radio-frequency augmented flame (58). The smallest particle size considered by each paper was 50 μm. Johnston (58) included a term to account for the radiative heat loss from the particles, a term which was considered negligible by Borgianni, et al. (59). Johnston also included another term to account for the heat gained from other emitting particles in the flame. In other respects, the analyses given in the two papers are similar. Dresvin (56) considered the heating and melting of a particle in a plasma jet and obtained equations similar to those of Johnston (58). In the discussion below, Johnston's approach is closely followed because of his more fully developed treatment.

For a spherical particle moving in a gas stream, the following heat balance holds:

$$\pi D^2 h(T_g - T_p) + h_r(T_g) = C_p \frac{dT_p}{dt} + \Delta H_{Td} \frac{dm}{dt} + \pi D^2 \varepsilon \sigma T_p^4 \left(1 - \frac{\pi D^2 nr}{4}\right) \qquad (3)$$

where D = diameter of the particle, m

h = heat-transfer coefficient, $WK^{-1}m^{-2}$

T_g = temperature of the hot gas, K

T_p = temperature of the particle, K

h_r = radiative heat-transfer coefficient, WK^{-1}

C_p = thermal capacity of the particle, JK^{-1}

t = elapsed time, s

ΔH_{Td} = enthalpy of decomposition (or vaporization), Jg^{-1}

m = mass of the particle, g

ε = emissivity of the particle

σ = Stefan-Boltzmann constant, $Wm^{-2}K^{-4}$

n = number density, m^{-3}

r = radius of interaction, can be considered radius of the column of particle-containing gas, m.

In Equation 3 the first term represents the heat transferred from the hot gas to the particle. The second term represents the heat gained by the particle from radiation of the gas. Although this term was considered negligible by the authors of both papers cited above, this heat transfer process may determine the temperature of the particle before it reaches the plasma region, i.e., the particle may be heated by radiation as it travels to the plasma. The first term on the right hand side represents the increase in the temperature of the particle. The rate of decomposition (or vaporization) is represented by the second term. The last term represents the heat lost by radiation from the particle along with the heat gained from other particles.

The heat transfer coefficient for a sphere moving in

a gas stream is given by

$$h = \frac{\kappa(Nu)}{D} \tag{4}$$

where κ = thermal conductivity of the gas, $Wm^{-1}K^{-1}$

(Nu) = Nusselt number.

The Nusselt number of a particle is given by

$$(Nu) = [2 + 0.6\ (Re)^{1/2}(Pr)^{1/3}] \tag{5}$$

where (Re) = Reynolds number

(Pr) = Prandtl number.

These numbers are defined below:

$$(Re) = \frac{Dv\rho_g}{\mu}$$

$$(Pr) = \frac{c_p\mu}{\kappa} \tag{6}$$

where v = velocity of the particle relative to the gas, ms^{-1}

ρ_g = density of the gas, gm^{-3}

μ = viscosity of the gas, $gs^{-1}m^{-1}$

c_p = specific heat of the gas, $Jg^{-1}K^{-1}$.

If it is assumed that there are no temperature gradients within the particle, the analysis of Equation 3 can be divided into four cases representing different stages of the vaporization process. In each of these cases, an elapsed

time period is calculated, viz., t_1, t_2, t_3 and t_4.

Case 1

The first period (t_1) is the time needed to heat the particle to its melting point. Equation 3 reduces to

$$\pi D^2 h(T_g - T_p) = C_p \frac{dT_p}{dt} . \qquad (7)$$

The thermal heat capacity of the particle is given by

$$C_p = \left(\frac{\pi}{6}\right) D^3 \rho_p c_p' \qquad (8)$$

where ρ_p = density of the particle, gm^{-3}

c_p' = specific heat of the particle, cal $g^{-1}K^{-1}$.

Equation 4,5,6 and 8 can be substituted into Equation 7 giving

$$\pi DK(T_g - T_p)\left[2 + 0.6 \left(\frac{Dv\rho_g}{\mu}\right)^{1/2} \left(\frac{c_p \mu}{\kappa}\right)^{1/3}\right] = \frac{\pi}{6} D^3 \rho_p c_p' \frac{dT_p}{dt} . \qquad (9)$$

The problems involved in applying this equation to the calculation of the time needed to heat the particle to its melting point are manifold. As the particle heats up, the diameter (D) and, therefore, the density (ρ_p) may change. These changes would also affect the velocity of the particle relative to the gas (v) since the velocity is partially determined by the viscous drag which is diameter sensitive. Also, the plasma is not isothermal. Thus, the gas temperature (T_g) experienced by the particle is not constant but is

position and, therefore, time dependent (64,92). Since the thermal conductivity (κ), viscosity (μ) and density (ρ_g) of the gas are all temperature dependent, these quantities are also time dependent. In addition, as the gas traverses the plasma it is heated, changing its velocity. This could have an effect on the velocity of the particle relative to the gas (v).

If the assumption is made that the change in these variables can be neglected, Equation 9 can be integrated to give

$$t_1 = \left[\ln \frac{T_g - T_{p_o}}{T_g - T_p} \right] \frac{D^2 c_p \rho_p}{6 \kappa (Nu)} \quad . \qquad (10)$$

Case 2

The second period (t_2) is the time it takes the particle to melt. This depends on the mass and the latent heat of fusion of the particle. If it is assumed that the temperature of the particle remains constant, the following relationship exists:

$$\pi D_o \kappa (Nu)(T_g - T_p) = \frac{dm}{dt} L_f + \pi D_o^2 \varepsilon \sigma T_p^4 \left(1 - \frac{\pi D_o^2 nr}{4}\right) \qquad (11)$$

where L_f = latent heat of fusion of the particle, Jg^{-1}

D_o = initial diameter of the particle, m.

The arguments given in Case 1 concerning the time dependence of (Nu), T_g and κ apply here as well. Similar arguments can

be presented concerning the number density of particles (n). Again, if these changes can be neglected, Equation 11 can be integrated to give

$$t_2 = \frac{D_o^2 \rho_p L_f}{(Nu)\kappa(T_g - T_p) - D_o \varepsilon \sigma T_p^4 (1 - \frac{\pi D_o^2 nr}{4})} \quad (12)$$

Case 3

Once the particle is melted, the liquid phase will heat up from the melting point to the decomposition or vaporization point in the time period t_3. The heat balance equation can be expressed as

$$\pi D \kappa (Nu)(T_g - T_p) = \frac{\pi}{6} D^3 \rho_p c_p' \frac{dT_p}{dt} + \pi D^2 \varepsilon \sigma T_p^4 (1 - \frac{\pi D^2 nr}{4}) \quad (13)$$

This equation can be rearranged for integration to give

$$\int_{T \text{ at MP}}^{T \text{ at decomp}} \frac{dT_p}{A - BT_p - CT_p^4} = \int_o^{t_3} F dt \quad (14)$$

where $A = \kappa(Nu)T_g$

$B = \kappa(Nu)$

$C = D\varepsilon\sigma(1 - \frac{\pi D^2 nr}{4})$

$F = 6/D^2 \rho_p c_p'$.

According to Johnston, this integral has to be solved numerically.[1]

---

[1]The F in Johnston's Equation 11 is the inverse of the one given above (58, p.375).

Once again it has been assumed that there is no significant time dependence of the variables which comprise A,B,C, and F, not necessarily a good assumption. As the liquid is heated, it will expand, changing the diameter and density of the droplet. This in turn will affect any variables which are diameter or density sensitive. Also, the argument expressed in Case 1 concerning the gas temperature and gas temperature dependent properties is still valid here.

In the development of Equations 13 and 14, it has been assumed that no vaporization takes place until the entire particle reaches the decomposition or vaporization temperature. However, the particle will start to decompose or vaporize before this temperature is reached.

Case 4

As the particle vaporizes, a portion of the heat which would normally be transferred to the surface of the particle is used to raise the enthalpy of the evaporating species from its value at T_p to its value at T_g (59). This means that the heat flux to the particle surface will be less than h. A new coefficient for heat transfer in the presence of mass counterflow can be defined as follows (59):

$$h' = h\left[\frac{\ln(1 + \Delta H_{ov}/\Delta H_{Td})}{\Delta H_{ov}/\Delta H_{Td}}\right] \qquad (15)$$

where h' = mass counterflow heat transfer coefficient

ΔH_{ov} = overall enthalpy change from T_p to T_g.

The expression in brackets is always less than one. Calling this expression λ, the heat balance equation for Case 4 can be written as

$$\pi D(Nu)\kappa(T_g-T_p)\lambda = \Delta H_{Td}\frac{dm}{dt} + \pi D^2\varepsilon\sigma T_p^4\left[1-\frac{\pi D^2 nr}{4}\right]. \quad (16)$$

This equation can be expressed in integral form,

$$\int_D^0 \frac{DdD}{A-BD+CD^3} = \int_0^{t_4} \frac{2d\iota}{\rho_p \Delta H_{Td}} \quad (17)$$

where $A = \lambda\kappa(Nu)(T_g-T_p)$

$B = \varepsilon\sigma T_p^4$

$C = \frac{1}{4}\pi nr\varepsilon\sigma T_p^4$

t_4 = time required for complete vaporization.

Johnston suggested that Equation 17 be integrated numerically in steps. If small enough steps were used, many of the objections raised in Cases 1-3 would be invalid here.

By combining the elapsed times t_1, t_2, t_3, and t_4 an estimate of the time which it will take to completely vaporize a particle can be obtained. Of course, if there are any phase changes or decomposition steps, these must also be accounted for by solving the appropriate equations.